Alma Mater Studiorum – Università di Bologna

DOTTORATO DI RICERCA IN GEOFISICA

CICLO XXIII

Facoltà di Scienze Fisiche, Matematiche e Naturali

Settore Scientifico disciplinare di afferenza: GEO/12

TITOLO

CLIMATE IMPACT STUDIES OF SEDIMENT TRANSPORT ON THE ADRIATIC COASTAL ZONE

Presentata da
Antonio Guarnieri

Relatore
Prof. Nadia Pinardi

Coordinatore
Prof. Michele Dragoni

Esame finale anno 2011

Correlatori

- Dr. Alejandro J. Souza
  National Ocenaography Center, Liverpool (United Kingdom)
- Dr. Paolo Oddo
  Istituto Nazionale di Geofisica e Vulcanologia, Bologna (Italy)

CONTENTS

Chapter 1

1. INTRODUCTION

1.1 General characteristics of the Adriatic Sea basin and of its circulation

The Adriatic Sea is a semi-enclosed, elongated basin of approximately 800 km of length and 200 km of width, exchanging waters with the rest of the Mediterranean Sea at its southern boundary, where the Otranto Strait marks the line of separation with the Ionian Sea (Figure 1.1). The basin is confined eastward with the Balcanic coast, westward and northward with the Italian coast. The bathymetry of the basin is very heterogeneous and it follows the well known three distinct regions of northern, central and southern Adriatic (Artegiani et al., 1997 a, and b): it starts from north gently sloping towards south until the isobath 100 m (northern Adriatic), where the Pomo Depression begins, reaching a maximum depth of about 250 meters, and ending at the Pelagosa Sill, between Vieste and Dubrovnik, which is the main topographic feature of the Central Adriatic. The southern part of the basin is characterized by a depression deeper than 1300 meters, with isobaths running parallel to the Italian and Balcanic coast lines respectively. Spanning from east to west the morphology of the coast is quite different as well: more regular and characterized mainly by sandy coastlines is the western side, while the eastern side is much more irregular, and presents mainly a rocky coastline and a considerable amount of islands, especially in front of Slovenia and Croatia.

The basin is characterized by a high input of fresh water, mainly due to the Po river (fig 1.1), situated in the Italian north-western coast, and to the Buna/Bojana river, a transboundary river between Albania and Montenegro, in the southern-east coast of the basin. These two rivers together, whose mean annual climatological flows are respectively 1585 m^3/s (Raicich, 1994) and 675 m^3/s (UNEP 1996), are responsible for almost the 40% of the runoff freshwater input in the basin, and strongly influence the dynamics of its general circulation, and these high freshwater fluxes strongly contribute to make it a dilution basin.

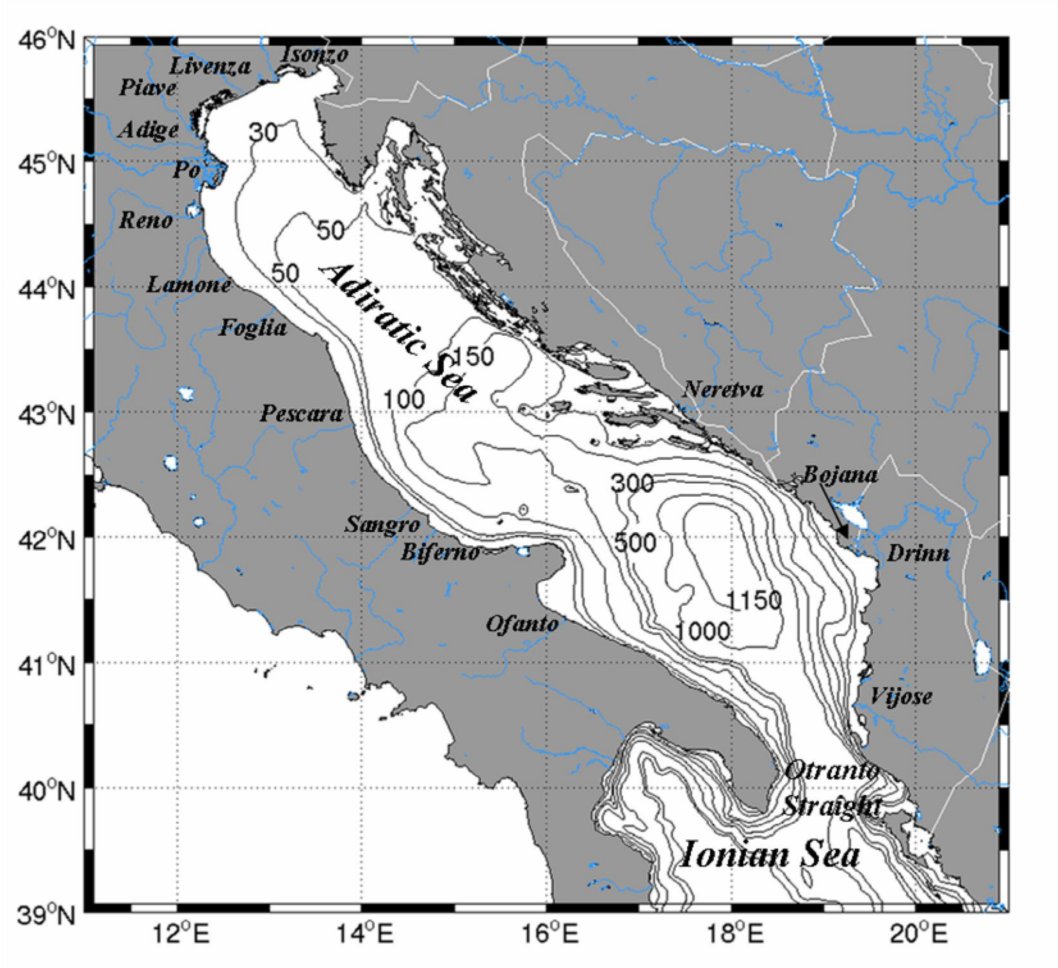

Figure 1.1: Adriatic Sea domain, bathymetry (solid contour lines), and main rivers discharging into the basin

The two main wind regimes that characterize this region are the Bora and the Sirocco winds. The former is a very cold and dry, north-easterly wind, presenting frequent strong spatial and temporal gradients (Cavaleri et al, 1981), and is strongly influenced by the orography of the Dynaric Alps, and usually confined to the northernmost part of the basin, while the latter is a much more humid wind, blowing along the basin longitudinal axis and fetching the whole basin from south-east to north-west, being thus often partly responsible of the sea level of the northern Adriatic region. These two regimes drive respectively the winter and autumn season, and give rise to the two corresponding main wave regimes of the Adriatic Sea, whose characteristics are quite different.

For what concerns the heat fluxes budget of the region different results have been presented in the literature, according to the different periods analyzed and methods used for the analysis. All the different analysis, though, show negative climatological annual heat budgets, varying from -54 Wm^{-2} (Chiaggiato et al. 2005), to much higher values of about -5 Wm^{-2} (Maggiore et al. 1998, Cardin and Gacic 2003). The most accepted values, after Artegiani et al. (1997a), range from -22 to -19 Wm^{-2} Recent findings from Oddo and Guarnieri (2011) propose a general heat budget very close to equilibrium, but slightly positive. In general the variability on the heat fluxes is very high from year to year (especially in the periods of heat losses), and has a very strong seasonal signal, inducing the basin to transfer heat to the atmosphere in Autumn (Nov, Dec) and early Winter (Jan, Feb, Mar, Apr), up to values of 350-400 W/m^2, especially during particularly strong Bora events, and to gain heat from the atmosphere in Spring (May, Jun) and Summer (Jul, Aug, Sep, Oct), with a less pronounced interannual variability.

The combination of the water and heat budgets just described gives an overall buoyancy budget on the basin which tends to be very close to zero, due to the balancing of the estuarine component of the circulation, driven by the strong input of runoff fresh water and typical of a dilution basin, and its anti-estuarine-like component, driven by the heat fluxes budget (Pinardi et al, 2006).

This variable geography and topography, together with the very high variability of the atmospheric forcings and with the strong impact of the river forcings contributes to create a very heterogeneous and interesting environment from a physical point of view.

1.2 Mechanism of tides and their characteristics in the Adriatic basin.

The periodical oscillations of the sea surface due to the combined effect of the gravitational attraction of the celestial bodies, in particular the sun and the moon, and of the rotation of the Earth are commonly known as *tides*. More generally we can define tides as the response to the ocean to the periodic fluctuations of the tide-raising forces of the Moon and the Sun, and this response is in the form of long waves, thus propagating through the ocean following the physics of long waves, interacting with each other and with the local peculiarities of the system, such as its geometry and topography in particular. This means that the tidal perturbation we can locally appreciate was not locally generated, but is the sum of the tidal waves travelling from far away, each one carrying its own experience along the way (after the *Canadian Hydrographic User's Guide*).

The dependence of the phenomenon from the mutual position of the Sun, the Earth and the Moon makes the intensity of the tidal processes variable in time according to the typical periods of these bodies themselves. The most tangible effect of this mechanism is the fluctuation of the tidal sea level in time, which can be represented as the sum of cosine functions as follows:

$$\eta(t) = \sum_{i=1}^{n} A_i \cos(w_i t + \varphi_i) \tag{1.1}$$

Where η (cm) is the total tidal resulting sea elevation, A_i (amplitude in cm) and φ_i (phase in degrees) are the tidal constituents or frequencies of tides, w_i (degrees/hour) is the frequency.

The tidal regime of the Adriatic basin is not very strong, but together with the coast off shore Tunisia, the Adriatic Sea represents the only area within the Mediterranean Sea where tides have a range of up to one meter. This happens particularly in its northernmost region, the Gulf of Trieste, where the amplitudes of the most energetic frequencies - M2 and K1 - reach approximately 27 and 18 cm respectively. As it is well known from many studies on the Adriatic tides the diurnal frequencies present weak amplitudes in the south of the basin and are enhanced moving northwards developing isopleth lines of amplitude perpendicular to the longitudinal axis of the basin. The semidiurnal frequencies as well show a strong enhancement in the northern part of the basin, presenting similar patterns of coamplitude lines, with a substantial difference: the formation of an anphidromic node situated in the centre of the basin between the Italian city of Ancona and the Croatian city of Zadar.

An important characteristics of the Adriatic tidal regime is that its major component is not a direct response to the astronomical influence of the Sun and the Moon, but is mainly linked to the astronomical tidal oscillations of the Ionian Sea, which induces forced oscillations of the Adriatic basin and phenomena of resonance, responsible for the amplification of the tidal wave amplitudes in the longitudinal direction, moving towards north. This suggests a behaviour of the Adriatic tides very similar to that one of seiches.

1.3 Sedimentological characteristics of the Adriatic basin and sediment dynamics

The coasts of the Adriatic Sea basin are mainly composed of sands, in particular for what concerns the Italian side (west side), while on the Balcanic one (east side) they appear to be mainly formed by rocks or gravel, with some exception of sands close to some river mouths (such as the Buna/Bojana river coastal area). Commonly the main sedimentological categories found along the western side of the basin and in general in its northernmost area go form mud (characterized by a diameter $\phi < 0.063$ mm) to sands ($0.063 < \phi < 2$ mm), spanning through all the diameters of the grains of the under-classes in which these two main categories can be subdivided, but with a prevalence of silt (0.031 mm $< \phi <$ 0.063 mm) very fine sands (0.062 mm $< \phi <$ 0.125 mm) and fine sands (0.125 mm $< \phi <$ 0.250 mm), as classified by Nota (1950).

The main input of these classes of sediments are the rivers of the Northern Adriatic (Isonzo, Tagliamento, Piave, Adige, and Po river), which guarantee a strong activity of sediment supply, even if the heavy human intervention on these rivers, and in particular on the Po river, with works of canalization and sand mining mainly, has definitely reduced the riverine sediment supply and the sediment deposition in the estuarine surrounding areas during the last decades. As an example the Po river, which is definitely the main supplier of sediment of the whole basin, with an estimated 70% of the total river input (Frascari et al. 1988) had been advancing its delta at a rate of approximately 47 m/yr between the end of the 19th century and the 1970s, when the delta formation process has experienced a fast slow down and appears now to be fairly stable (Correggiari et al. 2005, Nelson 1970). Besides the Po river the other big supplier of sediment to the Adriatic Sea is the Buna/Bojana river, in the south eastern part of the basin, even if detailed studies to quantify this sediment input have only recently been started (within the framework of the project Adricosm-Star)

1.4 Objectives and structure of the thesis

The interest in climate change has been growing in recent years, both from a practical and socio-economical point of view, and from a scientifical point of view. The approach to climate change studies through numerical models has started from the atmosphere, on a global scale, and was developed on this scale until the models were capable to reproduce the main climatic characteristics and dynamics of the recent observed climate at a certain degree of accuracy. Once this was achieved, thanks mainly to the higher computational resources available and to the effort science put into this issue, the space resolutions of the models have significantly increased, with a very positive impact on the results, which started to acquire an always increasing robustness and reliability. Moreover, the practical interests in climate change must have a local nature more than a global nature, since this is the scale that affects the lives of each one of us. For these reasons the next step into the study of climate, recently brought from a global approach to a local approach. This was possible in the atmosphere through numerical downscalings, which allow to capture and reproduce higher and higher spatial scales, together with the associated physical processes. The regionalization of the climate models in the ocean to investigate the local sea responses to climate change impacts is, on the contrary, something still very new, which we consider to be in the frame of pioneering activities in the field of oceanography.

To be really capable of simulating the environmental system that surrounds us in a very realistic way, a regional approach of the modelling is not enough, but it becomes necessary to integrate different numerical models in order to be able to reproduce always more and more processes, and to make the simulations as close to reality as possible. The present work wants to study and describe the effects of high frequency processes on the Adriatic Sea dynamics and on the coastal sediment transport of the basin, and to introduce a methodology of integration and regionalization of numerical models in the framework of climate change, in order to analyze its impact on the circulation, and, for the very first time, on the patterns of sediment transport in the coastal areas of the basin within future scenarios.

The thesis is organized as follows: chapter 2 presents a methodology to introduce the tidal processes in a baroclinic primitive equations Ocean General Circulation Model, and shows how well tides are consequently reproduced, analyzing also the impacts they have on the mean general circulation, on salt and heat transport and on mixing and stratification in the different seasons of the year. In chapter 3 a wave model and a sediment transport model are coupled with the OGCM presented in chapter 2, and the integrated resulting model is calibrated and validated, and used to evaluate the main characteristics of sediment transport in the coastal area of the Po river, and, for the first time, in the coastal area of the Buna/Bojana river, located in the south eastern part of the Adriatic Sea basin. In chapter 4 and 5 the simulation tool presented in the previous chapters is further coupled with models of atmosphere, hydrology, river flow, and waves under the climate change conditions of one of the scenarios of the *International Panel on Climate Change* (the so called *A1B* scenario), in order to evaluate the impact that climate change has on the main physical characteristics of the Adriatic Sea, such as circulation, temperature, salinity and sediment transport patterns of the coastal area of Albania and Montenegro in the period 2001-2030. Finally in chapter 6 we present the summary and some general conclusions of the work.

Chapter 2

2. MODELLING BAROCLINIC CIRCULATION WITH TIDAL COMPONENTS IN THE ADRIATIC SEA

2.1 **Introduction**

The very heterogeneous domain of the Adriatic Sea basin (fig 2.1) presented in section 1.1, together with the strong interannual and seasonal variability of the atmospheric forcings, and of the freshwater inputs, which are so important in a dilution basin such as the one here considered, reflect on the dynamics of the basin through some characteristics of its mean dynamics.

The circulation is generally cyclonic. The main surface circulation features are characterized by a southward current – WACC – (Western Adriatic Coastal Current) along the west coast, that has been divided in literature into three parts, Northern, Middle and Southern, according to their positions, whose variability is noticeable from season to season, and by a northward current flowing along the south eastern coast, the ESAC (Eastern Adriatic Coastal Current), detectable in all the seasons of the year but summer (Artegiani et al., 1997a). Beside these currents, three surface cyclonic gyres dominate respectively the north, middle, and south basin circulation, again showing an evident seasonal variability, but generally intensifying in autumn and, the southern and central gyres, in summer (Artegiani et al., 1997b). The WACC and the ESAC interconnect these three gyres, with a high intra-seasonal variability intensity. As anticipated above at the Strait of Otranto the Adriatic basin exchanges its waters with the rest of the Mediterranean Sea. Here we have an important inflow of relatively salty and hot waters coming from the Levantine Sea at intermediate depths, inflowing on the Balcanic side of the Strait (the Levantine Intermediate Waters - LIW), and constituting a heat and salt gain for the basin, acting in competition with the air-sea fluxes and the rivers respectively.

The tidal regime of the basin is not very strong, but together with the coast off shore Tunisia, the Adriatic Sea represents the only area within the Mediterranean Sea where tides have a range of up to one meter. This happens particularly in its northernmost region, the Gulf of Trieste, where the amplitudes of the most energetic tidal constituents - M2 and K1 - reach approximately 27 and 18 cm respectively.

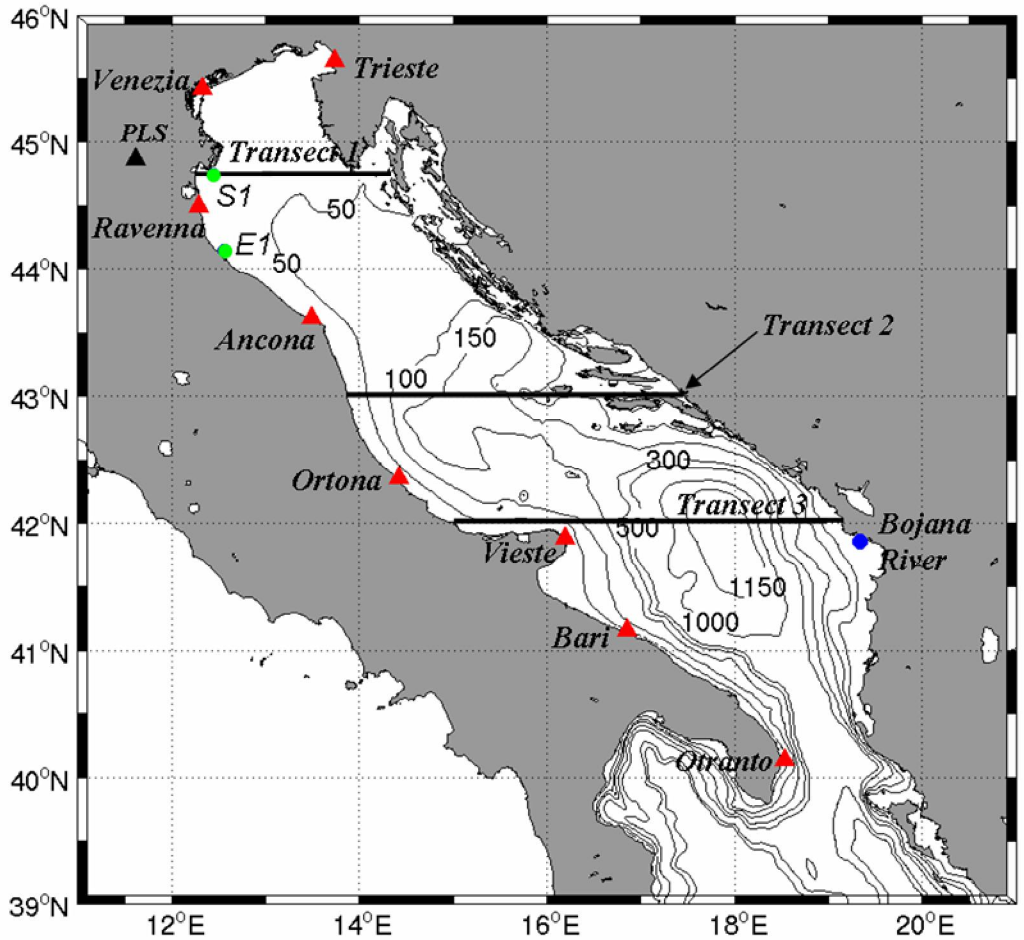

Figure 2.1: Domain of the Adriatic Sea model. The contour lines represent the bathymetry of the basin, the red triangles are the locations of the mareographic stations used for the model validation, while the blue dots are the locations of the E1 and S1 multi-parametric buoys

As it is well know from many studies on the Adriatic tides (Polli, 1960; Zore Armanda 1979; Mosetti, 1987; Malacic, 2000; Cushman and Naimie 2002), the diurnal frequencies present weak amplitudes in the south of the basin and are enhanced moving northward developing isopleth lines of amplitude perpendicular to the longitudinal axis of the basin. The semidiurnal frequencies as well show a strong enhancement in the northern basin, presenting similar patterns of coamplitude lines, with a substantial difference: the formation of an anphidromic node situated in the centre of the basin between the Italian city of Ancona and the Croatian city of Zadar. The little right panels of figure 2.2 show the well known cotidal and coamplitude lines, according to the modelling by Cushman-Roisin and Naimie (2002).

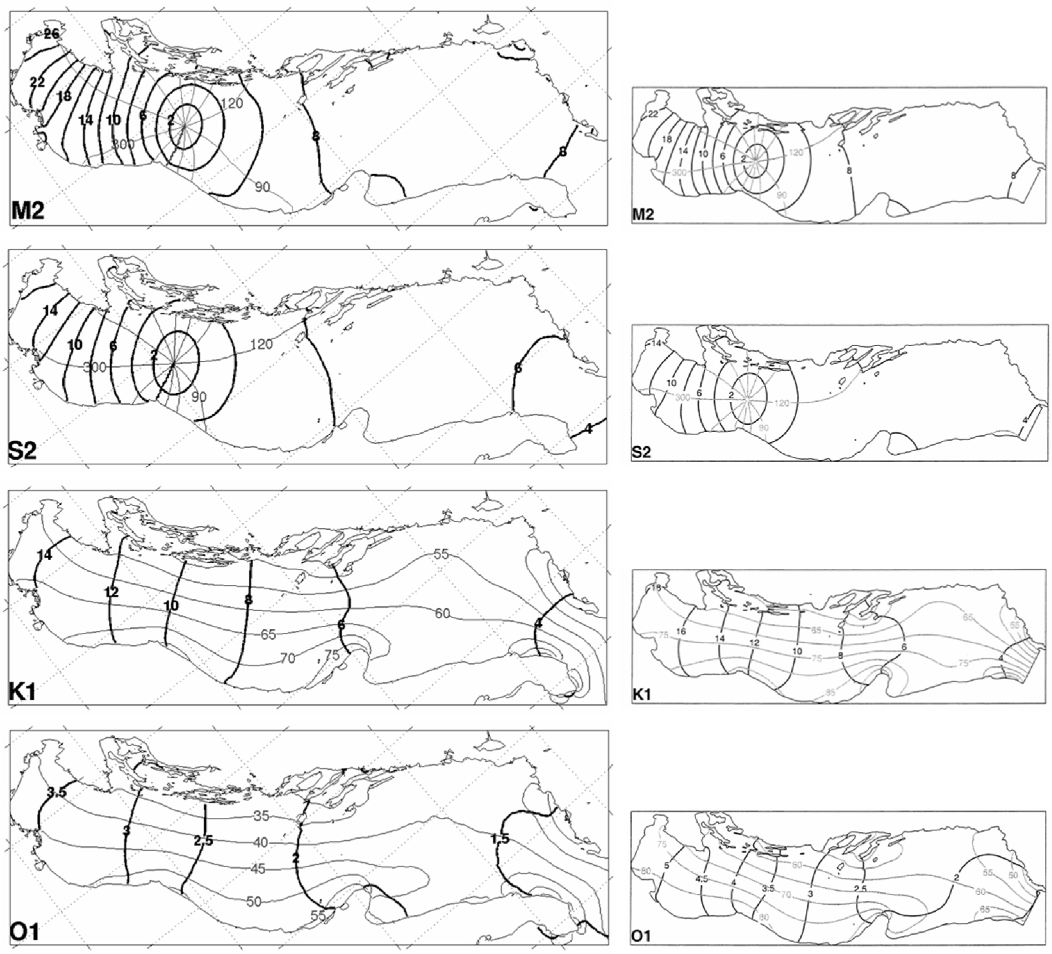

Figure 2.2: Amplitude and phase distribution of the M2, S2, K1 and O1 tidal constituents reproduced with the baroclinic model AREG2 (left bigger panels) and with the barotropic model by Cushman-Roisin and Naimie, 2002.

An important characteristics of the Adriatic tidal regime is that its major component is not a direct response to the astronomical influence of the Sun and the Moon, but it is mainly related to the astronomical tidal oscillations of the Ionian Sea, which induces forced oscillations of the Adriatic basin and phenomena of resonance, responsible for the amplification of the tidal wave amplitudes in the longitudinal direction, moving towards north. This suggests a behaviour of the Adriatic tides very similar to that of seiches.

According to Mosetti (1986) the diurnal and semidiurnal tides are produced by an incident and a reflected frictionless Kelvin wave, while Malacic et al. (2000) interpret the M2 constituent as a set of Kelvin waves propagating along the basin, and the K1 as a continental shelf wave propagating across the basin, and also show that the northern Adriatic basin behaves like a narrow rotating channel in which the instantaneous sea surface elevation (SSE) contours are aligned with the depth-averaged velocity vectors and in which the SSE is always higher to the right of the local current.

Tidal residual velocities have been recently computed by Cushman and Naimie (2002), to be a fraction of a centimetre per second (Cushman and Naimie 2002; Malacic et. al 2000), except for areas close to sharp coastlines, particularly near the Po area and within the Croatian islands, where their magnitude can reach up to 1-3 cm/s. Tidal currents were studied recently by Book et al. (2009) who shows how they tend to rotate almost completely in most of the areas of the Northern Adriatic, and how the sea elevations and phases increase northwestward and counter clockwise respectively, more evidently for semidiurnal than for diurnal tides. Evidence of diurnal thermocline oscillations driven by tidal flow in the central part of the basin have been proved by Mihanovic et al. (2009), in particular during the months of June, July and August, even if, at least in this area, the most energetic driver of the vertical isotherm oscillations turned out to be the diurnal wind variability, responsible of oscillations up to 18 meters, twice as much as those due to tidal activity.

Not much has been studied on the impact that tides have on the vertical mixing of the water column. Malacic et al. (2000) have studied the tidal mixing efficiency, arguing that in the northern region of the basin tides are too weak to mix it completely, supporting some of our findings of the present work.

In this thesis chapter we present (i) the methodology used to introduce tides in a new baroclinic circulation model of the Adriatic Sea - AREG2 - and quantify the importance of the tidal barotropic velocity in the formulation of the generalized Flather open boundary condition (Oddo and Pinardi 2008) (section 2), (ii) show how well tides are reproduced by a baroclinic model nested in a large scale general circulation model (section 3), and (iii) evaluate the impact of tides in the basin dynamics (section 4). In section 5 we propose some discussions and conclusions.

2.2 **The circulation model**

The circulation model used in this study – AREG2 (Adriatic REGional model) – is an implementation of the Princeton Ocean Model (POM, Blumberg and Mellor 1987) in the Adriatic Sea, already used in the past for modelling studies and operational forecasting at lower resolution (Zavatarelli et al. 2002, Zavatarelli and Pinardi 2003, Oddo et al. 2005, Oddo et al. 2006).

The model domain covers the entire Adriatic Sea (see figure 2.1) and presents a lateral open boundary line at 39° N, where it is nested into the operational Mediterranean Forecasting System (MFS) model (Pinardi et al. 2003, Tonani et al. 2008). The model horizontal resolution is approximately 1/45° and is implemented on 31 vertical sigma layers. The governing equations of the model are the equations of momentum and mass conservation (2.1 and 2.2 respectively), of advection-diffusion of salinity S and potential temperature θ (2.3 and 2.4 respectively), and the hydrostatic equation (2.5):

$$\frac{\partial(u,v)}{\partial t} + U \cdot \nabla(u,v) + f(-v,u) = -\frac{1}{\rho_0}\left(\frac{\partial p}{\partial x}, \frac{\partial p}{\partial y}\right) + \nabla_h \cdot \left(A_M \nabla(u,v)\right) + \frac{\partial}{\partial z}\left(K_M \frac{\partial(u,v)}{\partial z}\right) \tag{2.1}$$

$$\nabla \cdot U = 0 \tag{2.2}$$

$$\frac{\partial \theta}{\partial t} + U \cdot \nabla \theta = \frac{\alpha T}{\rho c_p}\frac{\partial p}{\partial t} + \nabla_h \cdot \left(A_M \nabla_h \theta\right) + \frac{\partial}{\partial z}\left(K_v \frac{\partial \theta}{\partial z}\right) \tag{2.3}$$

$$\frac{\partial S}{\partial t} + U \cdot \nabla S = \nabla_h \cdot \left(A_M \nabla_h S\right) + \frac{\partial}{\partial z}\left(K_v \frac{\partial S}{\partial z}\right) \tag{2.4}$$

$$\frac{\partial p}{\partial z} = \rho(S, \theta, p) g \tag{2.5}$$

where $U(u,v,w)$ is the field of velocity in a Cartesian coordinate system (x,y,z); p, g, ρ_0 are respectively pressure, gravity and a reference density value, f is the Coriolis parameter, A_M is the eddy viscosity coefficient, while K_M and K_v are the vertical mixing coefficients for momentum and tracers respectively. Finally c_p and α are the specific heat and the thermal expansion coefficient for water.

The vertical mixing coefficients K_M and K_v are calculated with a second-order turbulence closure submodel (Mellor and Yamada, 1982), while the eddy viscosity is parameterized following the scheme of Smagorinsky (1993). The advection part of the hydrodynamics equations are solved through a Monotonic Up-Stream Scheme for Conservation Law (MUSCL, Estubier and Lévy, 2000).

2.2.1 Vertical boundary conditions

The air-sea interaction is calculated through bulk formulae by means of the atmospheric forcings and of the sea surface temperature (SST) predicted by the model, and results in the following surface boundary conditions for heat (2.6) and momentum (2.7):

$$\rho_0 K_v \frac{\partial \theta}{\partial z} = \frac{1}{c_p}\left((1-Tr)Q_s - Q_B - Q_c - Q_h\right) \tag{2.6}$$

$$\rho_0 K_M \frac{\partial (u,v)}{\partial z} = (\tau x, \tau y) \tag{2.7}$$

where Tr is the coefficient of penetration of light into the water according to Jerlov (1976), Q_s is the short wave radiation incident to the sea surface, and is calculated through an astronomical formula according to Reed (1975, 1977), Q_B is the long wave radiation emitted back by the sea and is computed through the formula proposed by May (1986), while Q_c and Q_h are the latent and sensible heat fluxes respectively; τ_x and τ_y are the zonal and meridional components of the wind stress produced on the sea surface, computed according Hellerman and Rosenstein (1983).

The atmospheric forcings used are the reanalyses of the European Centre of Medium-Range Weather Forecast (ECMWF) at a horizontal resolution of 0.5 degrees, available every 6 hours.

For what concerns the surface boundary condition for the vertical velocities, realistic freshwater balance is used according to 2.8:

$$w\big|_{z=\eta} = \left(\frac{\partial \eta}{\partial t} + (u,v)\cdot\nabla\eta\right)\bigg|_{z=\eta} + (E - P - R) \tag{2.8}$$

where η is the sea surface elevation, E, P and R are evaporation, precipitation and river runoff respectively.

The precipitation used is the climatological dataset from Legates and Willmott (1990), while the fresh water runoff, except for the Po and the Buna/Bojana river, is taken from the climatology of Raicich (1994). The Po river flow values used are daily means observed at the cross section of Pontelagoscuro, a few tens of kilometres upstream the river's delta (see the black triangle fig 2.1 labelled *PLS*) provided by ARPA SIM Emilia Romagna, while the Buna/Bojana river climatological flow values of Raicich's have been substituted with those ones of UNEP 1996, recently investigated also by Marini et al. (2010).

At the bottom the vertical boundary condition for the continuity equation (2.2) results in:

$$w|_{z=-H} = -\left(u\frac{\partial H}{\partial x} + v\frac{\partial H}{\partial y} \right)_{z=-H} \tag{2.9}$$

where H is the still water depth, while the boundary condition for the hydrostatic approximation (eq. 2.5) is:

$$\rho_0 K_M \left(\frac{\partial(u,v)}{\partial z} \right)_{z=-H} = \left(\tau_{bx}, \tau_{by} \right) \tag{2.10}$$

where τ_{bx} and τ_{by} are the zonal and meridional components of the bottom stress $\vec{\tau}_b$, which is parameterized as:

$$\vec{\tau}_b = C_d \rho \left| \vec{U} \right| \vec{\boldsymbol{U}} \tag{2.11}$$

C_d is the bottom drag coefficient which follows the parameterization of equation 2.12:

$$C_d = \max\left\{ 0.0025; \left[\frac{\kappa}{\ln\left(\frac{\delta_b}{z_0} \right)} \right]^2 \right\} \tag{2.12}$$

Where κ is the Von Karman constant (equal to 0.40), z_0 is the bottom roughness length scale, and δ_b the thickness of the last model level above the bottom.

2.2.2 Lateral boundary conditions for nesting with tides

The approach used to account for lateral forcing of tides in the Adriatic Sea is similar to that used by Changshui et al. (2006) and by Xingang Lü et al. (2010) in the Yellow Sea, and derives from the formulation by Flather (1976) on the barotropic velocities at the open boundary line, generalized by Oddo and Pinardi (2008) as shown in equation (2.13):

$$V = V^{nesting} - \frac{\sqrt{gH}}{H}(\eta - \eta^{nesting}) \tag{2.13}$$

where V and η are the barotropic velocity normal to the boundary and the surface elevation (the absence of superscript means they refer to the nested model), $V^{nesting} = V^{MFS} + V^{tide}$, and $\eta^{nesting} = \eta^{MFS} + \eta^{tide}$, being the superscripts *MFS* and *tide* referred respectively to the Mediterranean Forecasting System model data and to the tidal data at the open boundary line, thus implying a linear combination of the two nesting components, one coming from the coarser circulation model and one from a specific barotropic tidal model. H is the topography and g is the gravitational acceleration. To be noted is that in all the areas of the model where the bathymetry is in the range from 0 to 10 meters, topography has been set to 10 meters.

The derivation of condition (2.13) starts from equating the continuity equation for the nesting and the nested models, under the hypothesis of mass conservation for both of them. These considerations bring to equation (2.13) only under the further assumptions that (i) the normal component of the phase speed is the linearized gravity wave speed ($C^n = \sqrt{gH}$), (ii) that the topographies at the boundary line are the same for the nesting and the nested models, and that (iii) they are much bigger than the surface elevation η.

The tidal fields at the open boundary were obtained implementing along the boundary line, on the same coordinates of the grid points of the circulation model, the OTPS (*OSU Tidal Prediction Software* of the Oregon University: http://volkov.oce.orst.edu/tides/otps.html) based on the Mediterranean regional solution obtained with the tidal inverse model OTIS (Egbert and Erofeeva, 2002) provided on a regular lon/lat grid at the horizontal resolution of 1/12° of degree. The constituents used to evaluate the tidal elevation and velocity where the 8 most important ones: M2, S2, N2, K2, K1, O1, P1, Q1.

As anticipated, a very similar approach had already been successfully used by Changshui et al. (2006) and by Xingang Lü et al. (2010) in the Yellow Sea, with the only difference that they omitted the tidal barotropic velocity (V^{tide}) in their formulation, while we included it, and we will show that - at least for the Adriatic Sea basin - it is rather important in the correct evaluation of the tidal harmonic constants around the basin, in spite of its little magnitude at the open boundary line.

2.3 **Simulation experiments**

2.3.1 Barotropic experiments

Under this configurationsimulations of the model have been performed in barotropic mode, setting temperature and salinity constant respectively to the value of 15°C and 38 PSU, and letting the model be forced only by tidal velocity and elevation at the open boundary line. This procedure has been applied to the M2 and K1 constituents, being respectively the two semidiurnal and diurnal most energetic constituents responsible for tidal oscillations in the Adriatic Sea basin. Following an underestimation of the resulting tidal amplitudes (not shown), mainly in the northern Adriatic region, some calibration has been done both on tidal elevation at the open boundary, and on the bottom roughness scale used in the parameterization of the bottom drag coefficient (eq. 2.12).

The final bottom roughness scale used is z_0=0.001m, while the tidal elevation at the boundary line was increased by 10%. Some investigations have also been carried out with the depth dependent bottom drag coefficient from the Chezy formula, letting vary the Strickler coefficient, but the results had not been as satisfactory.

2.3.2 Baroclinic experiments

The model described above has been used to carry out 9 year long baroclinic integrations, (see table 2.1), from January 2000 to December 2008.

In experiment INT1 the model was initialized from a previous integration of the same circulation model without tides (Guarnieri et al. 2010), and the formulation of the lateral boundary condition is the one of equation 2.13. To estimate the importance of the tidal barotropic velocity in the formulation of the lateral boundary condition the experiment INT2 was then carried out, where the tidal barotropic velocity term V^{tide} has been removed. Lastly, in order to investigate the impact of tides on the dynamics of the basin another experiment INT3 was carried out, removing completely the tidal forcings.

Experiment Name	Tides	Lateral Boundary Condition
INT1	Yes	$V=(V^{MFS}+V^{tide})-\frac{\sqrt{gH}}{H}(\eta-\eta^{MFS}-\eta^{tide})$
INT2	Yes	$V=V^{MFS}-\frac{\sqrt{gH}}{H}(\eta-\eta^{MFS}-\eta^{tide})$
INT3	No	$V=V^{MFS}-\frac{\sqrt{gH}}{H}(\eta-\eta^{MFS})$

Table 2.1: Naming conventions for simulation experiments carried out: the simulations differ for the inclusion of tides and the type of lateral boundary condition.

2.4 Results

2.4.1 Evaluation of the tidal harmonic constants

The tidal phases and amplitudes resulting from INT1 have been estimated through a harmonic analysis on the sea surface elevation using the methodology of Pawlowicz (2002) at each grid point of the model for the year 2003. The results of this analysis for the most important semidiurnal and diurnal constituents (M2, S2, K1, O1) are presented in the left panels of figure 2.2, where the cotidal lines are represented with the thinner curves and the co-amplitude lines are represented with the thicker lines. The right panels of the figure are the results from a barotropic model by Cushman-Roisin and Naimie (2002), considered here our reference model.

The figure shows that AREG2 is capable to reproduce most of the features of the diurnal and semidiurnal tidal constituents, both in terms of amplitudes and phases.

The semidiurnal tidal constituents M2 and S2 resulting from the simulation from AREG2 are overestimated in terms of amplitude compared to the results of Cushman's and Naimie's, which however underestimate the observed values of amplitude for the M2 constituent. On the other hand the diurnal components K1 and O1 resulting from AREG2 in the northernmost side of the basin are underestimated by approximately 2.5 cm and 1.5 cm respectively.

The same type of analysis was carried out comparing the model harmonic constants with the Italian mareographic stations. The locations of the stations are presented in figure 2.1 (red triangles). The comparison between the model and the observations is presented in table 2.2 for the period January 2000 - December 2008. The upper panel refers to the tidal amplitude, the lower one to the tide phase lag with respect to the local time (UTC+1). For each constituent the corresponding left column of the table shows the results of observations, the central column shows the results of simulations of AREG2 and the right one shows the absolute value of the percentage error, calculated, for amplitude and phase respectively, as it follows:

$$E_{\%}^{amp} = \left| \frac{A^0 - A^m}{A^0} \right| \times 100 \qquad (2.14)$$

$$E_{\%}^{pha} = \left| \frac{P^0 - P^m}{180} \right| \times 100 \qquad (2.15)$$

where *A* and *P* are the tidal amplitude and phase and the superscripts *o* and *m* refer to observations and model respectively. This means that the error in phase is 100% when the modelled phase has opposite direction with respect to the observations.

The main errors concern the simulation of the diurnal constituents, both in amplitude and in phase, and in particular of the O1 constituent. As recalled by

Cushman and Naimie (2002) the estimate of the phase of this constituent has always been problematic, and literature shows very different values at all stations; for example in Trieste its estimated phase ranges from 39° (Tsimplis et al., 1995) to 62° (Polli, 1960). Our model yields 39°, in accordance with Tsimplis et al., but the phase that we estimate from observations is 58°, evidencing a high discrepancy of approximately 11% (calculated according to eq. 2.15).

For what concerns the amplitudes, the most problematic constituent is again O1 in terms of percentage: the error versus the observations reaches 25%. The best result in amplitude is achieved for the reproduction of the most energetic frequency M2, with an average error around the basin of only 3%.

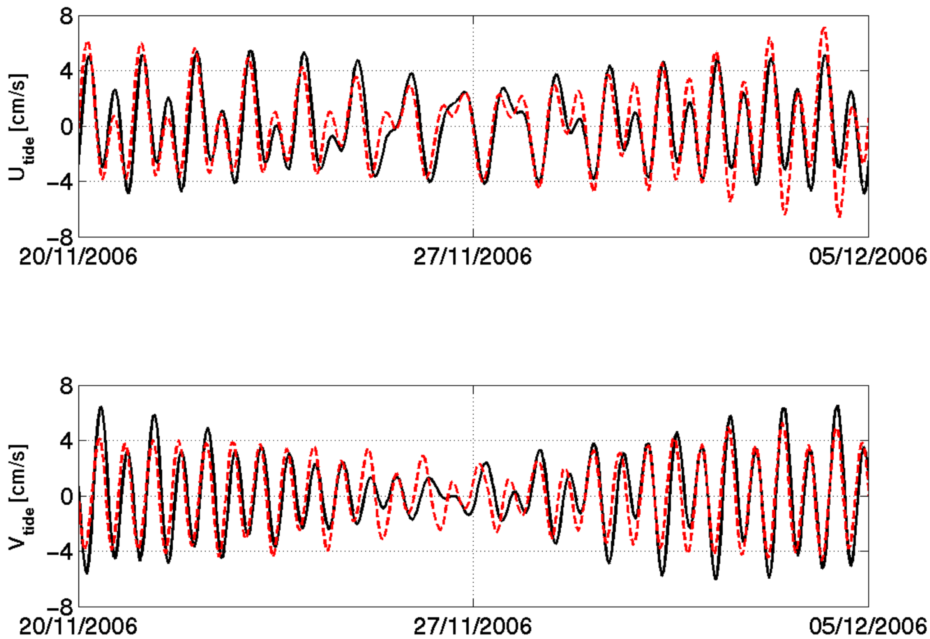

Figure 2.3: Validation of the bottom tidal currents at the Bouy E1. In the top panel the zonal component of velocity is presented, while the bottom panel shows the meridional component. The black solid line represents the observed data, and the dashed red line the model.

Station	AMPLITUDES (meters)																					
	M2			N2			S2			K2			O1			P1			K1			AVERAGE DIFFERENCE %
	Amp obs	Amp mod	Diff %	Amp obs	Amp mod	Diff %	Amp obs	Amp mod	Diff %	Amp obs	Amp mod	Diff %	Amp obs	Amp mod	Diff %	Amp obs	Amp mod	Diff %	Amp obs	Amp mod	Diff %	
Ancona	0,067	0,067	0	0,012	0,012	3	0,036	0,040	10	0,011	0,012	8	0,042	0,030	28	0,045	0,037	19	0,135	0,111	18	**12**
Bari	0,097	0,098	1	0,015	0,016	7	0,060	0,065	9	0,017	0,019	13	0,019	0,016	16	0,018	0,016	12	0,052	0,049	5	**9**
Ortona	0,069	0,065	6	0,012	0,010	11	0,048	0,050	3	0,015	0,015	2	0,030	0,022	26	0,031	0,026	17	0,092	0,078	15	**11**
Otranto	0,070	0,075	8	0,012	0,013	10	0,041	0,046	13	0,011	0,013	19	0,009	0,011	17	0,010	0,010	3	0,024	0,030	24	**13**
Ravenna	0,169	0,169	1	0,029	0,029	1	0,100	0,110	10	0,030	0,032	7	0,051	0,034	33	0,055	0,044	20	0,166	0,135	19	**13**
Trieste	0,267	0,263	1	0,045	0,052	17	0,160	0,177	10	0,048	0,052	8	0,053	0,037	31	0,063	0,048	23	0,182	0,149	18	**15**
Venezia	0,241	0,238	1	0,041	0,040	2	0,143	0,158	10	0,044	0,046	6	0,054	0,036	33	0,060	0,047	21	0,181	0,145	20	**13**
Vieste	0,095	0,097	2	0,016	0,016	0	0,061	0,066	9	0,017	0,020	13	0,018	0,015	19	0,020	0,016	20	0,053	0,048	11	**10**
AVERAGE DIFFERENCE %			**2**			**6**			**9**			**10**			**25**			**17**			**16**	**12**

Station	PHASES (degrees)																					
	M2			N2			S2			K2			O1			P1			K1			AVERAGE DIFFERENCE %
	Phase obs	Phase mod	Diff %	Phase obs	Phase mod	Diff%	Phase obs	Phase mod	Diff %	Phase obs	Phase mod	Diff %	Phase obs	Phase mod	Diff %	Phase obs	Phase mod	Diff %	Phase obs	Phase mod	Diff %	
Ancona	330	321	5	332	321	6	344	340	2	341	338	2	71	54	10	80	71	5	87	74	7	**5**
Bari	112	100	7	110	102	5	120	111	5	115	108	4	56	42	8	63	60	2	72	61	6	**5**
Ortona	93	86	4	90	85	3	101	101	0	95	97	1	68	52	9	78	69	5	83	72	6	**4**
Otranto	105	102	2	102	103	0	112	114	1	109	111	1	62	46	9	71	59	7	75	63	7	**4**
Ravenna	302	295	4	302	296	3	310	307	2	306	304	1	67	47	11	78	65	7	83	69	8	**5**
Trieste	278	273	3	278	275	2	287	284	2	283	281	1	58	39	11	65	56	5	71	59	7	**4**
Venezia	287	283	3	287	284	1	295	295	0	291	292	0	61	42	10	70	61	5	77	64	7	**4**
Vieste	102	97	3	102	98	2	111	110	1	105	106	0	77	57	11	84	75	5	91	78	7	**4**
AVERAGE DIFFERENCE %			**4**			**3**			**2**			**1**			**10**			**5**			**7**	**4**

Table 2.2: Upper panel: tide amplitude; lower panel: tide phase lag with respect to the local time (UTC+1). For each constituent the corresponding left column of the table shows the results of observations, the central column the results of simulations of AREG2, while the right column shows the absolute value of the percentage error

The validation of the tidal components of the system was also assessed for tidal currents at the location of the buoy E1 (Russo et al. 2009) (figure 2.1). The available data were only close to the bottom, at the depth of 8.5 meters. Table 2.3 shows the comparison between observed and modelled data in terms of major and minor tidal ellipse axes, and orientation. The analysis has been done on a short dataset, of just 2 months – November and December 2006, so the harmonic analysis showed good performance only on the three most energetic constituents M2, S2, and K1, and this is why they are the only ones presented. The reproduction of the model of the major ellipses is accurate, but generally underestimated, while the minor axes are overestimated for the semidiurnal components, and overestimated for the diurnal K1 frequency. In fig. 2.3 the validation of tides is shown in terms of zonal and meridional components of the current, respectively for the model (red dashed line) and for the observed data (black solid line). The fit of the curves is generally good, but sometimes they have a phase lag of 1 hour.

E1 STATION (Lon=12°34.219' Lat=44°08.599')						
CONSTITUENT	Major Axis (cm/s)		Minor Axis (cm/s)		Orientation (°)	
	OBS	MOD	OBS	MOD	OBS	MOD
M2	4.0	3.7	0.5	1.0	-49	-46
S2	2.5	2.3	0.1	0.4	-58	-50
K1	2.0	1.8	0.6	0.3	-10	-1

Table 2.3: Observed and modelled tidal ellipses at the buoy E1 for the depth 0f 8.5 m.

The comparison of the modelled baroclinic sea level with observed sea level at tide gauges is something that, to our knowledge, is usually never shown in the Adriatic Sea. In fact both the tidal and storm surge models are usually barotropic, thus they do not account for the variation of the sea level due to baroclinic processes. In particular, the component of the variation of the sea level due to the buoyancy forces, very important for the Adriatic sea basin, especially for the whole system of circulation influenced by the Po river, is not accounted for in barotropic models.

Figure 2.4 shows the comparison between the modelled sea surface height (SSH) in the baroclinic integration INT1 (red dashed lines) and the observed one (black solid line) at the mareographic stations previously mentioned (see tab. 2.2 and fig. 2.1).

The analysis has been done for the period January 2000 to December 2008 on a 1-hour-frequency time series. The first two panels of figure 2.4 represent the comparison for the mareograph in Trieste for a two week period of the month of April 2008, and the last two represent the comparison in Ravenna, for the same periods. In order to make sure of the consistency of the observed and modelled time series, and thus to make them comparable, the mean value of each dataset has been subtracted to the respective instantaneous values of SSH. The observed and modelled mean SSH values for Trieste are 7 cm and -9 cm respectively, for Ravenna they are 4 cm and -5 cm. Table 2.4 shows the root mean square error of the model SSH with respect to the observations for the analyzed stations.

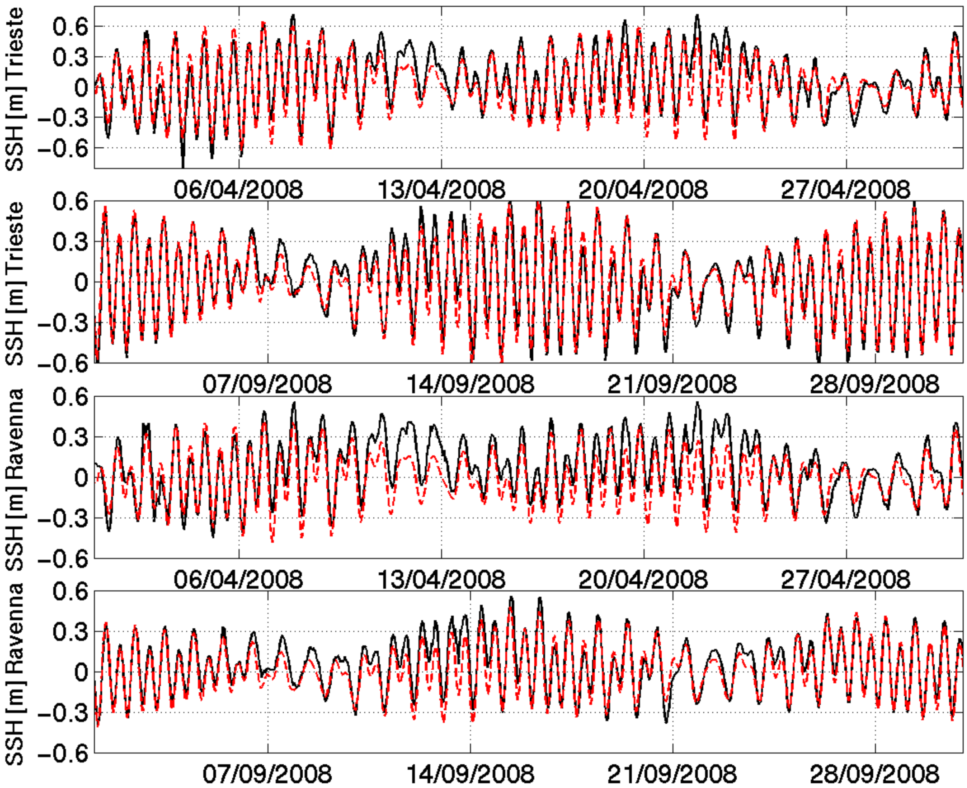

Figure 2.4: Comparison between modelled SSH of INT1 (dashed red line) and observed SSH (solid black line) at the Italian mareographic stations of Trieste (first and second panels) and Ravenna (third and fourth panels). The two datasets are on an hourly basis.

The error, calculated on the period 2000-2008 on 1 hour frequency data, ranges between 6 and 9 cm, and has a mean value around the basin of approximately 7 cm. It is defined as:

$$rmse_x = \frac{1}{N}\sqrt{\sum_{i=1}^{N}\left(x_i^o - x_i^m\right)^2} \tag{2.16}$$

where the superscripts *o* and *m* refer respectively to the observed and the modelled data. The error in the SSH representation can be addressed partly to the fact that not all the astronomical frequencies were used as input in the estimate of the tidal elevation and velocity at the open boundary (all the frequencies lower than the diurnal are missing), partly to errors in the model, probably mostly related to the model coastlines and bathymetry, extremely important in the vicinity of the coasts, where the tide gauges are installed, and most of all to errors in the atmospheric forcings and in the absence of atmospheric pressure in the model. The accuracy of the SSH simulation undergoes a degeneration counter clockwise, following the rotation of the tide. This is probably related to the fact that the total error in the estimate of the barotropic tide, treated as a surface gravity wave, increases inevitably with the increase of the space travelled because of an accumulation of errors.

However, the general good agreement in phase between the model and the observations is a hint that through the baroclinic combination of all the 8 considered tidal constituents the advective component of the tidal signal is well represented by the model.

ELEVATION MEAN ERRORS (cm)			
STATION	**RMSE**	**STATION**	**RMSE**
Ancona	8	*Ravenna*	8
Bari	6	*Trieste*	9
Ortona	7	*Venezia*	9
Otranto	6	*Vieste*	6
MEAN RMSE= 7 cm			

Table 2.4: Mean errors on the sea surface elevation for the simulation INT1.

2.4.2 Influence of the tidal velocity term in the open boundary condition

Experiment INT2 (tab. 2.1) allowed to estimate the importance of the tidal barotropic velocity in the formulation of the modified Flather boundary condition of equation (2.13). This integration was carried out from the beginning of December 2002 to the end of December 2003, and the first month of simulation was not used for the tidal analysis performed. The only difference between INT1 and INT2 is that in the open boundary condition (eq. 2.13) the barotropic velocity due to tides has been removed.

The results of the harmonic analysis on the sea surface height simulated by the model in terms of amplitudes and phases at the same mareographic stations and on the same period of time have been compared with those ones of the analysis of integration INT1. The comparison of the two datasets is shown in figure 2.5 for the two most energetic diurnal and semidiurnal constituents: M2, S2, O1, K1. The red triangles refer to integration INT2, while the black squares to integration INT1. The figure shows how the semidiurnal frequencies are well represented by the model of INT1, both in terms of amplitude and phase, and how important the barotropic velocity term is in the prescription of the tidal signal at the open boundary line. The reproduction of the diurnal frequencies (O1 and K1) is not as accurate as for the semidiurnal ones, but again we see how much the barotropic velocity term is important to better fit the tidal amplitude. The only exception where the absence of V^{tide} in equation (2.13) produces better results is for the phases of the O1 constituent, which, however, is responsible for very little values of amplitude, thus not very influent in the reproduction of the full sea surface elevation. In general the barotropic velocity term has a relevant influence in the prescription of tides in the Adriatic Sea, and in the diurnal constituents it can be responsible of up to 50% of the single amplitude signal simulated (is the case of K1 frequency) , while the influence in the phase lag appears to be much more confined (not higher than 8%, S2 and K1 constituent).

The analysis of the most realistic integration (INT1 – black squares of figure 2.5) shows also how the model tends to slightly overestimate the amplitudes of the semidiurnal frequencies and to more evidently underestimate those ones related to the diurnal ones. These discrepancies are much more marked in the diurnal constituent, which, however, is responsible for more confined tidal oscillations. On the other hand the modelled phases (INT1 – black squares of figure 2.5) are always underestimated, and the percentage error with respect to the observations increases significantly in the diurnal frequencies.

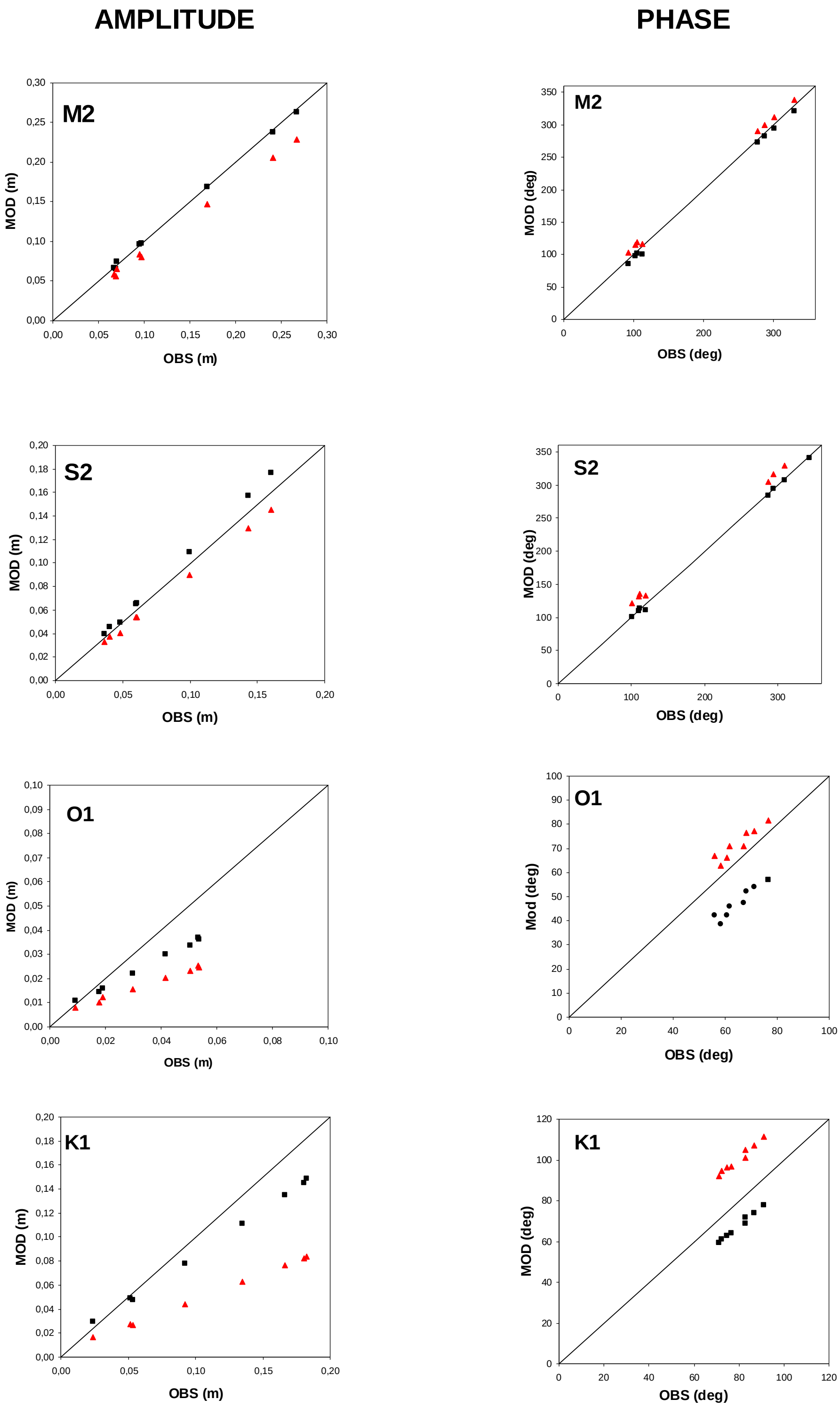

Figure 2.5: Validation of the amplitude and phases of the M2, S2, O1 and K1 tidal constituents for the integrations INT1 (black squares) and INT2 (red triangles). The harmonic analysis has been assessed on a 1 year long period. The observed data are on the x axis and the modelled ones on the y axis.

2.4.3 Validation of the model temperature, salinity, density, and SST

The daily mean simulated density, temperature and salinity of integration INT1 have been compared to approximately 2400 available profiles of CTDs sampled during the period 2001-2008. The locations of the stations are presented with the black stars in the map at the bottom of figure 2.6, while the skills of the model are shown in the profiles of the same figure. From top to bottom the mean profiles (averaged in time and space), biases (model-observations) and root mean square errors (calculated again according to equation (2.16)) are presented for density, salinity and temperature (left to right respectively). For all the three variables considered the shape of the simulated profiles are very similar to those observed, even if important biases and root mean square errors, are evidenced. In particular the model tends to be colder than the observations in the first 20 meters while model salinity is lower at depth and higher at the surface. The salinity bias at depth is the largest problem for the model that probably does not receive enough salty waters from the nesting Mediterranean model and does not have the overall correct effect of the rivers at the surface.

In general the simulated mixed layer depth is too diffuse in vertical and this may be due to the Mellor-Yamada (1982) vertical mixing scheme, that tends to over mix.

Also sea surface temperature (SST) has been investigated for the period 2003-2008, when satellite SST date were available. The basin mean SST bias is 0.8 °C averaged over the 6 years considered, and the root mean square error for the same period is approximately 1.3 °C, as figure 2.7 shows in the middle (bias: observations-model) and bottom (rmse) panels. In the top panel of the same figure the time series of the mean values of SST for the same period is shown (black stars are the observations and red ones are the model), evidencing how the seasonal cycle is well represented by the model, even if it has the tendency to be colder than the observations, especially during the hottest periods of the year when we may occasionally have errors of up to 4 or 5 degrees. To be noted is that the model grid points where the first sigma layer is deeper than 1.5 meters have not been used for the SST inter-comparison, and a threshold of at least 1000 grid points in the satellite observations has been used, under which the data were not considered for the inter-comparison.

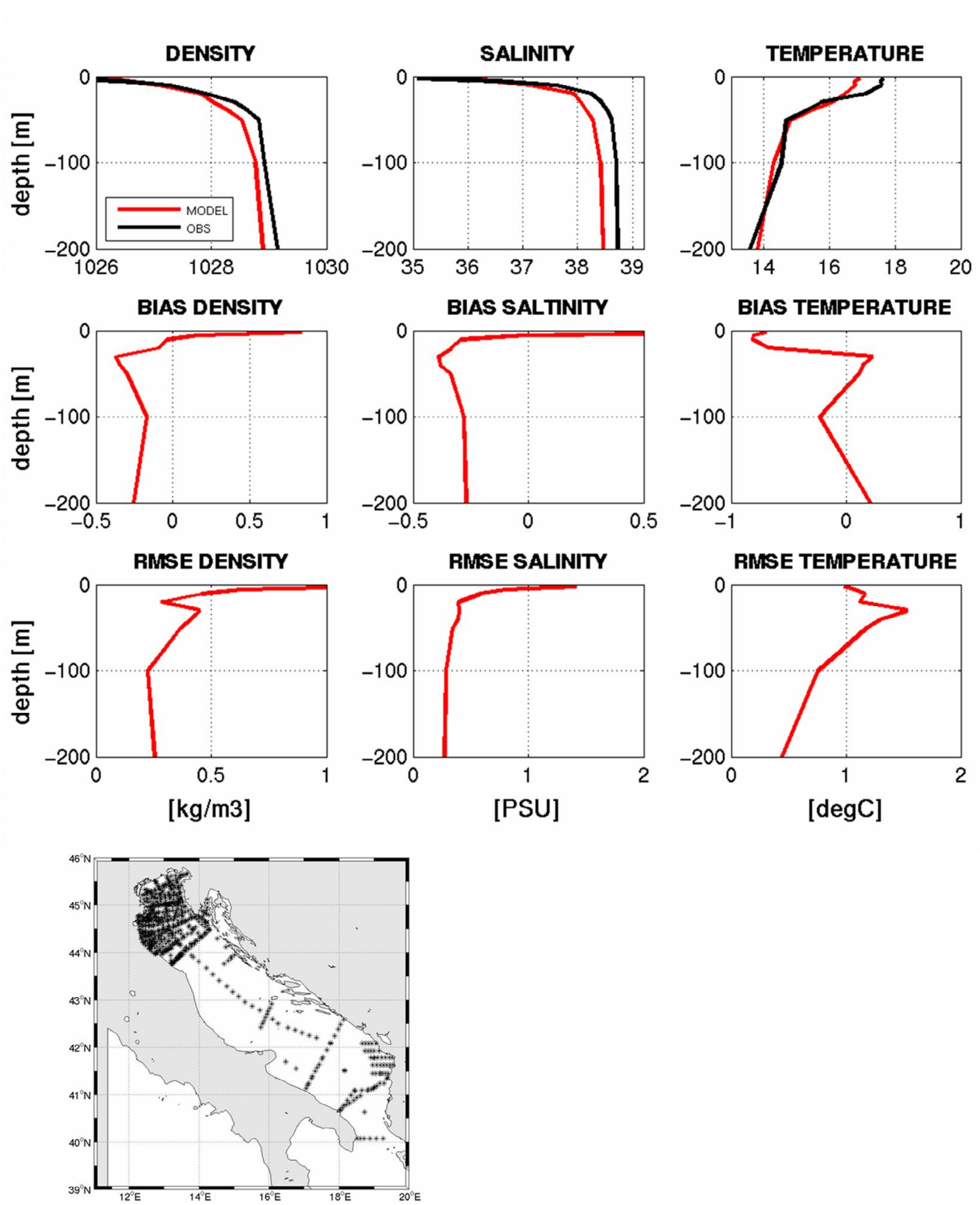

Figure 2.6: Observations-model comparison for density, salinity and temperature. The data refer to the mean spatial and time profiles sampled at the stations shown with black stars in the map in the bottom. The simulated data refer to daily means.

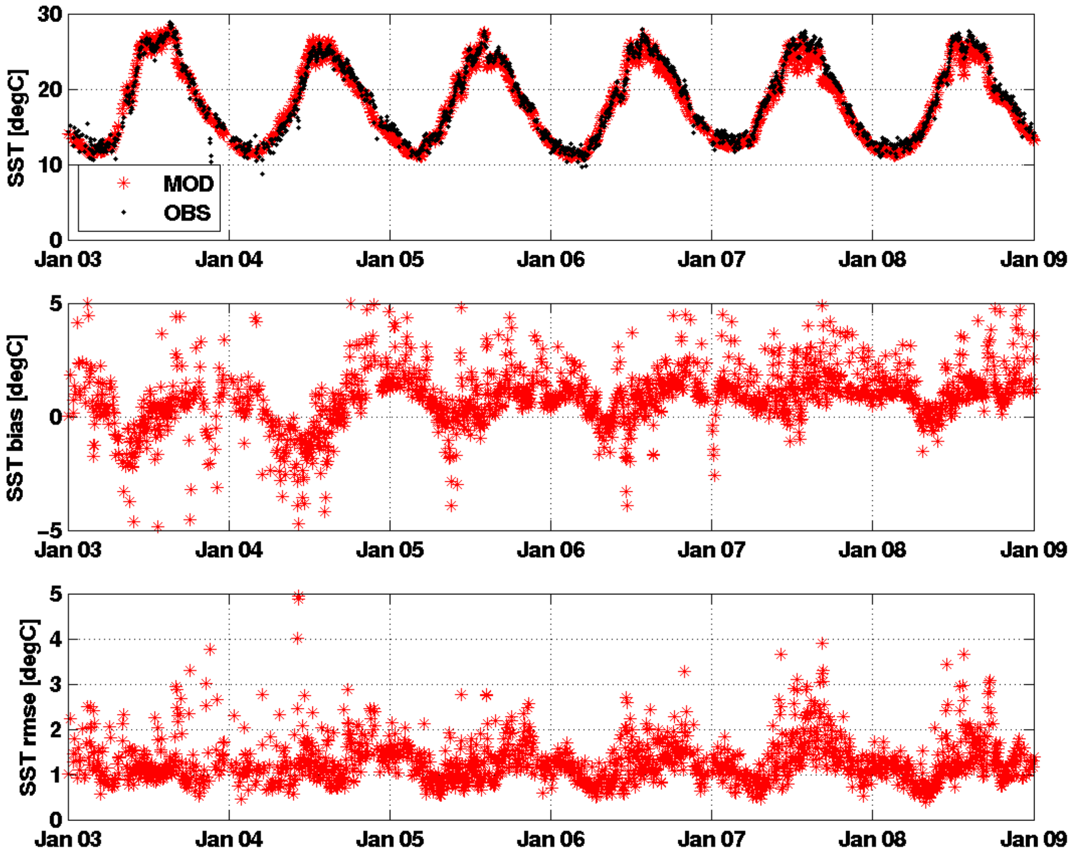

Figure 2.7: Validation of SST for the period 2003-2008: mean bias=0.8°C, RMSE=1.3°C. In the first panel the mean daily basin observed (black) SST is compared to the modelled (red) SST. The mid and bottom panels show bias and root mean square error respectively.

2.5 Impact of tides on the state variables and dynamics

In order to evaluate the impact of tides on the general circulation a third integration (INT3 – see table 2.1) was carried out, removing completely the tidal forcing. The integration INT3 was initialized with a snapshot of INT1 in January 2005 and run up to December 2006.

2.5.1 Tidal effects on temperature and salinity

Figure 2.8 shows the anomalies of temperature and salinity at the multi-parametric Buoys S1 and E1 (Bortoluzzi et al. 2006) (green dots of fig. 2.1) , for the periods from July 1st to October 1st 2006 for S1, and between the 1st of November and the 30th of December 2006 for E1. The data sampled by the buoys are approximately at the depth of 1.2 meters at S1 and of 1.6 meters at E1, with a frequency of 1 hour. Anomalies are referred to the months here analyzed. The buoy S1 is located just a few kilometres south of the Po river delta, clearly in a Region Of Freshwater Influence (ROFI, Sanchez-Arcilla and Simpson, 2002), with a bathymetry of approximately 20.5 meters (fig. 2.1). In this area a small anticyclonic gyre is often detected, which moves its centre causing the buoy to be caught or not within it, according to the variability of the local circulation. This, together with the very high variability in temperature and mostly in salinity directly related to the Po river fresh water input makes it a very difficult site to be represented by our numerical model, mostly because the rivers are introduced as vertical boundary conditions in terms of water fluxes at the surface, and not as lateral boundary conditions, which would most likely improve the performance in the representation of salinity, especially in ROFI regions. The E1 buoy as well is located at only a few miles from coast, in a region still strongly influenced by the Po river. For both of the sites, but mainly for S1, density is clearly driven by salinity. Both the models, with and without tides, are capable to represent the higher (only up to diurnal) and lower frequency cycles of surface temperature, even if the observed variability at the higher frequencies (diurnal and semidiurnal) is much stronger than the simulated one.

In general the model tends to be colder than the observations as shown before, and the mean correction in temperature due to the tidal processes is not very significant, smaller than 0.1°C (not shown).

Generally both models present much higher surface salinity than the observations, with an average bias on the considered periods of approximately 1.2 PSU at S1 (not shown) and of 0.3 PSU at E1 (not shown), and a root mean square error around 1.6 PSU and an 0.9 respectively (not shown).

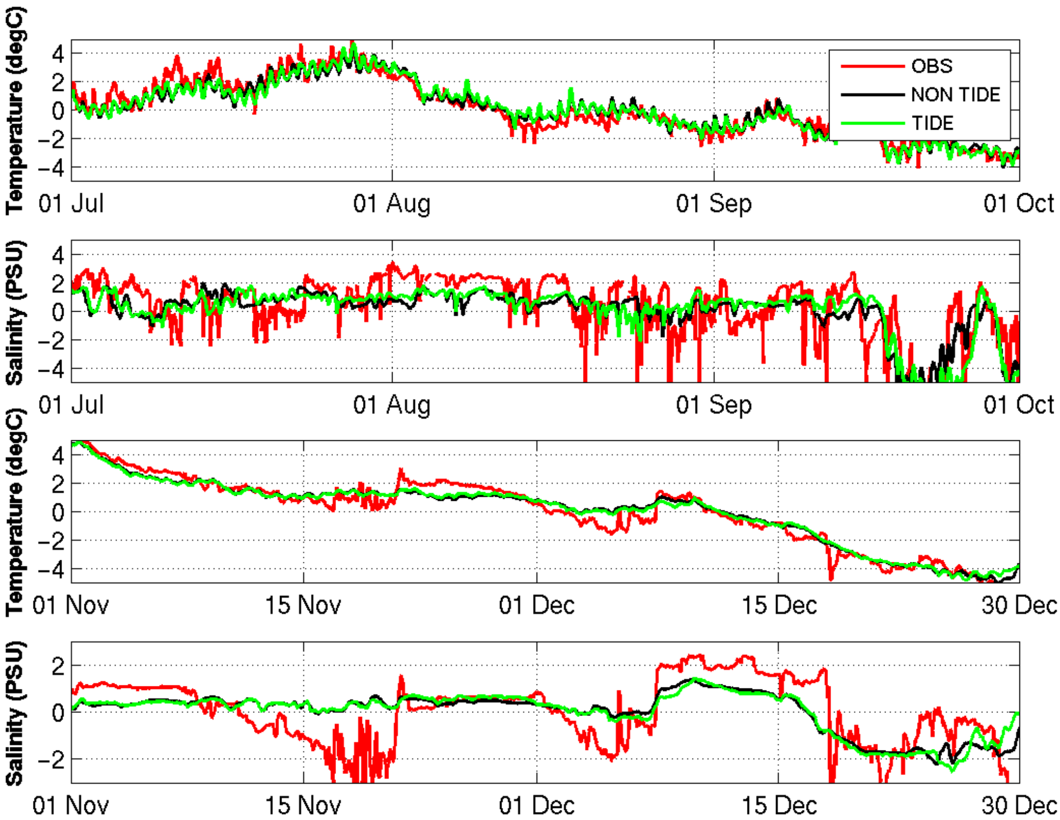

Figure 2.8: Temperature (°C, first and third panel) and salinity (PSU, second and fourth panel) anomalies at buoy S1 and E1 respectively. Data are taken at the surface (approximately 1.2 m) from July 1st to October 1st 2006 at S1, and from November 1st to December 31st at E1. The red, green and black line refer to observations, INT1, and INT3 results respectively.

Again, the parameterization of the rivers as vertical boundary condition causes wrong estimates of salinity, and is more evident at S1, much closer to the river mouth than E1. Moreover the model is probably too diffusive, causing a general tendency to be too salty, especially in correspondence of the negative peaks of observed anomalies, when the river activity is more important, as it happens in the second part of August 2006, when the river flow doubles, and mainly in the second part of September, when a high flood event occurred with discharge rates up to 4000 m^3/s, bringing down the salinity at S1 to a minimum of approximately 15 PSU, while the models are not able to reproduce values lower than approximately 29 PSU.

The mean improvements due to the introduction of tides do not seem to be very large when we look at time mean bias of density, salinity and temperature. However, the model with tides is capable to represent higher frequency variability, as shown in figure 2.9, where a zoom of the near bottom instantaneous transport of temperature and salinity at the buoy E1 is shown. Transports were calculated on hourly data as:

$Q_x = u_{bot} \cdot \mathrm{var}$ for the cross shore component and $Q_y = v_{bot} \cdot \mathrm{var}$ where u_{bot} and v_{bot} are the near bottom zonal and meridional components of velocity (m/s) respectively, and *var* is either temperature (°C) or salinity (PSU).

The time windows here presented are of 48 hours, and it is quite evident how the high frequency oscillations of transport are very well captured by INT1. As a confirmation of the impact that tidal frequencies have in transports there comes the spectral analysis undertaken on transports along and across shore, presented in figure 2.10. All the power spectra are referred to the near bottom transport at buoy E1, and the upper panels present salinity transport, while the lower ones temperature transports. The model with tides (green line) is capable to reproduce frequencies in very good agreement with the observations (red line).

It is remarkable that semidiurnal tidal frequencies have the strongest impact in the along shore transport, while the energy corresponding to the diurnal frequency is very low. Things change considering the transport across shore. Here the diurnal frequencies take over, and the associated energy has the same order of magnitude of the one associated to semidiurnal frequencies.

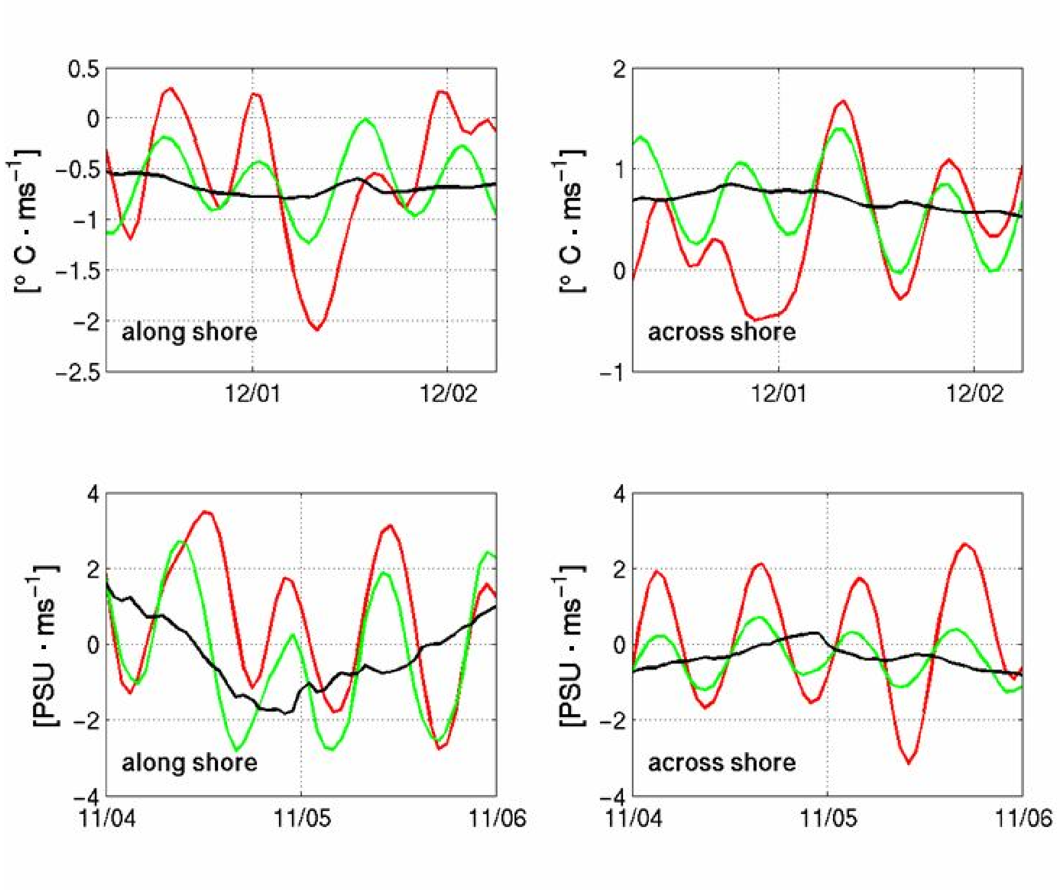

Figure 2.9: Modelled and observed bottom transport of temperature (top panels) and salinity (bottom panels) at buoy E1. Left and right panels refer respectively to along shore transport (positive is toward north) and to across shore transport (positive is toward open ocean). The red, green and black line refer respectively to estimates from observations, INT1, and INT3 results.

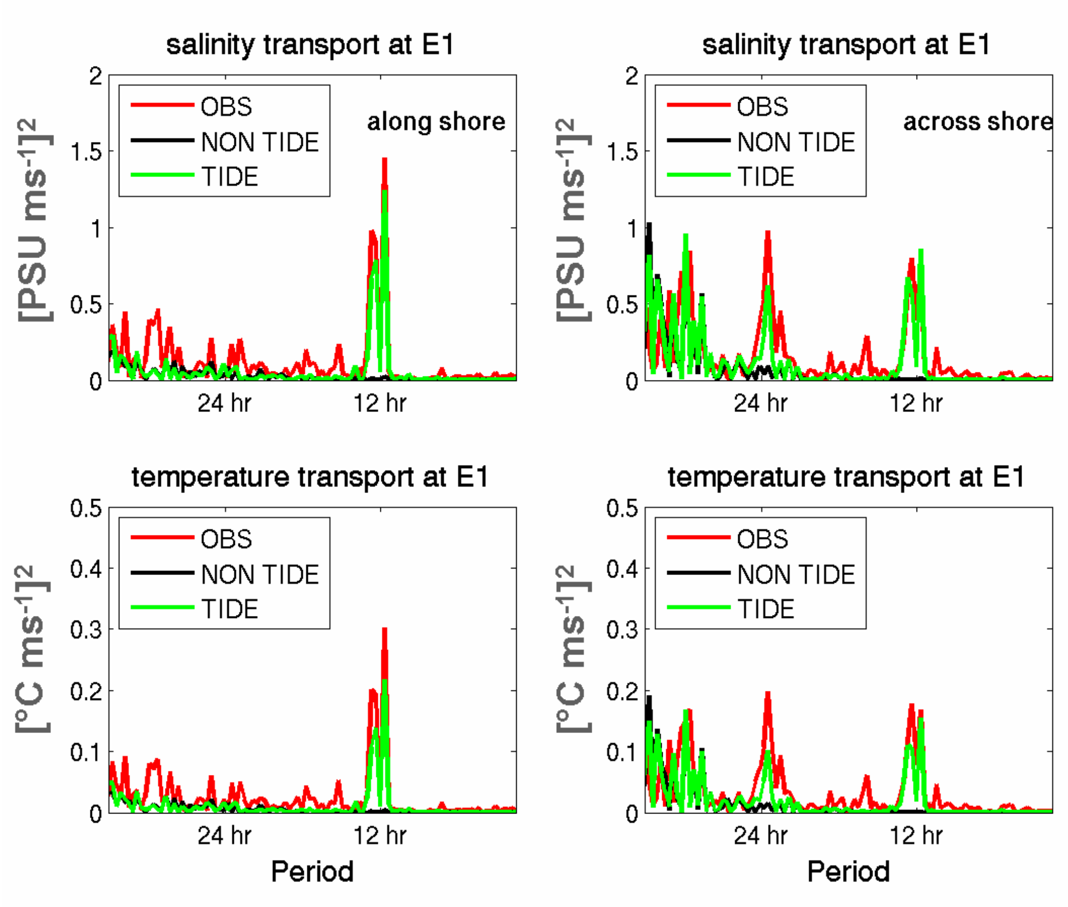

Figure 2.10: Power spectrum of along/across shore (left and right respectively) bottom transport of salinity and temperature (top and bottom panels respectively) at buoy E1.

2.5.2 Effects of tides on mixing and mean circulation

In ROFI regions such - as the one here analyzed - the stratification tends to be maintained by the continuous input of fresh water from the rivers, and is in competition with the stirring activity due to the atmospheric forcings at the surface and to frictions at the bottom (Simpson et al., 1990). In presence of tides the vertical shear acts on the horizontal density gradients, with the lighter surface waters moving faster seaward above the heavier, more saline waters in the lower layers and thus generating a stable structure (Simpson et al., 1990). During ebb tides the tidal activity produces a higher stratification, while during floods the tidal stirring will oppose to stratification to destroy the vertical structure towards a well mixed water column. Souza et al. (2008) indicate that the tidal induced stratification can have ranges of up to 4 PSU in ROFI regions where the circulation is strongly tidally driven, such as the Rhine region (North Sea).

In figure 2.11 an analysis of the difference between INT1 and INT3 results (tide-no tide) at the buoy S1 location is presented for the whole months of February 2006 (2.11*a*) and August 2006 (2.11*b*). The fields are hourly averaged. The green and black lines of panels *1a* and *1b* are the mixed layer depth of INT1 and INT3 respectively, while their difference is represented by the red line. The mixed layer depth has been calculated as the depth where the density difference with the density at the surface exceeds 0.01 kg/m^3. The blue line of panels *1a* and *1b* represents the wind stress (Pa) at the air-sea interface. The panels from 2 to 6 represent respectively the fields of difference between INT1 and INT3 for temperature (°C), salinity (PSU), density (kg/m^3), cross-shore current shear (s^{-1}), and vertical mixing coefficient for tracers (m^2/s) as defined in equations 2.3 and 2.4. The cross-shore current shear is $\frac{\partial u}{\partial z}$, where *z* the vertical direction and *u* the zonal velocity of the current. The black line of panels 2 to 6 represents the difference of SSH between the results of INT1 and INT3.

In summer time, when the water column is stratified, the diurnal cycle plays the main role in the oscillation of the mixed layer depth (MLD). This is hinted by the daily periodicity of the MLD very evident in panel *1b*. However tides surely induce a different stratification along the water column, as suggested by Simpson (1990) which is generally stronger, especially in periods of low atmospheric forcings. This is enlighten by the red line of panel *1b*, which is generally positive, except for the event of 5 to 8 of August. Evident is also the semidiurnal oscillation of salinity related to tides, which is present in both seasons but in winter it appears to be even more evident and enhanced after episodes of strong wind. A very clear example of this is the period from the 24th to the 28th of February 2006 (fig. 2.11-*3a* and 2.11-*4a*), which highlights a periodic semidiurnal vertical oscillation of salinity and density along the water column following ebb and flood tides

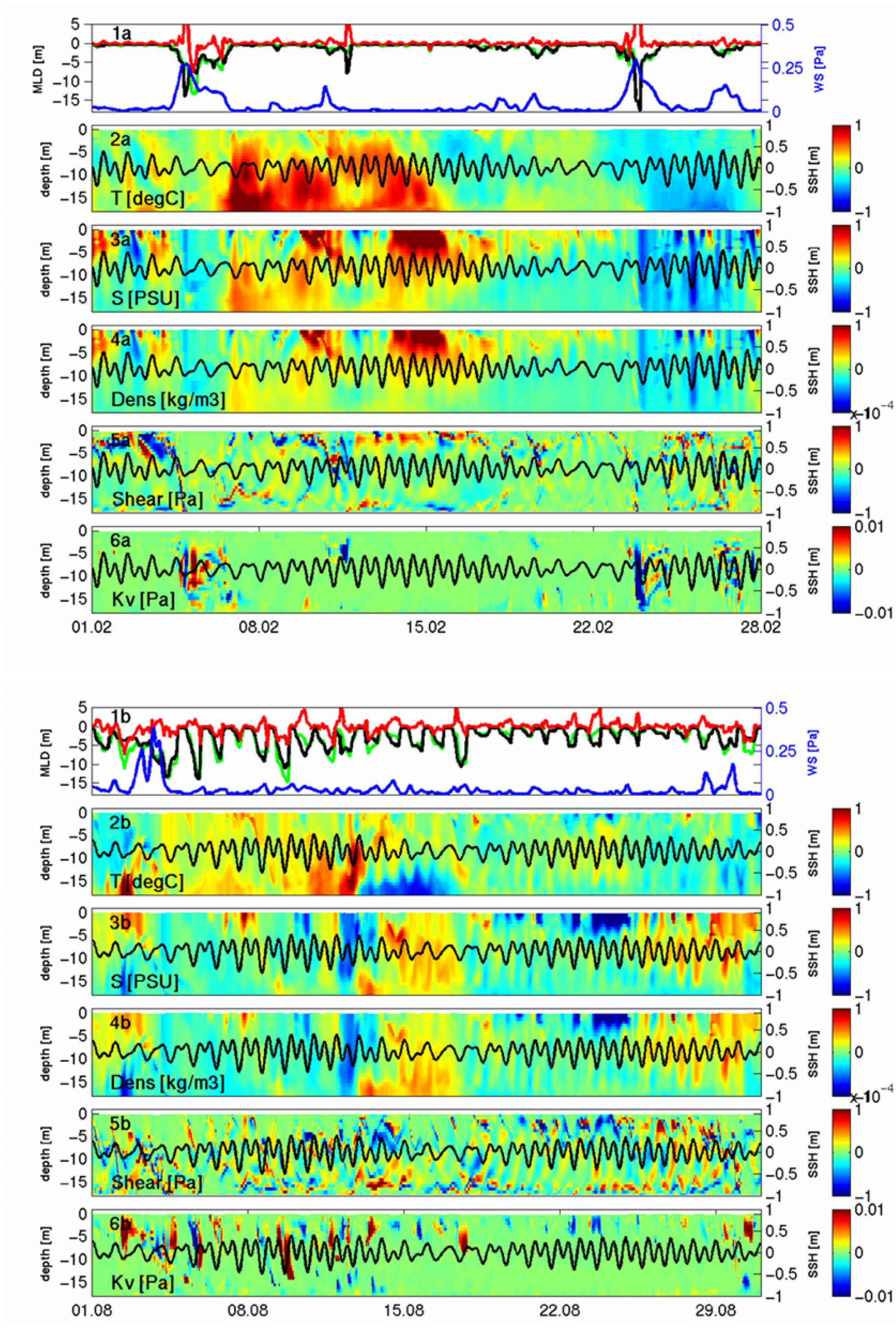

Figure 2.11: Analysis at buoy S1 location (lon=12.4575° E, lat=44.7424° N) of the difference between INT1 and INT3 results (Tide-NoTide), for the whole months of February (top) and August 2006 (bottom). In particular: 1. tidal (green line) and non tidal (black line) mixed layer depth (meters), and their difference (meters, red line); 2., 3., 4., 5. and 6. are the fields of difference of temperature (°C), salinity (PSU), density (Kg/m3), zonal velocity shear (Pascal) and vertical eddy diffusivity (m2/s) between INT1 and INT3 results, for the same location and time as the left panel.

(the black solid line represents the SSH in meters, and its amplitude is labelled in the right y-axis), according to the mechanism of stratification explained by Simpson et al. (1990) and recalled in the beginning of this section, with a half cycle of semidiurnal tide of stratification at ebbs, followed by a half cycle of semidiurnal tide at floods. Again the mechanism is visible in summer time from the 20th of August 2006 to the end of the month (fig. 2.11-*3b* and 2.11-*4b*). Differently to what happens for salinity, a semidiurnal tidal signal in the oscillation of temperature is visible only in summer time. In the Adriatic Sea, then, we do not have strong enough tides to cause a full stratification driven by tidal flow, which, in the analyzed Po ROFI region is mainly induced by the river fresh waters, but semidiurnal signals of salinity and density can be observed both in winter and in summer, while temperature oscillations are appreciable only in summer.

In some periods when differences in the vertical mixing (panels *6a* and *6b*) are not very marked, like the central part of February, the model highlights anyway very strong differences in temperature, salinity and density. The most evident example is the second week of February. This suggests a strong impact tides have on the advective component of motion, which is usually never underlined.

In figures 2.12 and 2.13, winter and summer sections across the basin in the northern, central and south regions (see fig. 2.1, transects 1, 2 and 3) are analyzed. The fields presented are differences between INT1 and INT3 of vertical mixing coefficient (m^2/s), temperature (°C), salinity (PSU) and meridional velocity from INT1 and INT3 (i.e. results of the simulation without tides are subtracted to those ones from the simulation with tides), averaged over the months of February 2006 (fig. 2.12) and August 2006 (fig 2.13). During winter the vertical mixing difference (panels *a, b, c*) appears to be quite variable both in time and space: in transect 1 the biggest differences are of order 10^{-3}, while in the deeper transects they reach the order 10^{-1}, and they are localized in the mid depths. On the other hand in summer (figure 2.13) the differences in vertical mixing are comparable among the three transects, of the order of 10^{-3}, just like transect 1 in winter time. This suggests again a stronger interaction in winter time between the vertical mixing and tides. In summer the dominant factor is the difference in advection of different water masses in the basin than in diffusion.

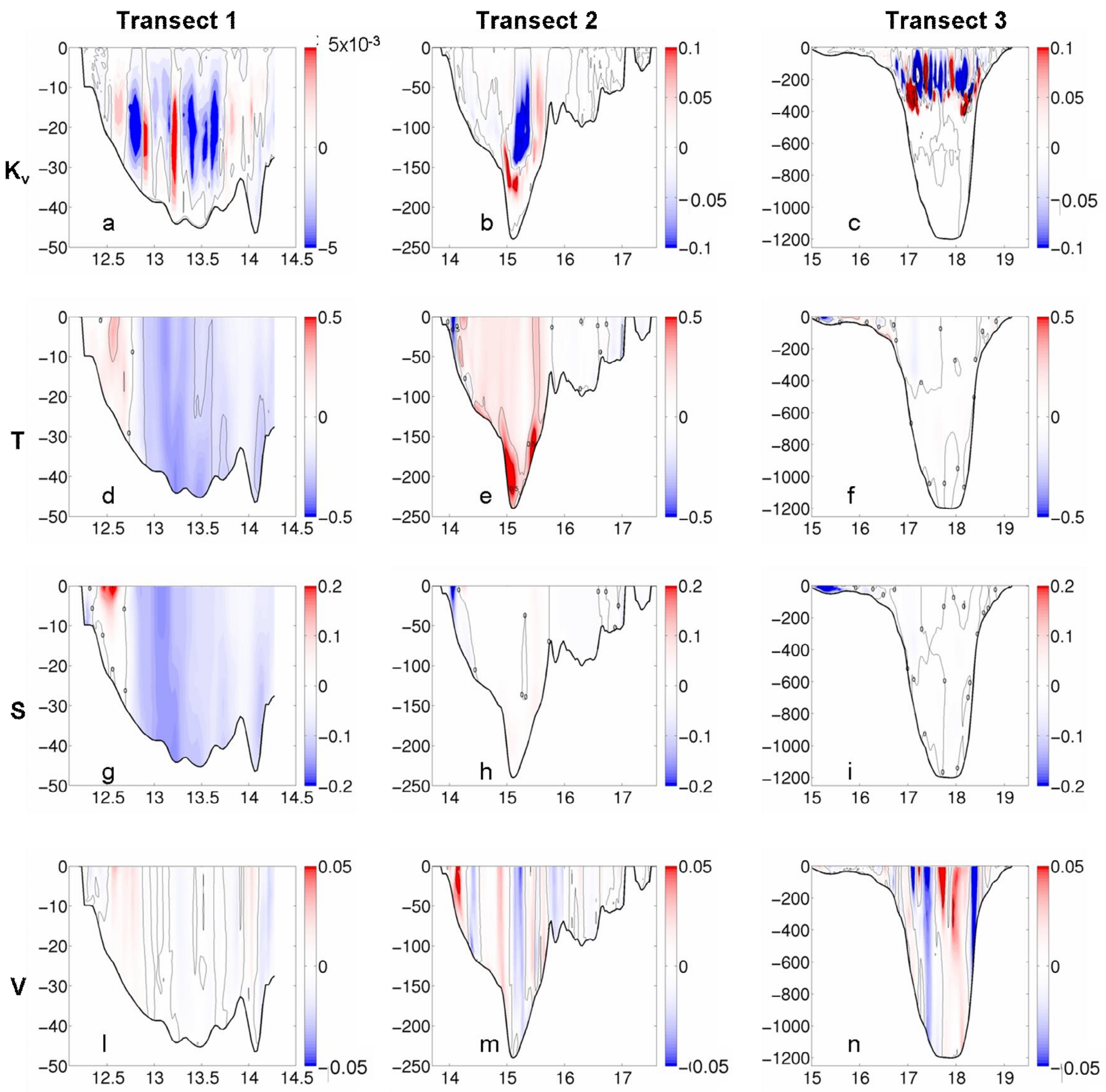

Figure 2.12: Transects 1, 2 and 3 (see fig. 2.1). The panels show the difference fields between INT1 and INT3 results for February 2006, and in particular they represent, from top to bottom: vertical mixing coefficient (eddy diffusivity, m^2/s), temperature (°C), salinity (PSU), and meridional velocity differences. The data have been averaged over the entire month.

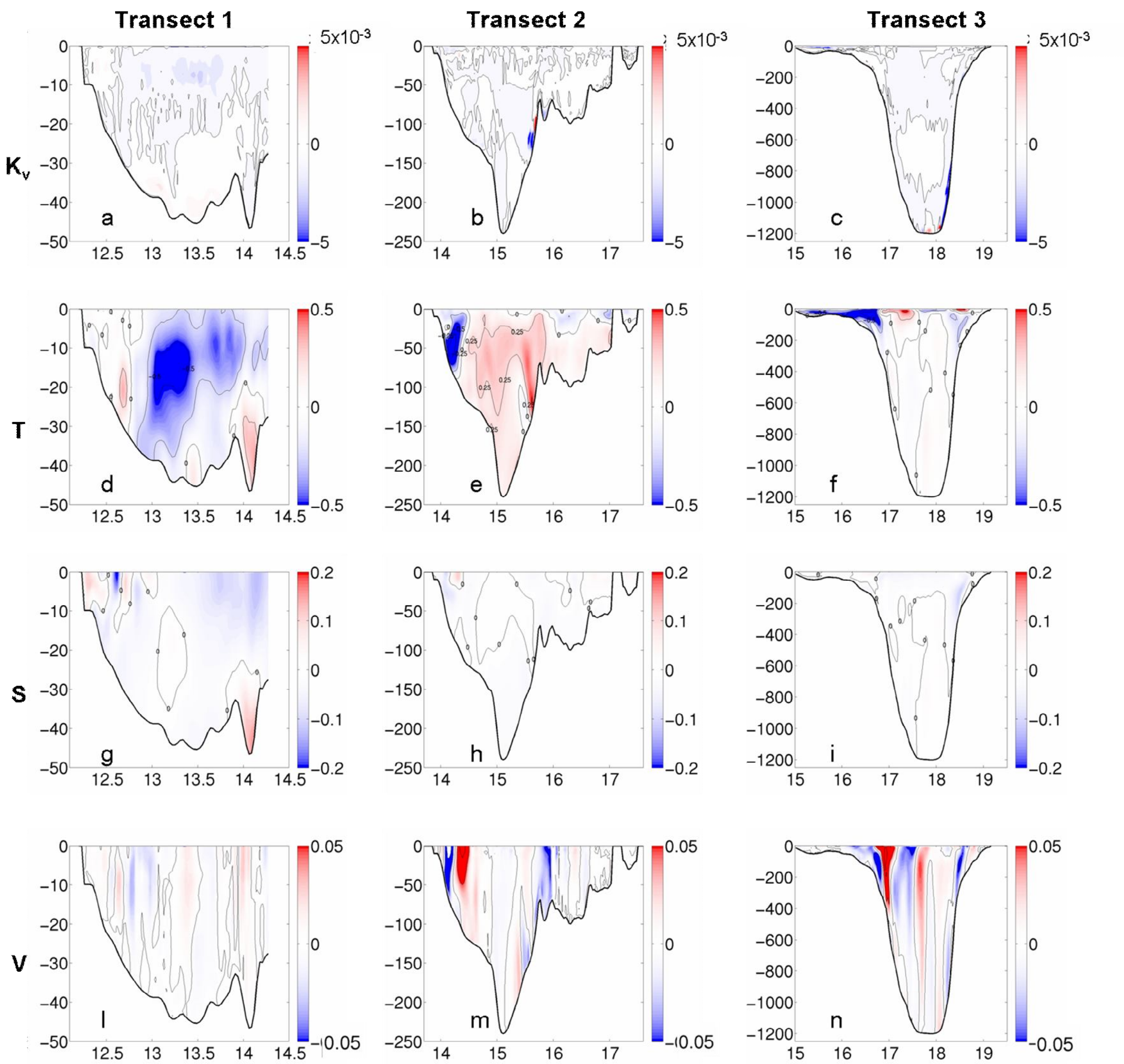

Figure 2.13: Same as fig. 2.12, but for the month of August 2006.

This is also supported by figure 2.14, which shows the mean circulation at 20 metres (upper panels) and at 100 metres (lower panels) simulated with INT1 (left panels) and INT3 (right panels). The red arrows and corresponding numbers in the figure highlight the areas with the most different patterns of circulation between the models with and without tides. Since the only difference between the two integrations is the tidal forcing, we can assume that the resulting mean circulation differences are related only to tides. It is remarkable how the WACC changes in the area of the Ancona Promontory, a zone of very high variability. In the model without tides (right top panel) the WACC (marked *1* in the figure) is located further off coast in this particular area, and a small anticyclone (*a*) is formed between the current and the coast. In the model with tides (left top panel), on the other hand, the WAAC (*1*) is much more constrained to the Promontory, and anticyclone (*a*) cannot form. This might be an effect of the anphidromic node. Another remarkable difference between the two integrations is the region of the southern Adriatic Pit, where a climatological cyclone is observed (Artegiani et al. 1997a and b). The results of INT1 for August 2006 show in this area two gyres (*3* and *4* upper left panel), both anticyclonic (even if climatologically the model reproduces one larger cyclone here, in accordance with literature), while INT3 shows two gyres of different sign (*3* and *4* right upper panel). Moreover the pattern of current *5* (in both upper panels) meanders in between the two gyres in the case of INT3, while it is shifted eastward in the case of INT1, embracing the two gyres *3* and *4*. The variability of the 20 meter deep currents along the Puglia Region also changes significantly. In fact eddy *2* of INT1 is much more confined to coast than it is in INT3, and an additional eddy (*6*) forms a little more south, still along coast.

The effect of tides show differences in advection also at depth, as presented in the lower panels of figure 2.14, where two small cyclones (*3* and *4* in the left panel) form in the model with tides INT1, while they are absent in the model without tides. On the contrary gyres *1* and *2* are still present in both models, maintaining the same signs they have at 20 meters, even if anticyclone *1* of INT3 changes its shape significantly, becoming more elongated southward.

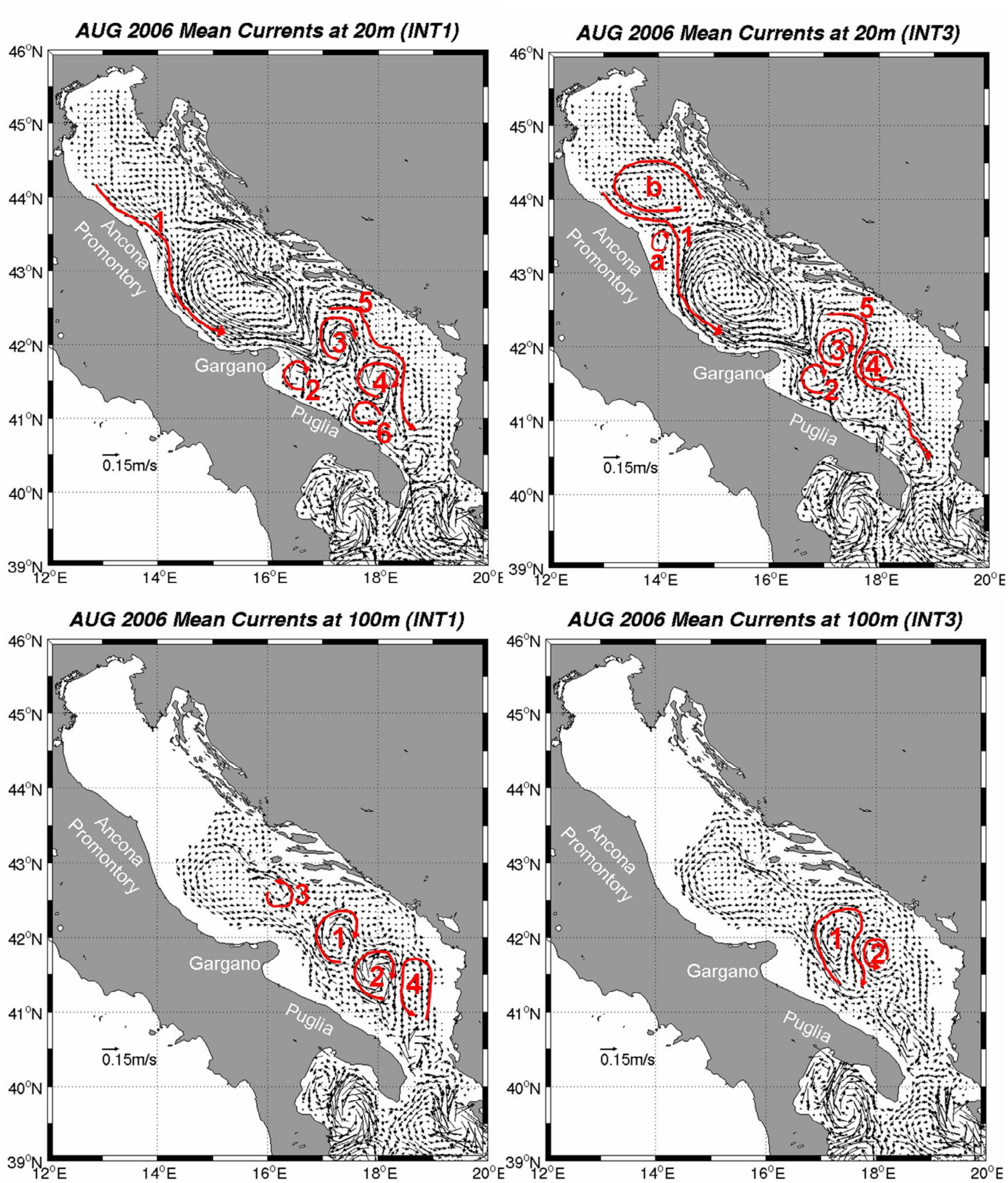

Figure 2.14: Mean currents of August 2006 at 10 meters (top panels) and 100 meters (bottom panels) for INT1 (left) and INT3 (right). The thick red arrows highlight the main differences between the two systems.

2.6 Summary and conclusions

Tides have been successfully introduced in a baroclinic primitive equation model of the Adriatic Sea. The new model has been widely validated over a decadal period of time in terms of temperature, salinity, density, SST and SSH. The main tidal constituents have been analyzed in terms of tidal amplitudes and phases, and the errors estimated versus the observed data were 2% and 4% respectively, for the amplitude and phase of the semidiurnal constituent, M2, while they generally increase for the diurnal constituents, reaching average values up to 16% for the amplitude of the diurnal component. Generally the errors on the phases are smaller than those in the amplitudes. Our results show for the first time the impact of the tidal barotropic velocity in the modified Flather (1976) boundary condition (Oddo and Pinardi 2008) is important to reproduce tidal amplitude and phases, particularly for the diurnal constituents. The full sea surface elevation was also analyzed in the period 2000-2008 for 8 mareographic stations around the basin, and the mean errors were found to range between 6 and 9 centimetres, with an average value of approximately 7 centimetres, probably due to the absence of pressure forcing in the model. Tidal currents have also been validated at a very coastal multi-parametric buoy offshore the Emilia-Romagna coast showing that the simulated velocities are realistic.

The baroclinicity of the model allowed to analyze for the first time the impact of tides on the dynamics and state variables of the system, and on the mixing of the water column in different seasons. The impact of tides in the near bottom transport of heat and salt in the ROFI region of the Po river is stronger along shore than across shore. In the along shore direction the tidal transport is almost completely associated to semidiurnal frequencies, while in the cross shore direction the transport related to diurnal frequencies becomes quite important too.

The mixing due to tides is also addressed, and we found similar conclusions to those of Malacic's (2000), finding that the tide induced mixing is present in the Northern Adriatic, even if it is not powerful enough to induce a complete mixing of the water column. Nevertheless, a clear oscillation of salinity and density, following the current shear stresses is found both in winter and summer, and it appears to be even more evident and enhanced in winter and after episodes of strong wind. In general tides showed to induce a higher stratification along the water column.

The comparison between the models with and without tides allowed also to highlight the two different temporal scales characterized by the effects of tides on the circulation: the fact that we often sea important differences in the distribution of mean temperatures and salinities between the model with tides and the model without tides, even in absence of big differences in vertical mixings, suggests that on long time scales tides have a stronger impact on advection rather than on diffusion.

Chapter 3

3. *NUMERICAL MODELLING OF SEDIMENT TRANSPORT IN THE ADRIATIC SEA*

3.1 Introduction

Interest in sediment transport in the Adriatic Sea has been growing recently. Sediments are fundamental vehicle for the transport of pollutants at sea (Frascari et al. 1998), and their concentration in the water column strongly influences the light penetration, impacting the physical properties of water and also the growth of phytoplankton in the subsurface (Vichi et al. 1998). The sediment transport is of major importance for coastal protection and coastal engineering in general, for sand mining at sea, or simply for tourism and recreational purposes (Warren and Johnsen, 1993).

The temporal large scale approach to the sediment transport issue in the Adriatic Sea, mostly supported with geological records and studies, has outlined some characteristics of the sedimentological properties of this area (fig. 3.1, after Frignani et al. 2005). In particular the most important depositional pattern is found all around the Po river delta, presenting accumulation rates up to 2 cm/yr according to Ravaioli et al. (PRISMA Project), or up to 6 cm/yr according to Palinkas 2005, and decreasing with the increase of bathymetry. Two other important depositional areas are found a few kilometres offshore the Ancona and the Gargano promontory, with accumulation rates ranging from 0.15 to 0.60 $grcm^{-2}yr^{-1}$ (Frignani et al, 2005).

As studied by Wang and Pinardi (2002) the two wind regimes of Bora and Scirocco have a very important role in understanding the sediment transport mechanism in the Adriatic Sea. These two winds can be responsible for the generation of strong wave activity, with significative wave heights of up to 4-5 meters in the northern part of the basin, with different characteristics. Scirocco comes from the south east, thus it has a much longer fetch than Bora, which blows parallel to the shortest side of the basin, and it generates waves with typical periods of up to 9-10 seconds, in contrast with Bora wind generated waves with

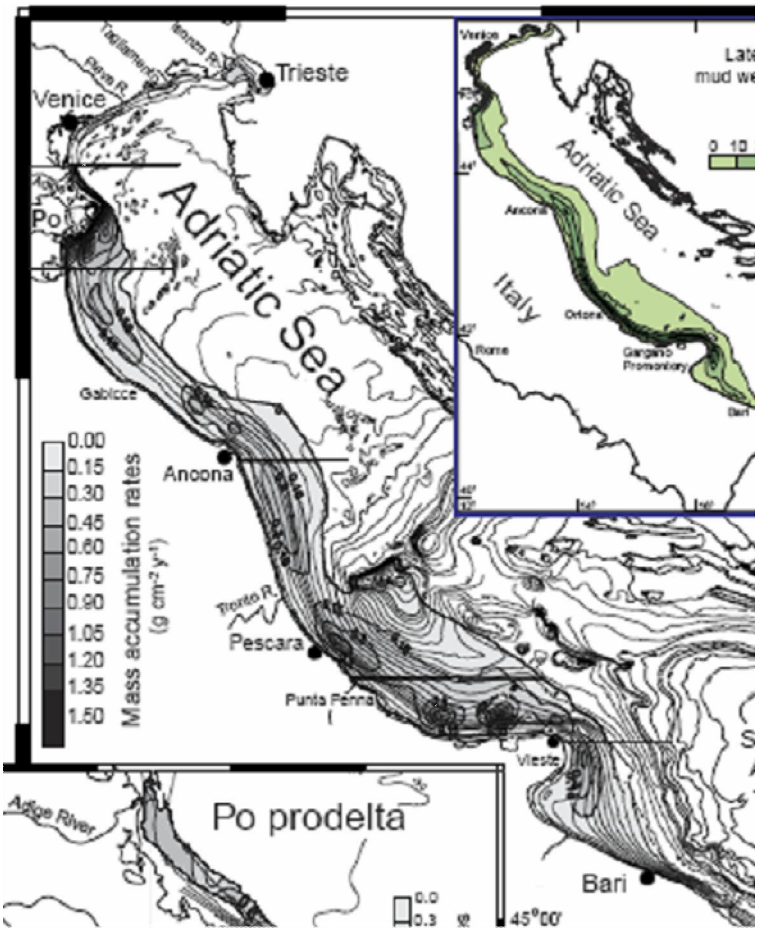

Figure 3.1:Accumulation rates (grcm^{-2}yr^{-1}) along the Italian coast. Image taken from Frignani et al. 2005.

shorter typical periods by a few seconds. This implies that less intense Scirocco winds can generate waves whose significative heights and bottom orbital velocities can be comparable with those generated by much more intense Bora winds (Wang and Pinardi 2002). The circulation as well is strongly affected by the wind regimes. In fact Bora tends to intensify the southwards circulation and intensify the WAAC and the related transport to south, while very strong events of Sirocco can even block and reverse the southward circulation, confining the sediment in the northernmost area of the basin. Wang and Pinardi (2002) outlined that the effects of these two different winds on sediment transport can be quite different, as they argue that the maximum southward transport occurs under Bora conditions and it exceeds that under Scirocco conditions by approximately a factor 4, while transport northward is maximum under Scirocco condition waves.

These results, though, were obtained with idealized Bora and Scirocco winds. Quite different results were obtained by Bever et al (2009), again simulating under idealized conditions the transport of sediment in the Po river vicinity of the basin. They always found a transport directed towards south, also under Scirocco conditions and in a control section north of the Po river delta, and a Bora wind associated transport lower by approximately three times the one associated to Scirocco. Wang et al. (2006) showed also the fundamental importance of the wave component in the study of sediment transport in coastal areas, and in particular the effects of the interaction between wave and current in the bottom boundary layer (BBL), arguing, on the contrary, that the tidal forcing produces small effects in sediment transport processes in the Northern Adriatic Sea.

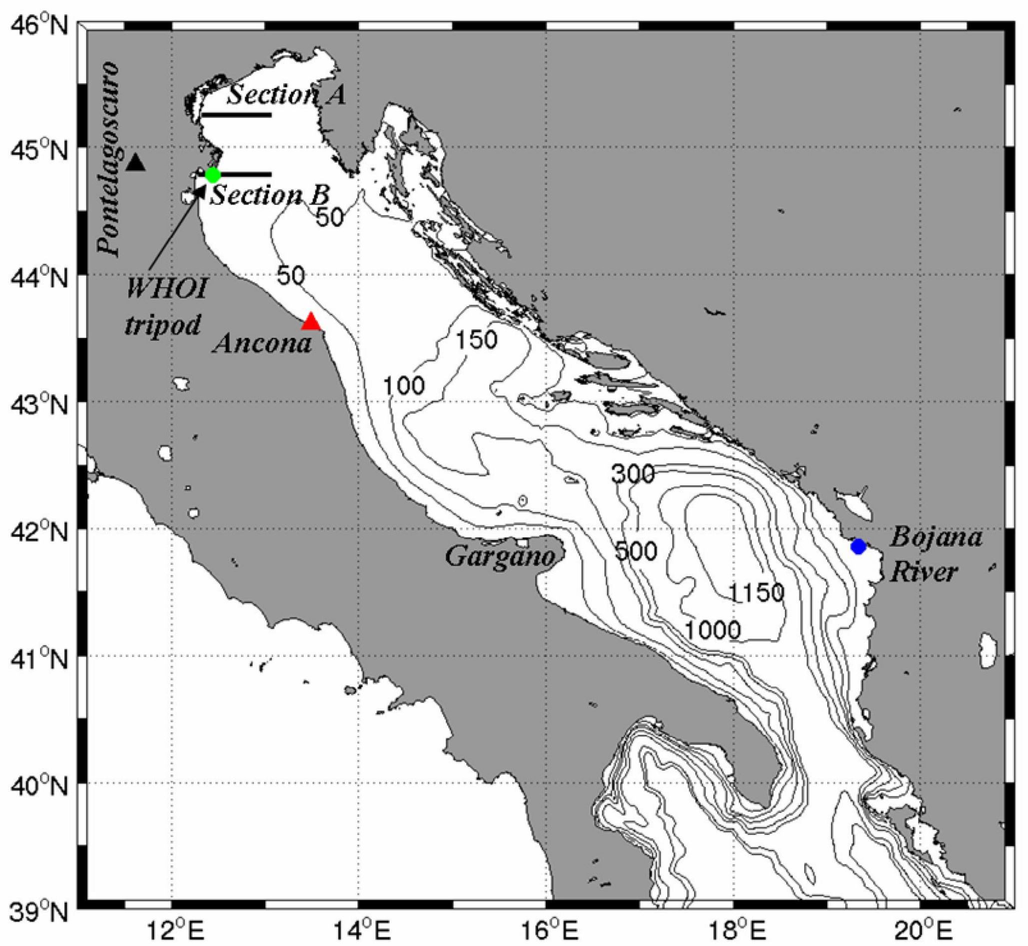

Figure 3.2: : Model domain and bathymetry.

In terms of sediment transport the Adriatic Sea (fig 3.2) is a very interesting area to be investigated, in particular the north-western part of the basin, where coasts are sandy, thus subjected to sediment movements, and where the Po river mainly, but also the rest of the several rivers out-flowing in the basin, are an important source of solid matter, acting at long term temporal scales. The other important source of sediment in the water column, acting at short temporal scales, is the process of sediment resuspension from the bottom of the sea. The motion of the fluid over the interface with the sea bottom creates a shear, proportional to the intensity of the motion, which can be responsible of the movement of the sediment grains previously deposited. This happens when the shear generated by the water exceeds a certain critical value for erosion. Resuspension involves directly the bottom boundary layer and its characteristics, in relation with the fluid motions within its limits and giving rise to highly non-linear friction processes, whose degree of complexity is closely related to the mechanisms that drive the motion itself, be them tides, waves, wind, density gradients etc.. (Grant and Madsen, 1986). It is now consolidated that the presence of surface short waves in the sea water is responsible for an evident increase in the bottom friction (Smith 1977, Grant and Madsen 1979, Cacchione & Drake 1982, Grant et al. 1984, Wang and Pinardi 2002), thus enhancing the sediment resuspension.

The purpose of this chapter is to show the implementation of a wave-sediment-current numerical simulation model in the Adriatic Sea, and its capability to predict the concentration and fluxes of sediment along the water column in the coastal zones of the basin. This model, coupled with the model described in chapter 2, will be used to investigate the changes in sediment transport patterns under climate change scenarios that will be presented in chapters 4 and 5.

The chapter is structured as follows: section 2 describes the wave model and the sediment transport submodel coupled with the ocean general circulation model presented in chapter 2. In section 3 the simulation experiment is described, while the corresponding results are discussed in section 4, where validation against available data is also given, together with some process analysis related to strong events of sediment transport in relationship with Bora and Scirocco wind regimes. In section 5 a summary and conclusions are offered.

3.2 **Description of the numerical models**

As anticipated in section 3.1 the wave activity is the major actor for the resuspension of sediments long the water column, so a realistic representation of waves is fundamental to be able to reproduce accurately the sediment dynamics at sea. The following two subsections describe the wave and sediment models.

3.2.1 The wave model SWAN

The model used for simulating the wave field was SWAN, a third generation spectral wave model developed by the Delft Univeristy Technology (see SWAN technical and scientific manual, Holthuijsen et al.,1989, Booij et al., 1999 and Ris et al.,1999). The model solves the spectral action balance equation without any a priori restrictions on the spectrum for the evolution of wave growth. This equation represents the effects of spatial propagation, refraction, shoaling, generation, dissipation and nonlinear wave-wave interactions. The model has been implemented on the Adriatic Sea domain of the Adriatic REGional model described on chapter 2, AREG2, using the same regular lon/lat grid, with a horizontal resolution of approximately 2.2 km, and the same bathymetry. The wave directions have been discretized by 18 bins of 20 degrees each. The model has been run in stationary mode, under the ECMWF atmospheric forcings at a horizontal resolution of 0.5° on a frequency of 6 hours. The bottom friction was computed by the Madsen scheme (1988) with the default equivalent bottom roughness length scale. The wave parameters calculated by SWAN were the wave direction, period, and orbital velocity.

The latter is the most important field in order to evaluate the maximum bottom shear stress due to the combined action of waves and currents, and it can be shown that for a monochromatic wave its distribution along the water column is given by:

$$u(z) = \eta_0 \omega \frac{\cosh(k(z+H))}{\sinh(kH)} \cos(kx - \omega t) \tag{3.1}$$

Where η_0 is the wave amplitude, ω is the radian or circular frequency, k is the wave number, H is the water depth, and z and x are respectively the vertical and horizontal component in a Cartesian coordinates system. The amplitude of the orbital velocity varies sinusoidally in time, reaching its minimum when $kx - \omega t = \pm \frac{n\pi}{2}$, and its maximum when $kx - \omega t = \pm n\pi$. In the framework of sediment transport and of sediment resuspension we are interested in the maximum bottom shear stress, thus in the maximum value of u at z=-H, so equation (3.1) becomes:

$$u'_{bott} = \frac{\eta_0 \omega}{\sinh(kH)} \tag{3.2}$$

Real waves are not monochromatic, so equation (3.2) for a realistic wave becomes:

$$u_{bott} = \sqrt{2}\left(\int_0^{2\pi} \int_0^{+\infty} \frac{\omega^2}{\sinh^2(kH)} S(\omega,\theta) d\omega d\theta \right)^{\frac{1}{2}} \tag{3.3}$$

where S is the wave spectrum distributing the energy over directions θ and frequencies ω. In sediment transport representative wave bottom velocities are usually referred to as defined by Grant and Madsen (1979, 1994):

$$u_w = \frac{u_{bott}}{\sqrt{2}} \tag{3.4}$$

Figure 3.3 presents the validation of the wave model in the WHOI location (Traykowski et al. 2007), close to the Po river delta (see fig 3.2). The bathymetry of the site is approximately 13 meters. The presented data are the representative bottom orbital velocity. The black line represents the observations, while the red line represents the modelled data. HC_i and DS_i refer respectively to high concentration (turbidity flow) and diluted suspension events of sediment transport, as classified by Traykovski et al. (2007). In spite of the coarseness of the wind field forcing the SWAN model, both in time and space, the response of the model appears to be quite good, even if some overestimation of the medium amplitude peaks is evident, particularly in the period between January and March 2003.

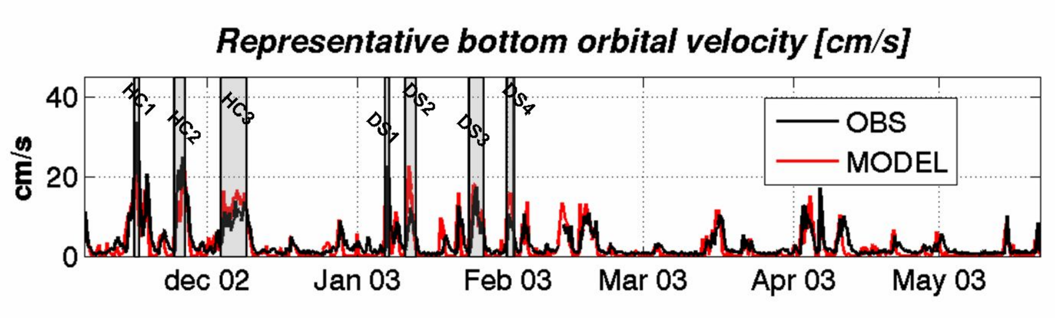

Figure 3.3: Validation of the representative bottom orbital velocity (as defined by Madsen 1979) and the SWAN implementation of this work. The black line represents the observed data, while the red line represents the modelled ones. HC and DS refer respectively to high concentration (turbidity flow) and diluted suspension events of sediment transport, as classified by Traykovski et al., 2007

3.2.2 The sediment transport submodel

The sediment transport submodel is based on the equation of advection-diffusion for a passive tracer in an incompressible fluid:

$$\frac{\partial C}{\partial t}+\frac{\partial}{\partial x}(uC)+\frac{\partial}{\partial y}(vC)+\frac{\partial}{\partial z}[(w+w_s)C]=\frac{\partial}{\partial z}(K_v\frac{\partial C}{\partial z})+A_M\nabla_h^2 C \tag{3.5}$$

where *x, y, z* are the spatial coordinates of a Cartesian system, and the corresponding velocity components are **u**=(*u*,*v*,*w*). *C* is the concentration of the sediment suspended along the water column, while K_v and A_M are respectively the vertical mixing coefficient and eddy viscosity, which do not differ from those used for the diffusion of salt and heat, as described in equation (2.3). K_v is given by the turbulence closure submodel of Mellor-Yamada 2.5 (1982). The w_s term in equation (3.5) represents the sediment settling velocity. It can be estimated by means of the Stokes law as it follows:

$$w_s=\frac{gd^2}{18\nu}\left(\frac{\rho_s}{\rho_w}-1\right) \tag{3.6}$$

where ρ *(kg/m^3)* is density and the subscripts *s* and *w* indicate sediment and water respectively, *g* *(m/s^2)* is gravity, ν *(m^2/s)* is kinematic viscosity of water, and *d (m)* is the mean diameter of the sediment grains.

Equation (3.6) is valid for a sediment concentration that does not affect the water motion and the sediments are assumed not to flocculate, so the model is suitable for non-cohesive sediments only.

3.2.3 Parameterization of the resuspension/deposition processes

Equation 3.5 needs initial and vertical as well as lateral boundary conditions to be solved.

The bottom boundary condition sediment flux can be represented as:

$$K_v \frac{\partial C}{\partial z}\Big|_{z=-H} - w_s C = S \tag{3.7}$$

where *H* is bathymetry, and *S* is the sediment flux expressed in $kgm\text{-}^{2}s^{-1}$.

The parameterization of *S* is based on the approach of Ariathurai and Krone (1976) for non-cohesive sediment, based on the concept of critical stresses for deposition and erosion: if the maximum stress at the interface between the sea bed and the sea water is higher than a critical value for erosion we have a flux of sediment from the seabed into the water column (erosion) linearly proportional to the ratio between the bottom maximum stress and the critical stress for erosion, vice versa we have a flux of sediment in the opposite direction, from the water column to the seabed (deposition), linearly proportional to the ratio between the bottom maximum stress and a critical stress for deposition. This is also the approach used by Wang and Pinardi (2002) and by Wang et al, (2006).

However, we argue that this approach has three main deficiencies: firstly it introduces a non-physical concept of critical stress for deposition, secondly it does not allow for sediment to be deposited in those periods of time when we have resuspension, as if gravity attraction was not acting due to high shear stresses, and finally there is not any limit to erosion, as if the sea bed was always provided with an infinitive amount of non-compact matter available for resuspension. For these reasons the parameterization used at the bottom boundary was modified, with respect to the formulation of Wang and Pinardi (2002) according to equation (3.8):

$$S = \begin{cases} S_0\left(\frac{|\vec{\tau}_b|}{\tau_c} - 1\right) \frac{B_i}{\sum_{i=1}^{N} B_i} & \text{for } |\vec{\tau}_b| > \tau_c \quad \text{and } B_i > 0 \qquad \text{(a)} \\ -C_b w_s & \text{for any } |\vec{\tau}_b| \qquad \text{(b)} \end{cases} \tag{3.8}$$

where S_0 *(kgm^2s^{-1})* is the erodibility of the sea bed, locally dependent; $|\vec{\tau}_b|$ and τ_c *(N/m^2)* are the amplitude of maximum bottom shear stress (due to wave, to current, or to their non-linear interaction), and of the critical stress for erosion respectively. C_b is the suspended sediment concentration at the last σ layer above bathymetry, and w_s is the sediment settling velocity (*m/s*). B_i is the sediment bed mass in kgm^{-2} for the i^{th} class of the N classes of sediment totally simulated (Souza et al. 2007).

In this parameterization there is no dependency from the bottom maximum stress (nor for the critical stress of deposition, which is an arguable concept) in case of deposition (3.8b), and the erosive sediment flux (3.8a) has been limited by the introduction of the ratio between the sediment bed mass of the i^{th} class of sediment and the total amount of sediment on the bottom. The conservation of each class of sediment mass at the bottom is given by:

$$\frac{\partial B_i}{\partial t} = -\frac{\partial C_i}{\partial t}\delta_b \tag{3.9}$$

where δ_b is the thickness of the last σ layer, allowing for deposition and erosion when $B_i>0$, and deposition only when $B_i=0$ (Souza et al. 2007). This modification allows to limit the sediment flux for each class of sediments only if on the bottom there is available sediments for erosion. Moreover the flux for each one of the classes is proportional to its amount with respect to the total sediments present on the bottom.

For what concerns the surface boundary sediment flux we used the following condition:

$$K_v \frac{\partial C}{\partial z}\Big|_{z=\eta} = S_{riv} \tag{3.10}$$

where S_{riv} is the sediment input in $kgm^{-2}s^{-1}$ supplied by each one of the rivers in the model, and η is the elevation of sea surface.

The lateral inflow of sediment at the open boundary was assumed to be zero.

3.2.4 The bottom stress formulation

In case of absence of waves the bottom stress $\vec{\tau}_b$ is due to the near bottom current u_c:

$$\vec{\tau}_b = C_d \rho |\vec{\boldsymbol{u}}_c| \vec{\boldsymbol{u}}_c \tag{3.11}$$

With the bottom drag coefficient C_d, defined according to Janssen (1991):

$$C_d = \max\left\{0.0025; \left[\frac{\kappa}{\ln\left(\frac{(\delta_b)}{z_0}\right)}\right]^2\right\} \tag{3.12}$$

where κ is the von Karman constant, set to 0.40, z_0 is the scale of the bottom roughness, which was here assumed to be 1 *mm*, and δ_b is the thickness of the last model level above the bottom. The inferior limit of 0.0025 for C_d is introduced to prevent the bottom drag to be too low in the domain of deep waters.

In the more complex case of currents and waves acting together on the bottom they interact non-linearly, and the resulting bottom maximum shear stress τ_b amplitude can be estimated by the parameterization of Grant and Madsen (1979).

$$\tau_b = \frac{1}{2} f_{cw} \rho \left(u_c^2 + u_w^2 + 2 u_c u_w \cos\theta \right) \tag{3.13}$$

where u_w is the amplitude of the representative bottom orbital velocity (see eq. (3.4), θ is the angle between wave and current direction, and f_{cw} is the wave-current friction factor that takes into account the non linear interaction between currents and waves. The estimate of f_{cw} can be done through an iterative procedure as proposed by Grant and Madsen (1979) and summarized by Lou et al. (2000). The same procedure was used by Wang and Pinardi (2002), and is here proposed in Appendix A, after Lou et al. (2000).

3.3 The winter 2002-2003 sediment transport experiment

The sediments model described in the section above has been used to reproduce the strong sediment transport processes occurred in autumn 2002 - winter 2003 (Traykovski et al. 2007, Fain et al., 2007). During this period the Po river flood (with flows up to 8000 m^3/s) occurred as well as several events of Scirocco and Bora, causing very high significative wave heights close to the coast near the Po river, with resulting representative bottom orbital velocities of up to 40 cm/s (fig. 3.3). In the same period measurements on sediment concentrations, sediment fluxes, and currents were carried out at the *WHOI* tripod (fig. 3.2) (Traykovski et al. 2007).

3.3.1 Numerical experiment design

The simulation started on August 6th 2002 and the initial conditions used were taken from the simulation of the model without the wave-current-sediment coupling. In terms of sediments the model was initialized with a sediment bed mass of 1 kg/m^2 constant over the whole domain for each class of sediment considered, while the concentration C along the water column was set to 0.002 kg/m^3 constant in the whole domain. Two classes of sediments were considered, following Wang and Pinardi (2002) and Wang et al. (2006): a class of finer sediments with a diameter of approximately *17 µm* and a corresponding settling velocity of 10^{-5} m/s, and a coarser class of sediments with a diameter of approximately *55 μm* and a corresponding settling velocity of 10^{-4} m/s. The critical shear stress for erosion used was $\tau_c=0.02\ Pa$ for both classes of sediment, and constant in space and time. The erodibility coefficient S_0 was set to 10^{-6} $kgm^{-2}s^{-1}$. This parameter is an empirical constant, and it is strongly locally dependent. Unfortunately we are not aware of measurements taken for the bottom erodibility in the Adriatic Sea, so we used this parameter for the calibration of the model, and the final value used is in the range of the values found in literature, ranging from 10^{-4} to 10^{-7} $kgm^{-2}s^{-1}$. For what concerns the lateral boundary conditions for sediment the different rivers were treated differently. Following the estimate of Frascari et al. (1988) of a total input of sediments from all the Adriatic rivers of approximately 20 MT/year, and considering that the Po river contributes for about 70% of this input, we equally spread the remaining 30% of sediment supply to the other rivers of the basin, estimating a flux of approximately 450 kg/s for the Po river, and of approximately 6.50 kg/s for all the other rivers. To take into account the great flood occurred in Autumn 2002 and Winter 2003 which could not be described with climatological values for sediment flux input, this was estimated parametrically, linearly dependent from the river flow as follows:

$$Q_s = \frac{Q_w}{12000} \text{ for } Q_w \leq 3500\,\mathrm{m^3s^{-1}} \tag{3.14a}$$

$$Q_s = \frac{Q_w}{5500} \text{ for } Q_w > 3500\,\mathrm{m^3s^{-1}} \tag{3.14b}$$

where Q_s (m^3s^{-1}) is the flow of solid suspended matter, and Q_w (m^3s^{-1}) is the water flow.

Figure 3.4 shows the flow and sediment concentration (first and second panel respectively) prescribed to the model as boundary conditions for the surface water and sediment fluxes during the period 2002-2003. The data of flow are the observed values of discharge at the cross section of Pontelagoscuro (see black triangle of fig. 3.2), while the data on sediment concentration at the mouths of the Po river (second panel) are the parameterized reconstruction of suspended

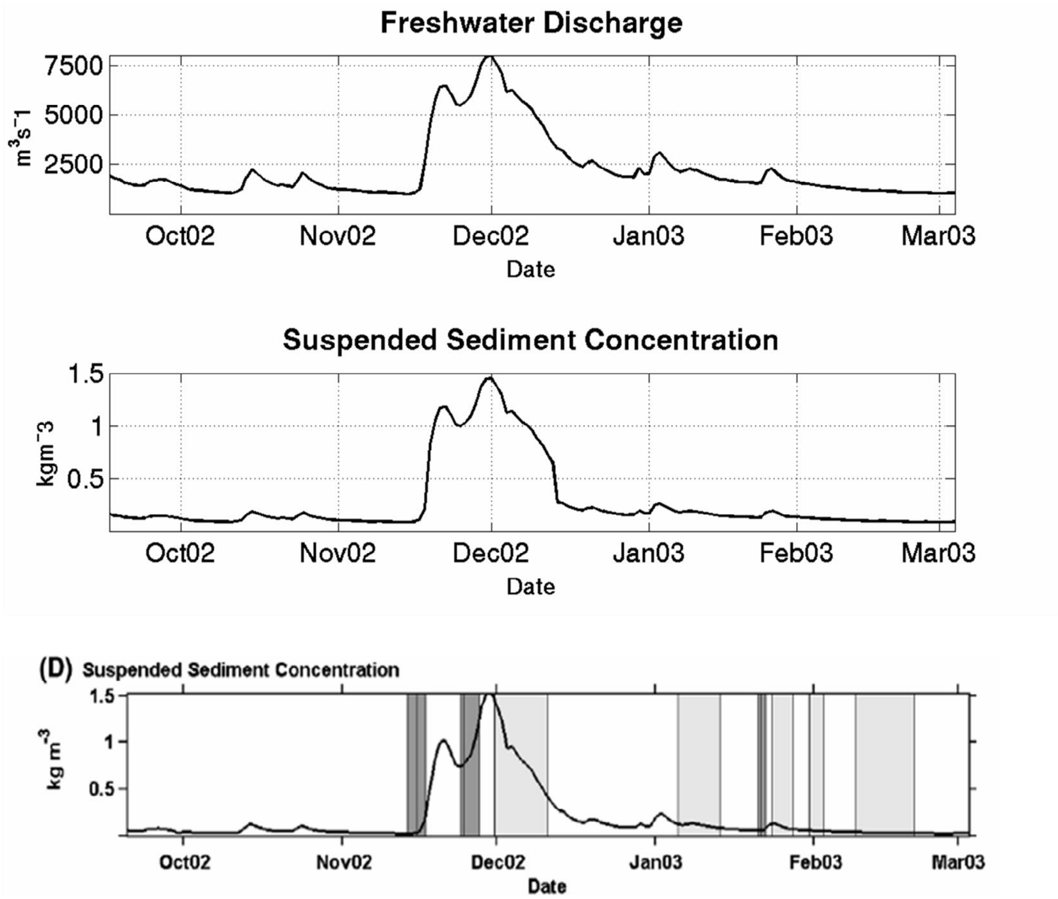

Figure 3.4: Flow (top panel) and sediment concentration (two bottom panels) conditions in the Po river delta, from October 2002 to March 2003. The flow data are the observations at Pontelagoscuro. The concentration data of the second panel are obtained through a flow dependent parameterization used in the model to emulate the data of concentration used by Bever et al. 2009 (bottom panel).

sediment at the river delta. For the rest of the time the concentration of suspended sediment associated to the Po river was fixed to 450 Kg/s

3.4 **Results**

3.4.1 Model validation

One of the most important physical quantity in the model is the bottom stress. Due to the absence of measured data on this parameter, we compared our results with the one of a 1D bottom boundary layer model implemented in the Adriatic Sea

(Traykowski et al, 2007). The results are shown in figure 3.5, and refer to the bottom stress estimated at the location of the WHOI tripod (see figure 3.2).

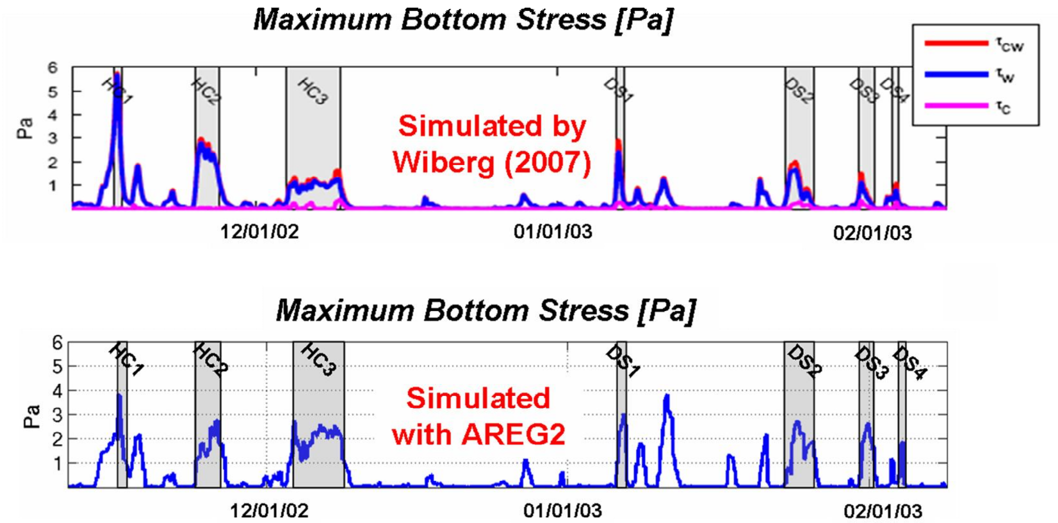

Figure 3.5: Bottom stress (Pa) at the location of the WHOI tripod, simulated by Wiberg et al. (top panel) with a 1D bottom boundary layer model, and with AREG2 (bottom panel).

Figure 3.5 shows that both the models simulate a similar behavior of the bottom stress. Most of the events are overestimated by AREG2, and probably they are related to the errors of the wave model (fig 3.3), which overestimates the same episodes, probably due to the coarseness both in space and time of the atmospheric forcings (0.5° of horizontal resolution and 6 hour frequency). The reference model (top panel of figure 3.5), on the contrary, is forced with the observed representative bottom wave orbital velocity and with the observed current velocity.

The sediment concentration along the water column during the big flood of Fall 2002 - Winter 2003 reached very high values, even up to 60 g/l during particularly strong storm events, such as the high concentration event occurred on November 16th and 17th, when very strong Scirocco winds generated waves up to 4.5 meters high in the northern part of the basin. In the upper panel of figure 3.6 the observed data by Traykowski et al. (2007) are presented, and in the shaded boxes three high concentration events (HC) and four diluted concentration events (DS) are evidenced.

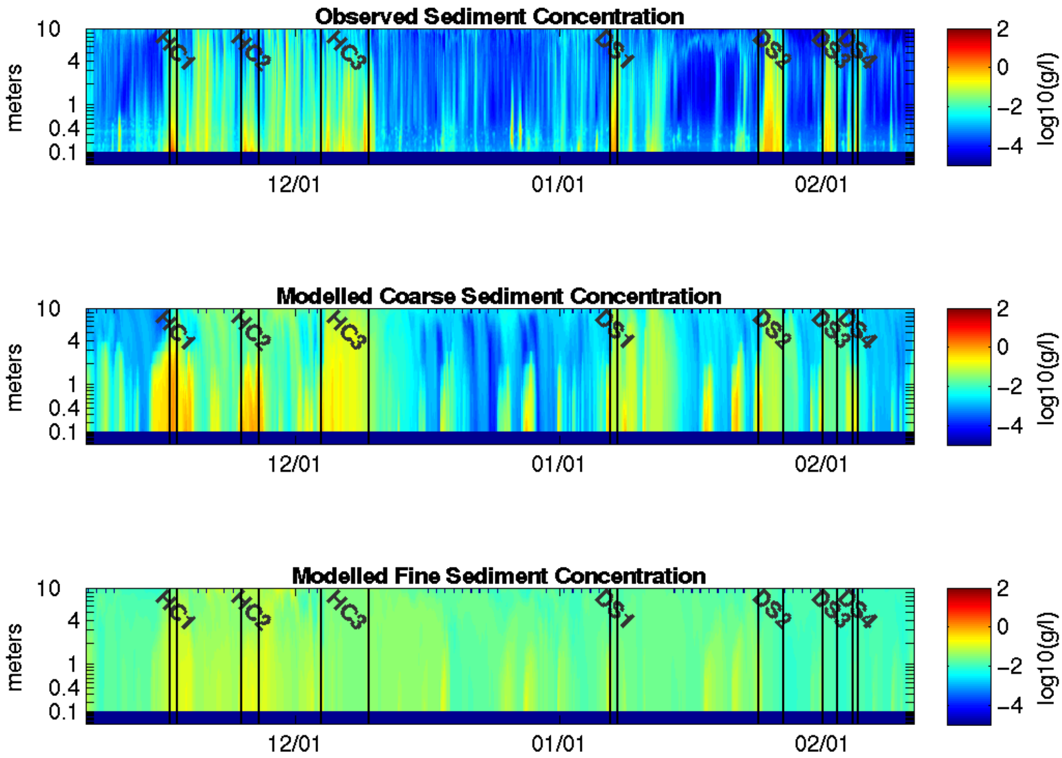

Figure 3.6: Concentration along the water column for the period November 2002-February 2003. Upper panel: observed sediment concentration data at WHOI tripod (Traykovski et al. 2007). Mid panel: modelled coarse sediment concentratoin. Bottom panel: modelled fine sediment concentration. The y axes refer to the height above the sea bottom (m).

The mid and bottom panels represent respectively the simulated coarse and fine sediment concentration along the water column for the same period of time. The first 10 centimeters above the bottom (cmab) have been masked out by a dark blue band because the model resolution is not high enough to be able to simulate this region, so close to the bottom, being the thickness of the bottom boundary layer in this location approximately 12 cm. The HC events are events of very high concentration at the bottom: within the first 5 cmab several g/l of concentration are fund, which the model is not capable to simulate, not just because of its resolution, but also because we are here in the field of turbidity flows. A more accurate analysis of the observed sediment concentrations versus the modelled ones underlines immediately some deficiencies of the model. First of all the predicted coarse sediment concentration is quite consistent with the observations, but if we sum it to the fine sediment concentration the vales a re too high during the periods of calm, and in the upper part of the water column. This means, on one hand, that the model is too erosive on the finest sediment, which tends always to be suspended along the water column, and on the other hand that the vertical mixing is also probably too high. In fact if we analyze events HC1 to HC3, also for the coarse sediment, we see that the high concentration of sediment reaches too far high along the water column compared to observations, and often the duration of resuspension is too long, as it happens for HC1 and HC3, even if, at least for these two cases, the reason can be addressed to the imprecise wave forcings (fig. 3.3). In other cases, on the contrary, such as diluted concentration events DS2 and DS3 the model underestimates the concentration of sediment in the lowest part of the water column. This time the reason is quite different, and the analysis of the mass bottom evolution in the location of the tripod for the considered period, shown in figure 3.7, helps us understand it.

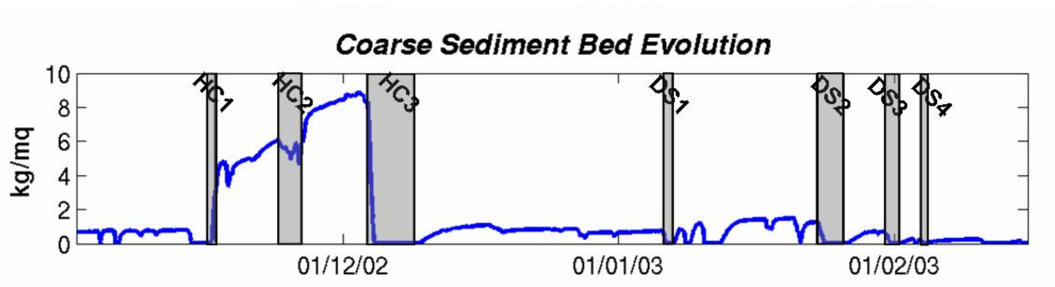

Figure 3.7: Evolution of the sea bottom in terms of mass of sediment per squared meter (kg/m^2) at WHOI tripod during the period November 2002 February 2003. Data are hourly means.

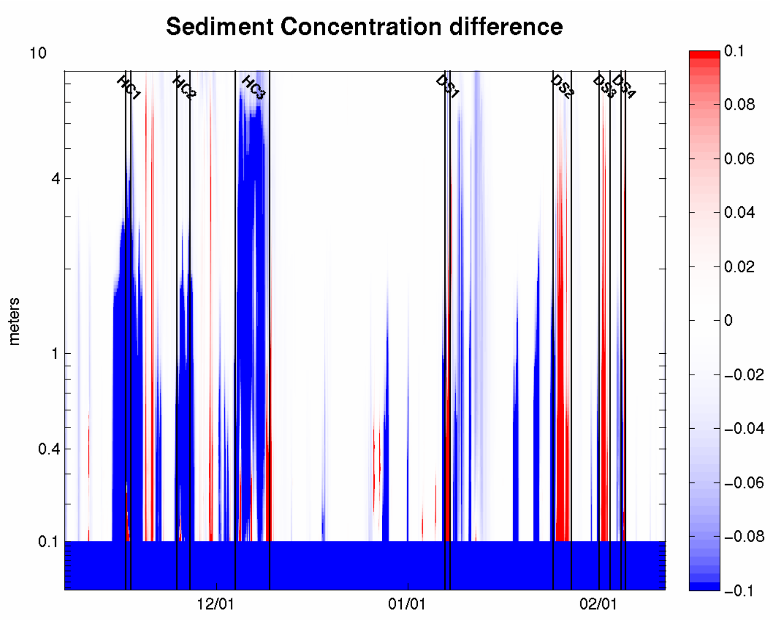

Figure 3.8: Field of difference of sediment concentration between observed and modelled data. The unit is g/l. Again the first 10 cmab are masked out.

In fact, in spite of predicted bottom shear stresses even higher than those predicted by the reference model the low values of sediment concentration in these events are due to the unavailability for erosion of sediment matter on the bottom. To better interpret the considerations just done, figure 3.8 shows the field of difference between the observed sediment concentration and the coarse sediment concentration measured in g/l. As anticipated, in the HC events the sediment is clearly too much diffused up along the water column, while the bottom boundary lacks of suspended sediment.

As it happens for the sediment concentration, where the modelled coarse class fits best the observations, this happens also for the sediment flux at the tripod WHOI, as shown in figure 3.9. The image represents the cumulative depth integrated sediment flux, from November 2002 to May 2003.

The analysis of figure 3.9 hints that the modelled events HC2 and HC3 are definitely not well represented, not only for the overestimation of the flux during the HC3 event, whose reasons have already been analyzed, but mainly because of the hydrodynamic component of the flux: the simulated flux is northward, while the observed one is southward. Starting from the end of the HC3 event, though, the fitting of the data, particularly for what concerns the coarse sediment is very good. In particular, the along shore simulated flux for coarse sediment is 1656 kg/m versus an observed value of approximately 1200 kg/cm from mid December 2002 to May 2003.

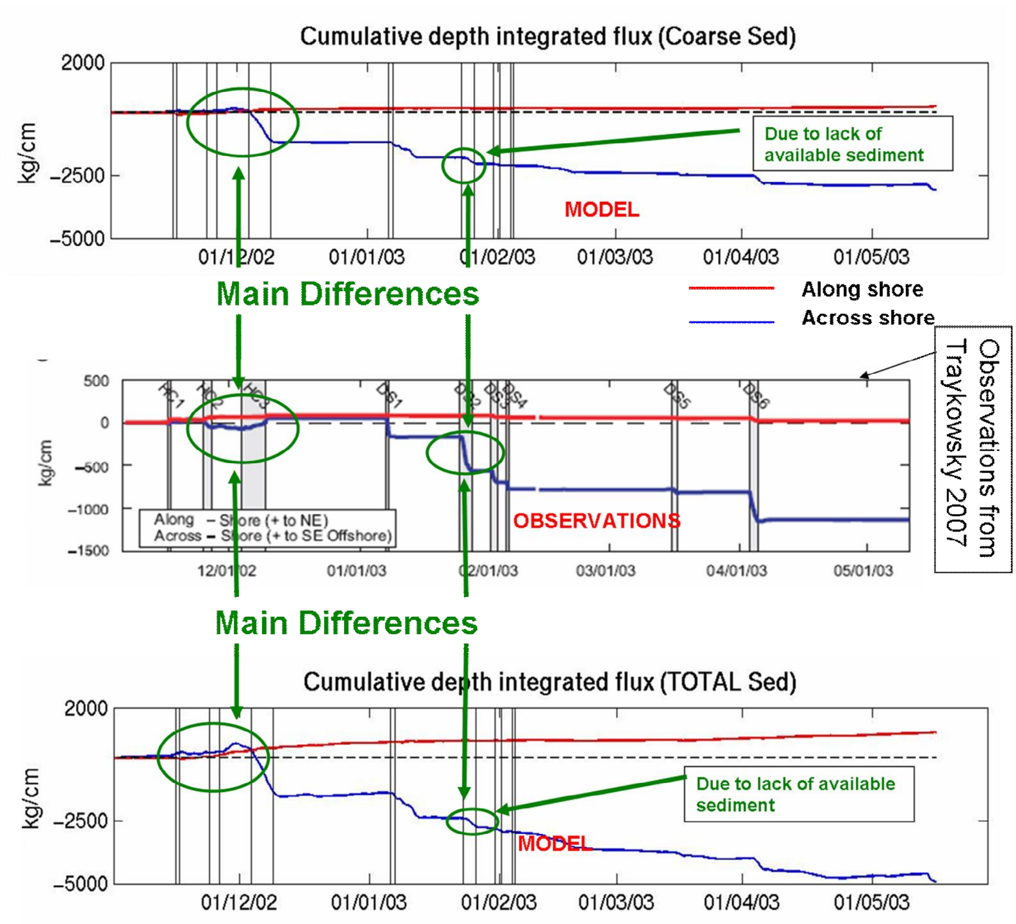

Figure 3.9: Depth integrated sediment flux ath the WHOI tripod, integrated from November 2002 to may 2003. The observed data are represented in the central panel, while the upper and lower ones respectively show the simulated values of sediment fluxes of the coarse and the total sediment. Red lines are fluxes across the coastline (positive to open sea, negative to the coast), blue lines are fluxes along the coast (positive northwards and negative southwards).

The cross-shore simulated flux for coarse sediment is slightly positive, while the observed one is slightly negative. If we consider the total sediment (fine plus coarse), a total flux of 3036 kg/cm is simulated in the same period (excluding the HC events).

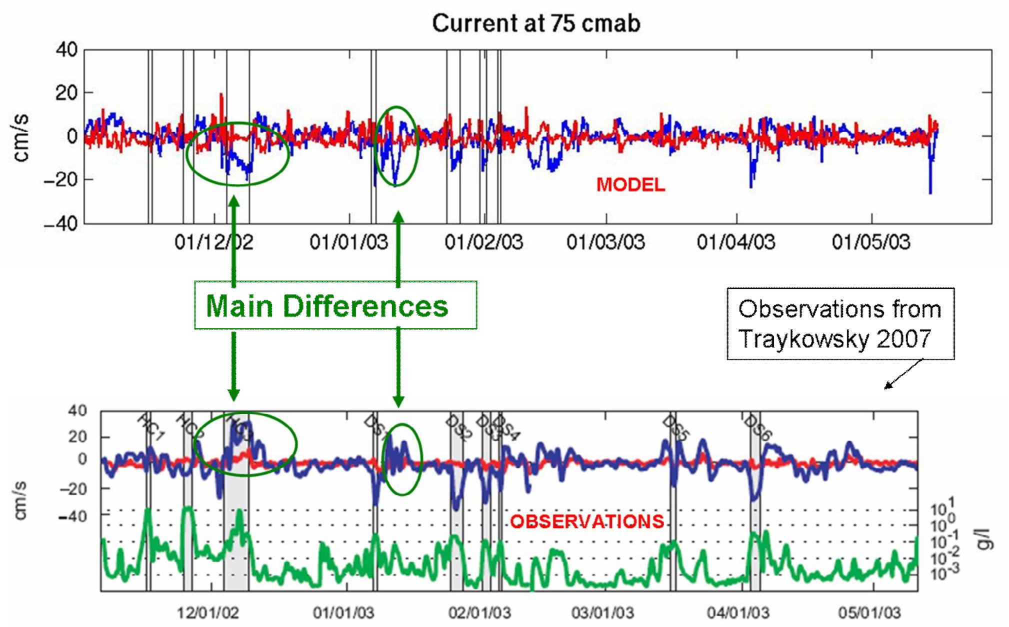

Figure 3.10: Modelled (upper panel) and observed (lower panel) current at 75 cmab. The red line represents across shore current, while the blue one represents the along shore currents. The main differences are in the HC3 event, where the model predicts an along shore current opposite to the observed one. The lower panel (taken from Traykowski et al. 2007) also shows (green line) the flux-weighted depth-averaged concentration, not available at the moment for the simulated data.

A confirmation of the problems due to hydrodynamics is given in figure 3.10, representing the along shore (blue line) and cross shore (red line) components of the current at 75 cm above the bottom, simulated and observed respectively in the top and bottom panel. The main differences in the currents are evidenced during event HC3 and in the days immediately after event DS1. The misprediction of this latter period, though, are not very significative in terms of fluxes, since the suspended sediment was almost negligible. On the contrary the errors in the representation of the currents during the former event (HC3) are responsible for a very high amount of sediment predicted to flow in the opposite direction of the observed fluxes.

All the validation comparisons showed so far were related to very short timescales, of the order of hours, such as the processes of sediment erosion for the single events. It is interesting though, to also have a look at the longer timescale processes, those that can help understand depositional patterns and sediment pathways in the domain. Figure 3.11 shows a comparison of the simulated accumulation rate of sediment in grm^{-2}yr^{-1}(left panel) with the observed data (right panel) taken from Frignani et al. (2005). Since the observations refer to the more coastal belt that encompasses the western Italian coast from the Po pro-delta down to the Gargano region the domain in the open sea has been masked out in the modelled results. As it was stated earlier the model is too erosive, especially in the regions where the fluvial input is not very significative, as it is for the Po delta. It is interesting to notice that the two main depocenters of the Po river delta and of the Ancona promontory are very well represented by the model. The majority of the sediments provided by the Po is deposited within the first tens of kilometres around its mouth, reaching high accumulation rates of approximately 1.50 gr/cm-^{2}yr^{-1}. Another part of the Po sediments and of the sediments eroded in the shallow coastal area during strong wind events between the Po river and Ancona are advected offshore the Ancona promontory, as confirmed by the observations by Frignani et al (fig 3.11, right panel). The missing sedimentation evidenced by the model in the coastal regions between the PO and Ancona and North of the Gargano can be also addressed to a lack of sediment input from the Apennine rivers, whose regime is torrential, and in years of particular strong floods, such as the one considered here, their estimated sediment input can be occasionally several times higher than the climatological here estimated, but we believe that the main problem is the too high erodibility of the sea bottom, due to the lack of a real physically based layer-submodel for the sea bottom.

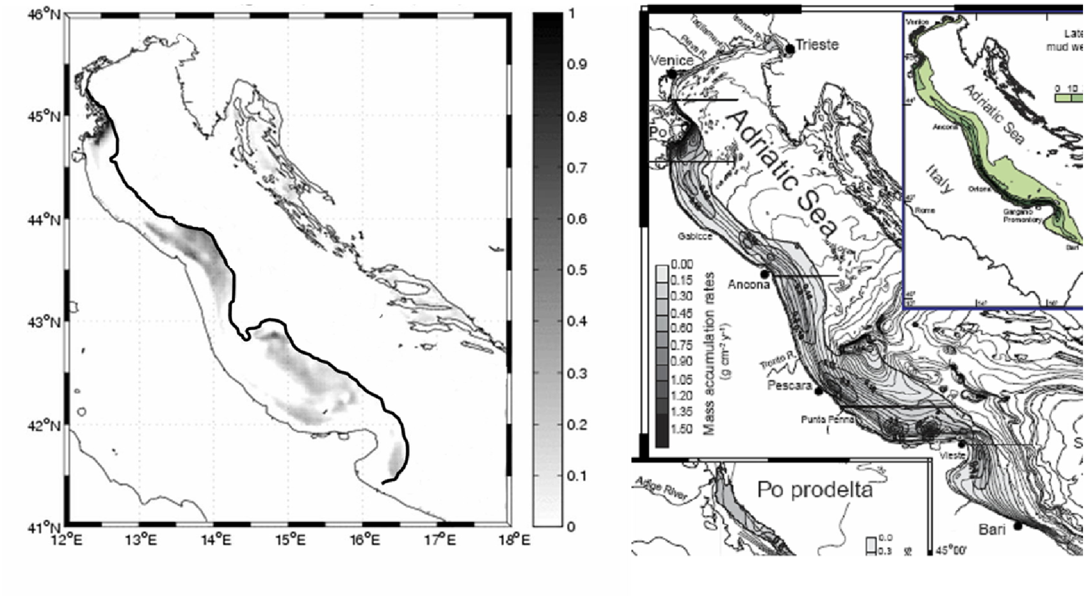

Figure 3.11: Comparison of the simulated accumulation rate of sediment (left panel) with the observed data taken from Frignani et al. (2005).

3.4.2 Analysis of different response of sediment transport to events of Bora and Scirocco

In order to understand the different impact that similar events of Scirocco and Bora can have on sediment transport we have analyzed the mean sediment transport, sediment concentration and currents for event HC1, when a storm of Scirocco occurred, and for event DS1, when the wind regime was of strong Bora. The duration of the two events was of 21 hours, and the maximum bottom shear stresses simulated were respectively of 3.8 Pa and of 3.0 Pa.

The results of the analysis are presented in figures 3.12 and 3.13, respectively for section A – a section north of the Po river delta – and for section B – the section of the tripod WHOI, south of the Po river delta (see figure 3.2).

It is interesting to notice how, in accordance with Bever et al., 2009, for both the Bora and Scirocco events the sediment fluxes at the northern section (section A) are directed southwards (the dashed lines mean a direction of the field pointing towards south. Opposite situation is for solid lines of figures 3.12 and 3.13), even if the Scirocco event had a particularly high intensity. Different results had been found by Wang and Pinardi, 2002, who had found a northward dominant sediment transport in their idealized simulations under Scirocco events also at their northern boundary. In contrast with what happens at section A, the very strong Scirocco HC1 event causes a significative reversal of the coastal circulation until longitude 12.6° E, that combined with the high sediment concentration in the lower part of the water column is responsible for an evident northward transport integrated over the whole transect at section B.

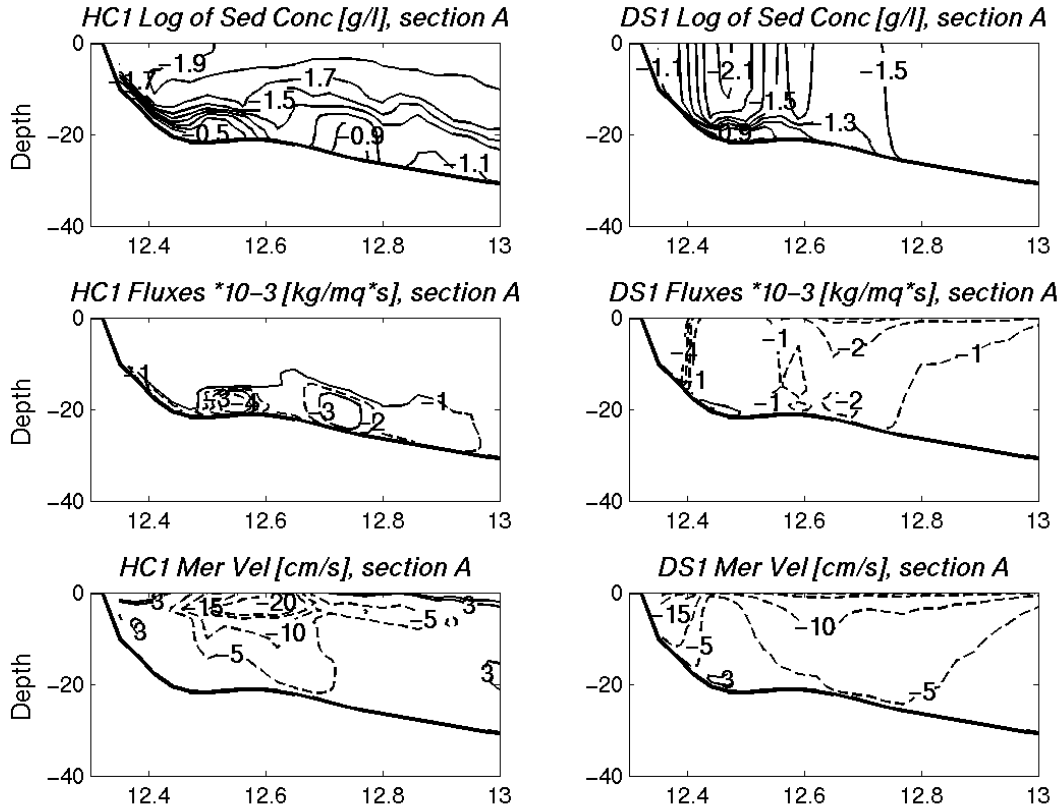

Figure 3.12: Section A: suspended sediment concentration (top), sediment fluxes (mid) and meridional currents (bottom) for a Scirocco (left) and a Bora (right) significative events for the events. The data have been averaged over the period of the events, whose duration was of 21 hours each. The dashed lines mean a direction of the field pointing towards south. Opposite situation is for solid lines

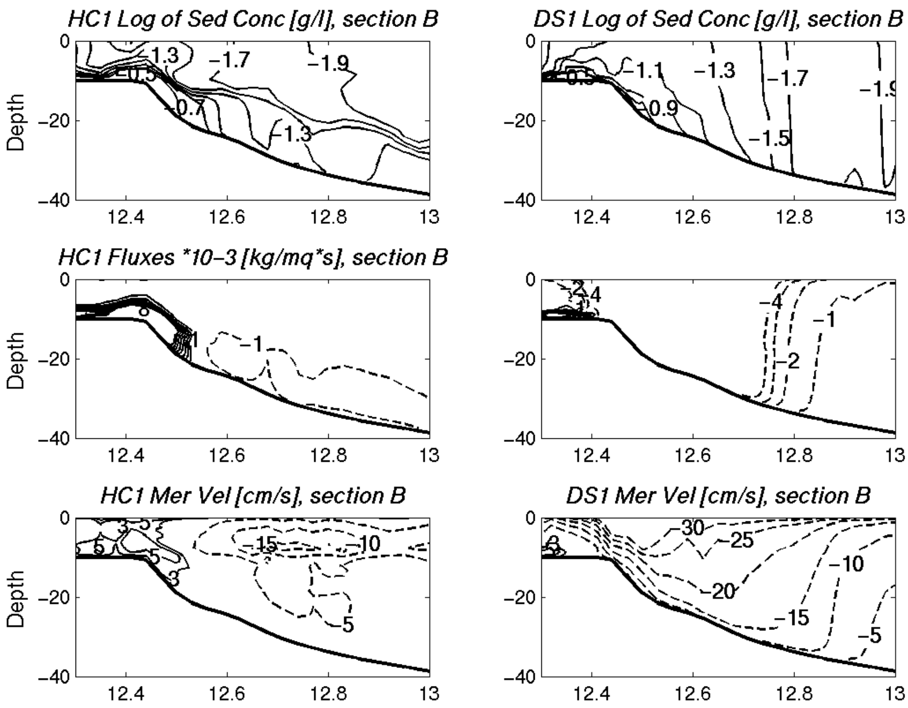

Figure 3.13: Same as figure 12, but for section B.

Table 3.1 below summarizes the total meridional transports along the y-axis of coarse and fine sediment integrated in time and in space for the two events HC1 and DS1 at the sections A and B. Positive transport is towards north and negative transport is towards south.

		EVENT	
		HC1 (Scirocco)	*DS1 (Bora)*
SECTION	*A*	Coarse Sediment: -994 tons	Coarse Sediment: -6246 tons
		Fine Sediment: -1427 tons	Fine Sediment: -3127 tons
	B	Coarse Sediment: 3671 tons	Coarse Sediment: -25894 tons
		Fine Sediment: -798 tons	Fine Sediment: -9887 tons

Table 3.1: Fine and coarse meridional transport of sediment at sections A and B for the events of Bora and Scirocco, respectively DS1 and HC1.

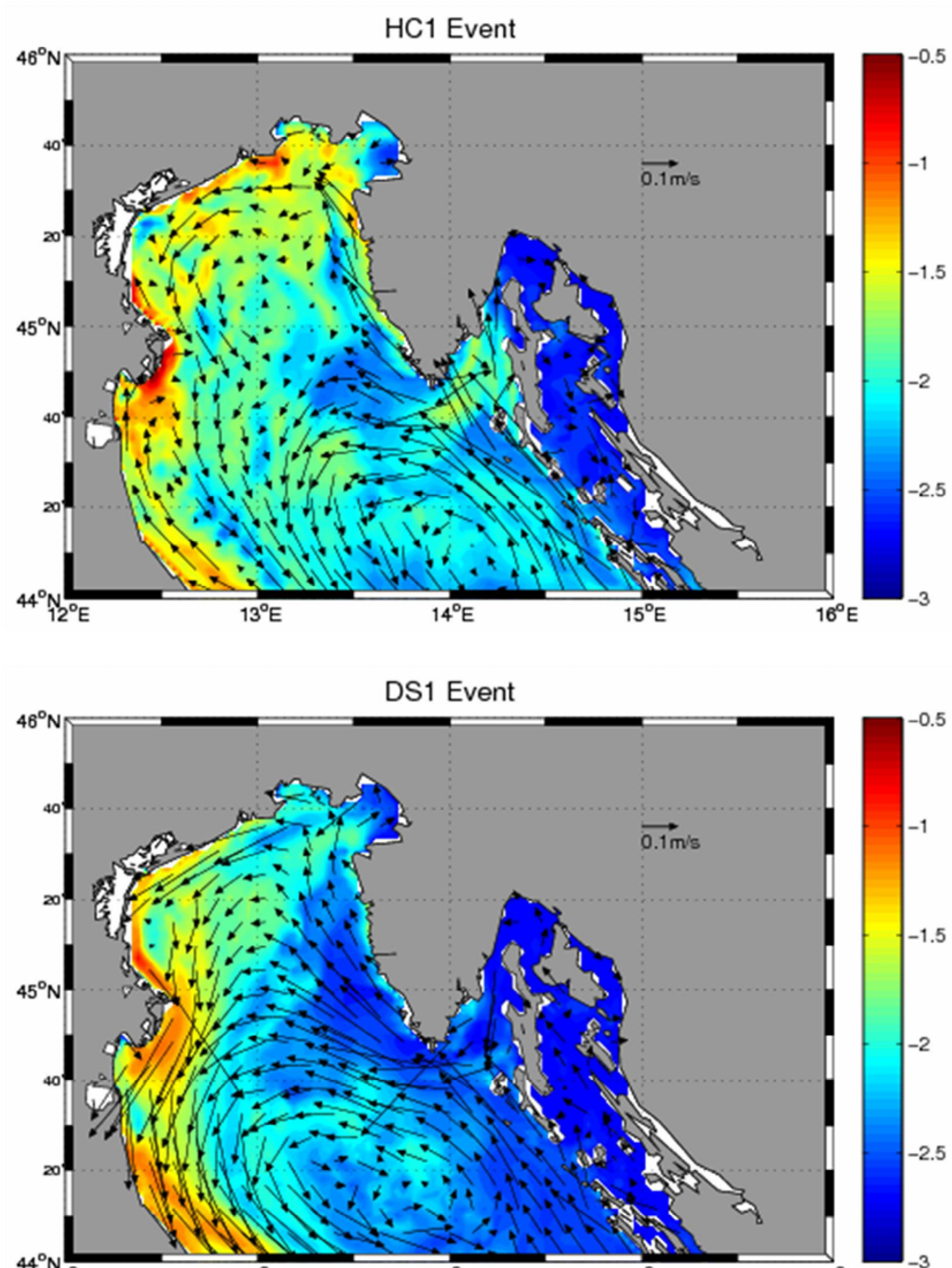

Figure 3.14: Modelled depth averaged currents (black arrows) and sediment concentration for the HC1 and DS1 events. The hourly modelled data have been time-averaged over the duration of the events.

Figure 3.14 shows the modelled depth averaged currents and sediment concentration for the HC1 and DS1 events, where the hourly data have been time-averaged over the duration of the events, respectively from November 13 2002 at 11:00 p.m. to November 14 2002 at 7:00 p.m., and from January 7 2003 at 00:00 to January 7 2003 at 8:00 p.m. During the event if Scirocco the cyclonic circulation of the northern Adriatic is weakened by the effect of the winds acting on the opposite direction of the more usual circulation. In particular the very coastal circulation is reversed up until the Po river delta, and the transport is northward, contrarily to what happens during the Bora event, when the cyclonic circulation is enhanced and its intensity along the western coast is up to 3-4 times that one we experience during Scirocco. Also the distribution of the sediment concentration presents different characteristics related to the forcing winds: during Scirocco we have a higher concentration all around the Po delta promontory than during Bora, but at the same time the very high values of suspended sediment concentration are more confined towards the river's delta, while in the Bora event the high concentrations are localized on a larger coastal strip. Scirocco wind conditions, though, are responsible for a more diffused and spread resuspension of the solid matter, also at higher bathymetries, and more towards the central part of the northern area of the basin. In general, strong Bora events tend to affect the sediment transport of a more confined portion of the northern basin, concentrated along its western coast, and the horizontal gradients of currents, sediment concentrations and horizontal sediment fluxes are much more pronounced, while the events of Scirocco tend to smooth these gradients, especially those of sediment concentration.

3.4.3 Depositional patterns in the Buna-Bojana coastal area

The Buna/Bojana (fig 3.2) river is the second largest freshwater runoff supplier to the Adriatic Sea basin. The river is situated in the transboundary region of Albania and Montenegro, and, as a result of the Project Adricosm-Star, funded by the Italian Ministry for Environment, Land and Sea, the surrounding coastal area is very sensitive to sediment transport, and very interesting to be investigated under this point of view. Moreover, this marine region has never been studied, to our knowledge, in terms of sediment transport and sediment depositional patterns earlier.

In the year 2003 the sediment transport model described above has been coupled with a river model of the Buna/Bojana river, developed in the framework of the Project Adricosm-Star, with the intent of analyzing the depositional patterns of this coastal area. Figure 3.15 shows the time-series of the river solid flow at the two branches of its delta. The conversion from solid flow to flux of sediment has been done dividing the solid flow by the density of the sediment, considered to be 1700 kg/m^3.

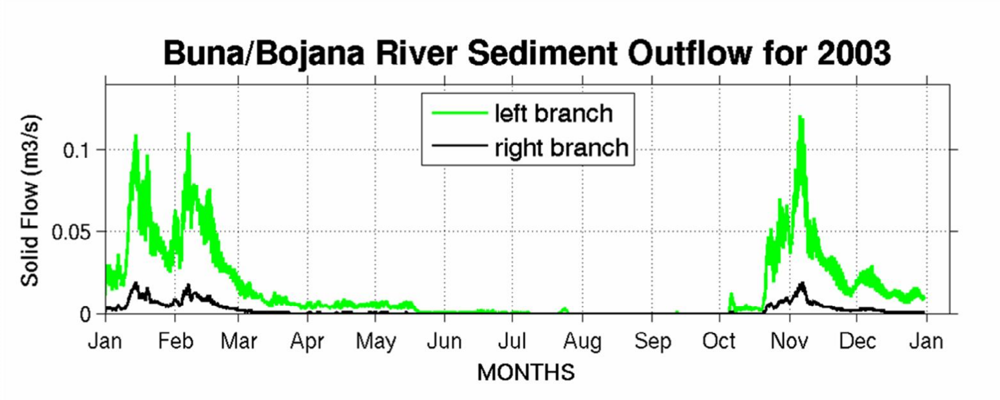

Figura 3.15: sediment supply simulated for the Buna/Bojana river for the year 2003 with the model MIKE11. The sediment input is shown in terms of solid flow (kg/m^3 of suspended sediment) per each one of the two branches forming the river delta.

The sediment transport model coupled to the Buna/Bojana river model was integrated for the year 2003, and figure 3.16 shows the results of the integration in the area of interest in terms of sedimentation (kgm^{-2}) averaged over the entire year. The figure shows two clear depositional areas marked with red ellipses (labelled *1* and *2*). One of them (*2*) is situated some 40/50 km offshore the coast, a north-west of the river delta, while the other one (*1*) is located along the coast towards the Bokakotorska Bay. Beside these two important depocenters predicted by the sediment model, the whole coastal area surrounding the Bojana River delta and the Bay of the Drinn appear to be an area of deposition for the sediment coming from the river. Unfortunately the results of the sedimentological analysis on the cores collected along the coastal area of Montenegro collected during the Project Adricosm-Star are not ready yet to support the presented model results.

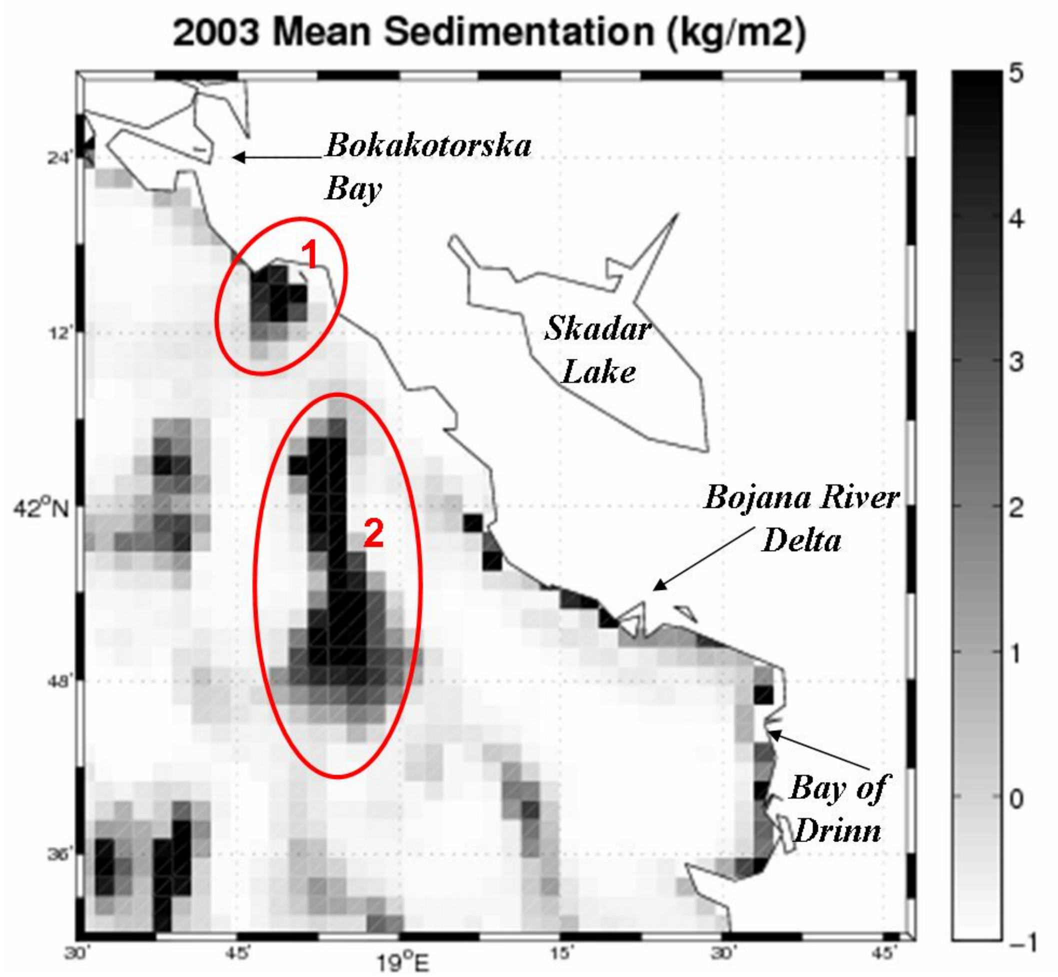

Figure 3.16: Pattern of mean sedimentation (kg/m2) for the year 2003 in the coastal area of Montenegro and Albania. White is erosion, while black is deposition.

3.5 Summary and conclusions

In the present chapter the integration of an Ocean General Circulation Model, based on the Princeton Ocean Model (Blumberg and Mellor, 1987), with a wave model (SWAN) and a sediment transport submodel was described. The sediment transport submodel consists of the back-bone of the model implemented and described by Wang and Pinardi, 2002, and by Wang et al. (2006), which has here been upgraded in terms of space resolution, and corrected in the formulation of the bottom sediment fluxes parameterization. The coupling between the dynamics and sediment models with the wave model is done off-line, meaning that firstly the waves are separately simulated on the entire domain of the OCGM (Ocean General Circulation Model) for the needed period, and then the parameters needed for the sediment transport model (i.e. wave direction, period and bottom orbital velocity) are taken from the OGCM as an input. The coupling is done at the same time resolution as the wind field, which in this case is 6 hours, then the wave parameters are linearly interpolated in time to fill in the temporal gaps. The integration of the sediment submodel with the dynamics model, on the contrary, is done on-line, and the coupling is done at each internal time step of the OGCM.

The parameterization of the combined wave-current interaction is based on the theory of Grant and Madsen, 1979 and 1986), while the parameterization of the bottom boundary layer fluxes of sediment was based on the theory of Ariathurai and Krone (1976) for non-cohesive solid matter, and has been corrected to limit the vertical fluxes at the sea/bottom interface, and to make them more realistic. Some assumptions besides that of non-cohesiveness of the sediments have been assumed, such as the Newtonian behaviour of the fluid, and the non dependency of the water density from the suspended sediment concentration. Moreover the sediment simulated was gathered into two only classes of grains, according to their dimensions: a finer class with diameter of approximately $17\mu m$ and setteling velocity $w_s=10^{-5}\ m/s$ and a coarser class with diameter of $55\mu m$ and setteling velocity $w_s=10^{-4}\ m/s$. These two classes have been considered equally contributing to the sediment supply from the rivers, and equally present in the bottom. These numerous simplifying assumptions are most likely behind some of the problems evidenced by the integrated model.

The model has been tested on an a realistic integration of one and a half years between August 2002 and December 2003, and the period of time corresponding to the big flood of the Po river of November-December 2002, and the successive moths, particularly interesting for the occurrence of particularly strong events of Bora and Scirocco have been analyzed. The model has been validated by means of comparison with available data on sediment concentration along the water column at high frequency (hourly) in a very coastal location near the Po river, and with published literature on these events.

First of all, in spite of the very low time and space frequency of the wind data (ECMWF, 6 hours, 0.5° horizontal resolution) forcing the wave model, the wave input provided to the sediment submodel proved to fid considerably well the wave bottom orbital velocity, necessary for a correct estimate of the maximum bottom shear stress. It was shown that the model is very sensitive to this input, and relatively small misprediction of the wave field can cause high errors in the estimate of the bottom maximum combined stresses, which is reasonable, considering the nonlinearity of the processes.

The simulated maximum bottom stresses, compared to those simulated by a 1-dimensional bottom boundary layer dedicated model, seem quite realistic, confirming that its parameterization and the estimate of the combined wave-current fiction factor work well. It is to be noted here that the coupling with the waves dos not only affect the resuspension of the sediment, but also the hydrodynamics part of the model. In fact the activity of the waves on the bottom boundary is responsible for an increased bottom roughness, and consequently for an increase in the bottom drag coefficient, which acts directly on the currents, changing the vertical profile of velocities. A supplementary analysis, not shown here has been undertaken to see the impact that the introduction of new physics and new processes on the bottom boundary layer, and particularly affecting the bottom drag coefficient, could possibly have on the representation of tides, but the result of the analysis, conducted on the years 2003 and 2008, showed that the differences in the estimate of tidal amplitudes and phases around the Adriatic Sea obtained by the wave-coupled model and by the uncoupled model are negligible. The quality of the tidal estimates remains than unchanged with the increase of the complexity of the model.

The validation of simulated sediment concentration and fluxes along the water column during Autumn 2002 and Winter 2003 showed that our model is capable to represent the major dynamics of sediment transport at sea, and to reproduce well the strong storm events in regions of very strong sediment activities, such as the depocenter around the Po river.

The high concentration events (fig. 3.6), i.e. those events were the near bottom concentration at the bottom are of the order of magnitude of several g/l, but confined in the first centimetres above the bottom are represented worse thank the diluted events: the very high near bottom concentrations, within the first 10 cmab, are impossible to be represented due to the vertical model resolution, causing a lack of sediment near bed, while the vertical mixing seems too strong, and probably the characterization of the sediment grains not accurate enough, in fact the modelled sediment concentrations along the water columns are too homogeneous compared to observations, where we have a much stronger vertical gradient of concentration (values up to 50 g/l at the bottom and 10^{-2} - 10^{-3} g/l at the surface). For these reasons the DS events, much more diluted in the water column and presenting much less pronounced vertical gradients of suspended sediment concentration are much better represented. Events DS1 and DS4 are well represented, while DS2 and DS3 are under-estimated. The reason of this underestimation can probably be found in the lack of available material for erosion, not in problems in the parameterization of sediment flux at the water-sea bottom.

The other big issue of sediment transport beside the correct representation of the sediment concentration, is related to sediment fluxes, which strongly depend on this latter, but also on the velocity fields. Particularly problematic under this point of view are the events HC2 and HC3, where the direction of the modelled transport is opposite to that one of the observed transport. These errors, combined to the overestimation of the concentration of suspended sediment, which this time can also be addressed to a wrong wave field, and consequently to a wrong maximum combined bottom stress (cfr. figg. 3.2 and 3.5), are responsible for a the very high misprediction of sediment transport of the event HC3. A part from this episode totally missed, though, the transport of the model, both along and across shore proved to be very similar to the estimated measured transport. So, ff we only consider the period from mid December to May, so excluding these HC events, the modelled values of cumulative vertically integrated transport along shelf are very similar to those observed (1656 kg/cm and approximately 1200 kg/cm respectively).

This analysis seems to present a reliable model of sediment transport, but what is very important to be noted is that all the modelled data of sediment fluxes and of sediment concentration fit much better the observations if we only consider the modelled coarse sediment (*d=0.055 mm and* $w_s = 10^{-4}$ *m/s*). In fact if we consider the sum between coarse and fine sediment we always have a background value ranging between 0.01 and 0.05 g/l, due to fine sediment which is always in suspension, and that we do not see in the observed data.

The analysis of the yearly accumulation rates (fig. 3.11) leads us to the same conclusions on the limit of the presented model:

1. the erosive component of the model is too strong, and not well balanced between the two different grain classes;
2. a very simplified representation of the sea bottom such as the one presented, combined with the several assumptions adopted (constant critical shear stress for erosion in time and space, and equal in magnitude for all the classes of sediment considered) is not enough to be able to reproduce correctly the long timescales of sediment transport, such as maps of erosion/deposition patterns, at least far away from important sources of sediment.

We believe that these problems can only be solved introducing two important correctionsto the sediment model:

1. Introduce a variable critical stress of erosion both in time and space, inversely dependent on bathymetry, and directly dependent on the compacting time of the sediment available for erosion;
2. Formulate a sea bottom submodel considering the use of an active layer with variable thickness where the deposited sediment is available for erosion, also related to the granulometry of the solid matter.

Chapter 4

4. *CLIMATE IMPACTS ON THE COASTAL CIRCULATION FOR THE PERIOD 2001-2030*

4.1 **Introduction**

It has been recently accepted by the majority of the scientific international community that the Earth has been going through a period of observed global warming, whose effects are obviously reflected on the climate of the atmosphere and of the oceans, so much related with each other. The impossibility of the science of climate to recreate ad-hoc experiments that can be scientifically approached and studied, and the big uncertainties that the science of climate still has to face, together with political and socio-economical issues, strongly contribute to make it still not fully accepted and quite controversial. Nevertheless, though, both the scientifical and the non-scientifical communities are starting to accept more and more the instruments that science has in order to investigate the future dynamics and main issues on the planet's changing climate and on all the practical effects that this may lead to: rise of the sea level, change in the intensity and distribution of storms and precipitations, change in the duration of intense events, increase of desertification of the southernmost parts of Europe and northernmost parts of Africa, etc..

For what concerns Europe, a general trend of increase in air temperature is well consolidated and shown, of up to 0.9°C in the XX century (Jones and Moberg 2003), even if recent periods generally show much higher trends, of up to 0.41°C/decade in the period 1979-2005 (Jones and Moberg 2003). In general temperatures are expected to increase more in extreme seasons, such as winter and summer, and between these two more in winter than in summer (Jones and Moberg 2003), and the increase in maxima on a yearly basis will be much more evident in Central and Southern Europe than in Northern Europe (Räisänen et al. 2004, Kjellström et al. 2007), and the trend seems to be related to the increase of hot extremes more than to the decrease of cold extremes (Tank et al. 2002, Tank and Können, 2003).

In terms of precipitations the expected projections for Europe show a general decrease in the eastern part of the Mediterranean basin, and substantially non detectable variations in its western side (Norrant and Douguedroit, 2006) even if an increase of precipitation per wet day is detected in most of the basin. According to Beniston et al. (2007) both heavy summer and winter precipitations will decrease in the southern of Europe, and increase in its northern regions, and this, combined with the increase of frequency, intensity and duration of heat waves (Beniston et al., 2007) will cause Mediterranean droughts to start earlier during the year and last longer, especially in the most affected regions, such as the Alps, Southern Greece, Spain and Portugal and the south-eastern Adriatic basin. Generally the response to temperature and heat waves are quite consistent from model to model, while the response to other parameters such as precipitations or winds seem to be more dependent from the model used for their estimates (Beniston et al., 2007).

All these changes in atmospheric conditions, among which the most commonly accepted and consolidated is the general increase in the air temperature over the majority of the Mediterranean domain and in all the seasons of the year, will likely be responsible for several effects on the ecosystems and on the socio-economical texture of society. This is why a future-oriented, scientifically based Integrated Coastal Zone Management (ICZM) is of fundamental importance to correctly approach the planning of the natural resources and of the possible mitigations to the changes that climate will bring in the near future. This is possible only by means of numerical simulation models.

The approach to the study of climate changes through numerical models has started on a global scale, and was developed on this scale until the models were able to reproduce fairly well the main climatic characteristics of the recent observed climate. Once this was achieved, thanks to the higher computational resources available, the space resolutions of the models have significantly increased, with a very positive impact on the models' results, which started to acquire an always increasing robustness and reliability. Moreover, the practical interests to climate change follow a local nature more than a global one, and these are the reasons why the next step in the study of climate changes brought from a global approach to a local approach. This has been possible in the atmosphere through numerical downscalings, which allow to capture and reproduce higher and higher spatial scales, together with the associated physical processes. The regionalization of the climate models in the ocean to investigate the local sea responses to climate change impacts is, on the contrary, something still very new, which we consider to be in the frame of pioneering activities in the field of oceanography and connected to climate studies, and it will be the object of the present and of the next chapters of this thesis.

The other very important way of approaching the problem of how realistic and reliable a platform of climatic ICZM can be, beside the local approach, is related to the integration of numerical models with each other in order to be able to simulate the hydrological water cycle in more and more realistic ways. In the present chapter the attention will be focused on the integration of atmospheric, hydrological, river and ocean circulation models under the conditions of one of the scenarios of climate change of the *International Panel on Climate Change* (the so called *A1B* scenario), in order to evaluate the impact that climate change has on the sea circulation and main parameters, such as temperature and salinity. Such an integration of models was undertaken in the study area of Albania and Montenegro (fig. 4.1). This is a region still not very much investigated, but very interesting from a hydrological point of view, where, in particular, the Buna/Bojana river plays an important role for the circulation and for the sediment transport at sea, with the second highest average flow of the Adriatic Sea basin, of approximately 675 m^3/s. In chapter 4.2 the integration of the different numerical models – implemented and simulated within the framework of the project Adricosm-Star (funded by the Italian Ministry for Environment, Land and Sea) by other project partners - will be presented together with the configuration and general conditions of the OGCM forced under climate change conditions, while in chapter 4.3 a brief overview of the single integrated models forcing the ocean model will be given. In chapter 4.4 the reliability of the climatic ocean circulation model will be assessed through its validation versus observed data, while the overview of the results in terms of changing in circulation, temperature and salinity due to climate impacts is given in chapter 4.5. We summarize the work done and present the main scientific conclusions in section 4.6.

Figure 4.1: Study case area of Montenegro and Albania regions where the integration of atmospheric, hydrology, river and ocean models took place.

4.2 Climate coupled integration in the time window 2001-2030 under the *A1B IPCC* scenario

4.2.1 Description of the 2001-2030 integration

To investigate the changes of circulation, temperature and salinity due to the impacts of climate changes, the Adriatic REGional model described in Chapter 2 (i.e. general circulation model coupled with tides) has been integrated for 30 years, in the time window 2001-2030. This climatic integration is the result of a chain of numerical model couplings, schematized in figure 4.2.

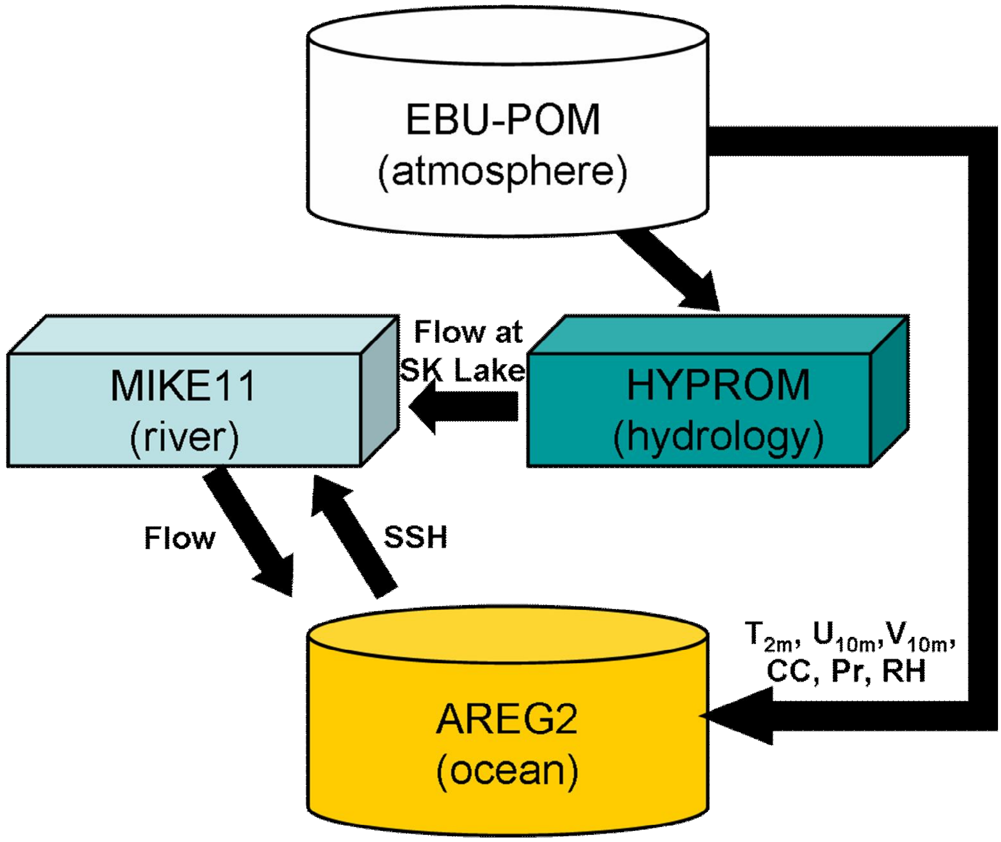

Figure 4.2: Scheme of coupling of numerical models used in the scenario simulation. CC, Pr and RH stand respectively for cloud cover, precipitation, and relative humidity. SK stands for Skadar.

The atmospheric forcings are the core of the climatic couplings (upper compartment of figure 4.2). They are provided by the integration of the EBU-POM coupled (ocean-atmosphere) model that downscaled the *A1B IPCC* scenario from the SINTEX model (Gualdi et al. 2003b, Gualdi et al. 2008) at global scale to a Mediterranean regional scale. The dynamical downscaling allowed to reach a horizontal resolution of 0.25° on the regional downscaled atmospheric model, starting from a horizontal resolution of 1.125° of the global model. The frequency of the atmospheric forcings is of 6 hours. The land compartment that links the atmosphere with the ocean (central compartment of figure 4.2) was modelled by means of two more numerical models:

- The atmosphere-hydrology coupled system "HYPROM", which simulated the complex surface and sub-surface hydrology of the Skadar Lake and of its upstream hydrological catchment, by taking in input the necessary data from the EBU-POM model, downscaled once more at a higher horizontal resolution, and giving as output the flow (m^3/s) at starting cross section of the Buna/Bojana river, i.e. the outflow of the Skadar Lake (red dot in fig. 4.1).

- The MIKE11 model, which simulated at a very high resolution (approximately 200 metres) the flow of the Buna/Bojana river from the Skadar Lake all the way down to the outflow in the Adriatic Sea, taking in input the output of the hydrological model (in terms of flow, m^3/s), and as downstream boundary condition the sea surface height provided by the ocean model. To do this the ocean model was simulated twice: first without being coupled with the river, in order to provide the SSH at the river's mouth, and then being coupled with the river outflow.

For what concerns the oceanographic model AREG2 the general configuration and conditions of the climatic simulation under the A1B scenario of the IPCC are summarized in table 4.1. The model has been initialized in January 2001 from instantaneous conditions of the model used for integration INT1 described in Chapter 2. The river flows used in input as lateral conditions are the monthly climatological means from the climatology of Raicich (1996) as modified according to the variations presented in Chapter 2, except for the Bojana river. For this river the climatological monthly means have been used until the year 2019, then for the last 10 years of the scenario simulations the model was coupled off-line with the river model MIKE11, implemented and validated in this implementation by the private company S.G.I. SPA

Experiment conditions

Time Frame	Jan 2001- Dec 2030
Model	AREG 2km with tides (POM based)
Initial Conditions	AREG2 interannual simulation
Bojana River Runoff	Observed monthly clim. (2001-2019) Hourly Modelled data (2020-2030)
Other Rivers' Runoff	Raicich modified climatology (2001-2030)
Atmospheric Forcings	EBU-POM Atm Model (0.25°)
IPCC Scenario	A1B
L.O.B.C	MFS Daily Climatology (1998-2008)
Output Frequency	Daily (Daily Means)

Table 4.1: General conditions of the climate change scenario integrated simulation of the ocean model AREG2.

As for the hydrological and river models, the atmospheric forcings are those of the coupled climatic regional model EBU-POM, implemented on the entire Mediterranean Sea. In the next chapter a brief overview of the data forcing the ocean model will be given. Lastly, the open boundary conditions used for the integration of the OGCM were a daily climatology of the Mediterranean Forecasting System data (Tonani et al.) 2008 calculated over the period 1998-2008.

4.3 **The forcings of the circulation model**

4.3.1 The atmospheric model: EBU-POM

As anticipated in chapter 4.2 the atmospheric forcings are the core of the integration of climate change scenarios, since all the models of the integrated system schematized in figure 4.2 are forced by them.

EBU-POM is an air-sea coupled regional climate model, in which the atmospheric component is composed of the limited area model developed by Janjic, and detailed model description can be found in Janjic (1977, 1979, 1989, 1990, 1994, 1999) and Mesinger et al. (1998), while the oceanographic component consists of the P.O.M. model (Blumberg and Mellor 1986). The two models are two-way coupled, and their interaction takes place every time-step of the atmospheric model (approximately 180 seconds). In this implementation the atmospheric model is resolved over the domain with a horizontal resolution of 0.25°, on 32 vertical levels, up to 100 mb, while the ocean model has 21 σ-layers on a horizontal resolution of 0.2°. The model uses as lateral open boundary conditions the output of the global model SX-G, which is composed of ECHAM4 (Rockner et al., 1996) at 1.125° of horizontal resolution and 19 vertical levels in the atmosphere, and of OPA (Madec et al., 1998) at 2° of horizontal resolution on 19 vertical levels in the ocean. Figure 4.3 (courtesy of V. Đurđević, University of Belgrade) represents the domains of the two models, where the dark blue region refers to the ocean component, and the light blue region to the atmospheric component.

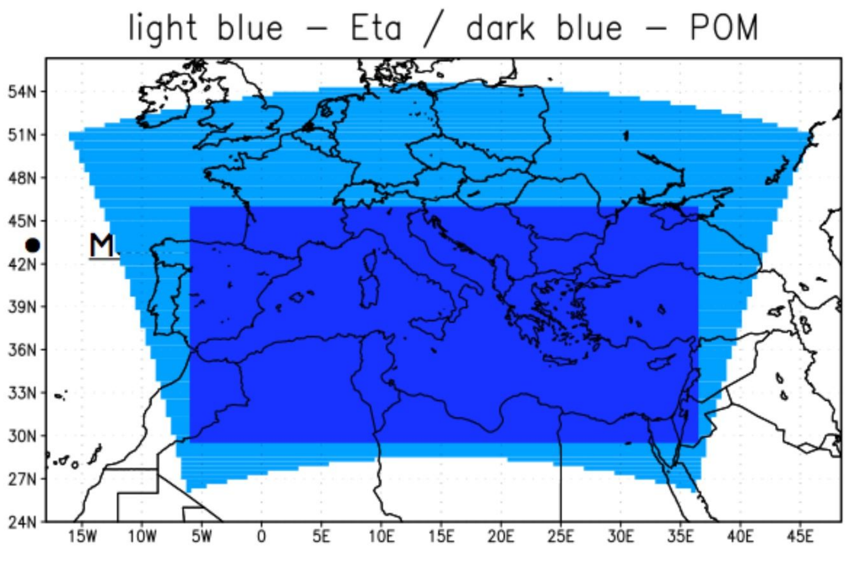

Figure 4.3: Domains of the coupled air-sea regional model EBU-POM. This image is a courtesy of V.Đurđević, University of Belgrade.

For the climate future scenario simulations the atmosphere was assumed to have a constant composition, and the greenhouse profile used was that one of the A1B scenario of IPCC, which assumes an increase in equivalent CO_2 of approximately 70% in the period 2000-2030 (which corresponds to an increase of approximately a factor 2 from the beginning to the end of the 21st century). Figure 4.4 shows the evolution of the equivalent concentration of CO_2 in the atmosphere for some of the IPCC scenarios. The A1B scenario is represented with the magenta curve.

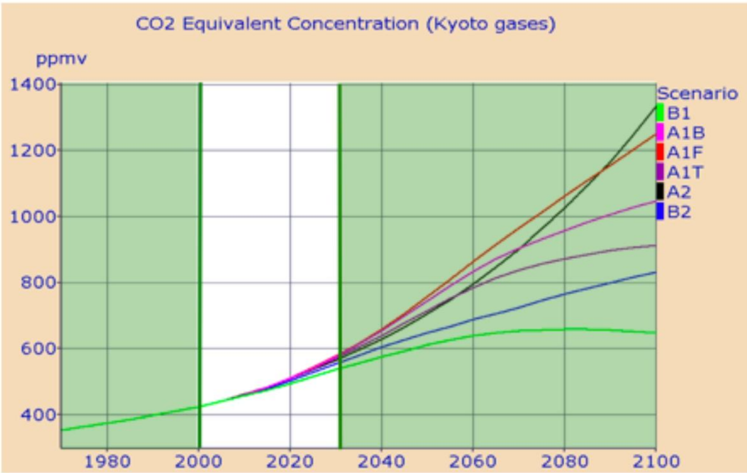

Figure 4.4: Equivalent concentration of CO_2 in the atmosphere for some of the IPCC scenarios. This image is a courtesy of V.Đurđević, University of Belgrade.

The results of these atmospheric simulations (Djurdjevic, V., and Rajkovic B. 2010), undertaken by the University of Belgrade in the framework of the Project SINTA (http://www.earth-prints.org/bitstream/2122/4675/1/SINTA_FInal%20Science%20Report%20_October%202008.pdf) and Adricosm-Star (http://gnoo.bo.ingv.it/adricosm-star/) showed the following major results:

- A general increase in the air temperature over the whole Mediterranean Sea region. Over the Adriatic Sea the increase of temperature for the period 2001-2030 with respect to the period 1960-1990 referred to the whole year is of approximately 0.6°/0.8° (see fig. 4.5, left panel). The increase is much higher in summer than in the other seasons, when the highest variations reach values up to 1 degrees in the northern and central regions of the Adriatic Basin.

- A general decrease in the annual precipitation with respect to the same period (1960-1990). The decrease in the Adriatic basin ranges between 5 and 10% (see fig. 4.5, right panel).

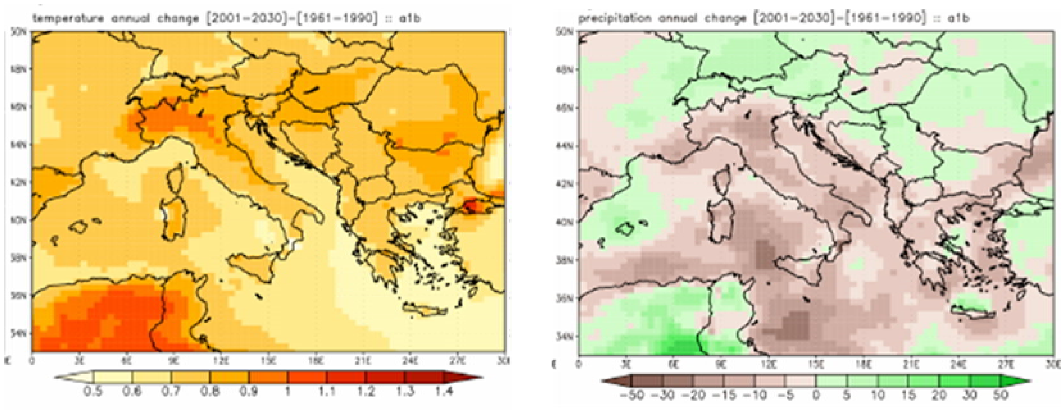

Figure 4.5: Air temperature at 2 metres and precipitation changes (left and right) over the Mediterranean Sea for the period 2001-2030 with respect to the period 1960-1990. The data are referred to the whole year period. This image is a courtesy of V.Đurđević, University of Belgrade.

The atmospheric model and data concerning the climate simulations used for the present work have been implemented and produced by researchers of the University of Belgrade.

4.3.2 The hydrological coupled model: HYPROM

The HYdrological PRediction MOdel (HYPROM, Nicovic et al. 2010) is a coupled system (land-atmosphere) that integrates four different modules in order to produce simulation of rivers runoff. The four modules are:

1) *Atmospheric module.* The *Non-hydrostatic Meteorological Model* (*NMM* - Janjic et al. 2003) was used. In this implementation it covers the Adriatic Sea domain with a horizontal resolution of 12 km and a vertical resolution of 36 layers, covering up to 20 km;

2) *Land surface module.* The *NOAH Land Surface Model (LSM* - Chen et al. 1996*)* was used. In this implementation it covers the simulated domain with 4 layers up to the depth of 2 metres underground and, with a horizontal resolution of 1 km. Under the NMM forcing surface parameters (wind, pressure, specific humidity, temperature, precipitation, long and short wave radiation), *NOAH LSM* is using several prognostic variables: soil moisture, soil temperature, snow height, snow density and canopy moisture. The process of evapotranspiration is also included.

The most important output of this module is the surface water runoff, which consists of the portion of precipitation that can not be infiltrated into the soil because of its saturated conditions. Additional components of runoff come from the subsurface and lateral drainage of the soil moisture, mostly depending on the terrain slope. The land surface model uses 17 types of soil and 24 types of vegetation.

3) S*urface module.* This bi-dimensional module forces the surface water towards the river network under gravity and according to gradients of water height in the catchment; a full system of continuity and motion equations is applied, and friction, in both South-North and West-East directions, is controlled by the Manning's friction term. The orography, the catchment area and the river network are derived from USGS-HYDRO 1 km data set;

4) *River-routing module.* It is the last module of the integrated hydrological system HYPROM, and its main role is to govern the water motion downstream towards the catchment's outlet. This module is one dimensional, and it is also based on continuity and momentum equations.

The HYPROM integrated system has been implemented over the Skadar Lake hydrological catchment (fig. 4.1) and integrated over the period 2020-2030 to give an hourly time-series of flow (m^3/s) at the outflow location of the Skadar Lake (red dot of fig. 4.1), under climate change scenarios at the time frequency of 1 hour. The atmospheric component was coupled with the EBU-POM results for the same period of time. The Skadar Lake was not simulated with a physically based realistic lake model, but parameterized in terms of flow at its downstream section, where the Buna/Bojana river starts.

The hydrology model and data concerning the climate simulations used for the present work have been implemented and produced by researchers of the private company SEWA (South-East Weather Agency, Belgrade, Republic of Serbia).

4.3.3 The river model: MIKE 11

MIKE11 is a very consolidated commercial river model, developed by the Danish Hydraulic Institute, world widely used for simulations of river flows, sediment transport and water quality. The model, solving through finite difference the mono-dimensional equations of momentum and continuity for water, has been used for the simulation of the discharge of the Buna/Bojana river into the Adriatic Sea for the period 2020-2030. The model was forced in input at the Skadar Lake outlet with the scenario flow resulting from the hydrological integrated system HYPROM, described in chapter 4.3.2. Figure 4.6 shows the Buna/Bojana river flow at the river's delta used in the climate integration of the OGCM AREG2. As summarized in table 4.1 in the period 2001-2019 the data used are climatological monthly means (m^3/s), while the simulated scenario hourly discharge is used in the period 2020-2030.

It is important to notice how the decrease in precipitation over the Balcanic region outlined in chapter 4.3.1 is reflected in the decrease of the flow of the Buna/Bojana river in the period 2020-2030 compared to the climatological annual flow mean calculated over the years 1965-1990. This latter is in fact 646 m^3/s, while the former is 482 m^3/s.

The model and data concerning the Buna/Bojana river climate simulations used for the present work have been implemented and produced by the private company S.G.I. SPA (Studio Galli Ingegneria, Padova, Italy)

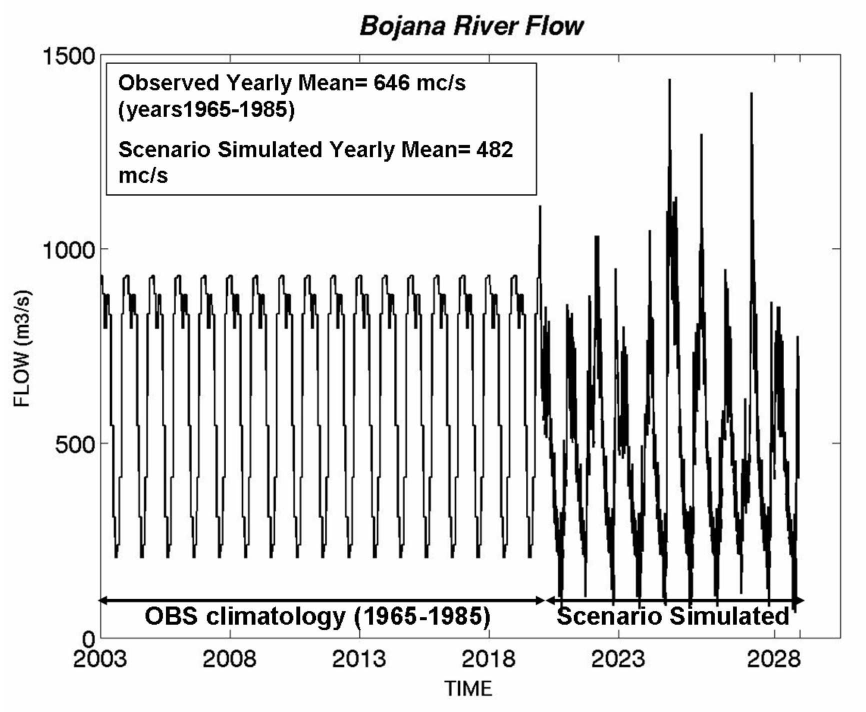

Figure 4.6: the Buna/Bojana river flow at the river's delta used in the climate integration of the OGCM. From 2001 to 2019 data are climatological (according to the period 1965-1990). In the period 2020-2030 data are the results of the scenario A1B integrated simulations.

4.4 **Validation of the climate change scenario model in the period 2001-2008**

As introduced in chapter 4.1, a very up-to-date and controversial issue concerning climate changes is related to the reliability of the climate models. Obviously numerical models have errors: atmospheric and oceanographic systems are highly multivariate, and this makes their study very complex and impossible to be solved analytically, furthermore all the simplifying assumptions in the governing equations of the systems, the errors brought by the parameterizations of some of the physical processes, by the discrete numerical approach - with all the deficiencies related to the spatial and temporal resolutions of the models – and by the errors in the boundary and initial conditions, all contribute to make the representation of the physical systems very difficult. This difficulty is surely enhanced introducing in the models the scenarios of climate change which inevitably bring more uncertainties into the systems. It is fundamental, though, that in spite of the errors they have, the climatic models are able to reproduce the general dynamics of the atmosphere and the oceans, and their general cycles.

To show the reliability of the climatic ocean model of the Adriatic Sea in the *A1B* scenario the model has been validated in terms of temperature salinity and density using the same data presented in Chapter 2.3.2. The result of the analysis is presented in figure 4.7 for the period 2002-2008 (the first year of integration was discarded since it was too close to the beginning of the integration), where the locations of the stations are presented with the black stars in the bottom map, while the behaviour of the model compared to the observations is shown in the upper profiles. From top to bottom the mean profiles (averaged in time and space), biases (model-observations) and root mean square errors (calculated according to equation (2.16)) are presented for density, salinity and temperature (left to right respectively). Observations are represented with the black line, and the modelled climatic scenario is represented with the red line. The simulated scenario results present small errors for both salinity and density, respectively smaller than 1.5 PSU and 1 kg/m^3. Such errors are in the range of errors of realistic models. Much bigger errors are evidenced in temperature (fig. 4.7, right panels). Contrarily to what happens for the realistic ocean model analysed in Chapter 2, the temperature of the scenario model has always a positive bias, meaning that the model represents always higher temperatures than those observed. The highest error is at the surface, within the first 50 metres of the water column, where it reaches a maximum value of almost 2.5°C. Also at much higher depths, however, the error is fairly large, and it is never lower than 1°C even at 200 metres of depth. It is interesting, though, to notice how the shapes of the mean temperature profiles (top right panel of fig. 4.7) are similar. This is very important from the point of view of climate change scenarios and in the perspective of the analysis of the evolution of a system in terms of relative differences – i.e. comparison of future situations with present situations - more than in terms of the exact scatter values of the main variables that describe the system itself. Figure 4.8 shows the evolution of the sea surface temperature in the period 2003-2008, by comparing the daily model data averaged over the entire domain of the basin with the satellite data, also spatially averaged. It is very important to see that the climatic model presents a positive bias of surface temperature which seems to be constant in time, without evidencing any diverging tendency trend from the observed data.

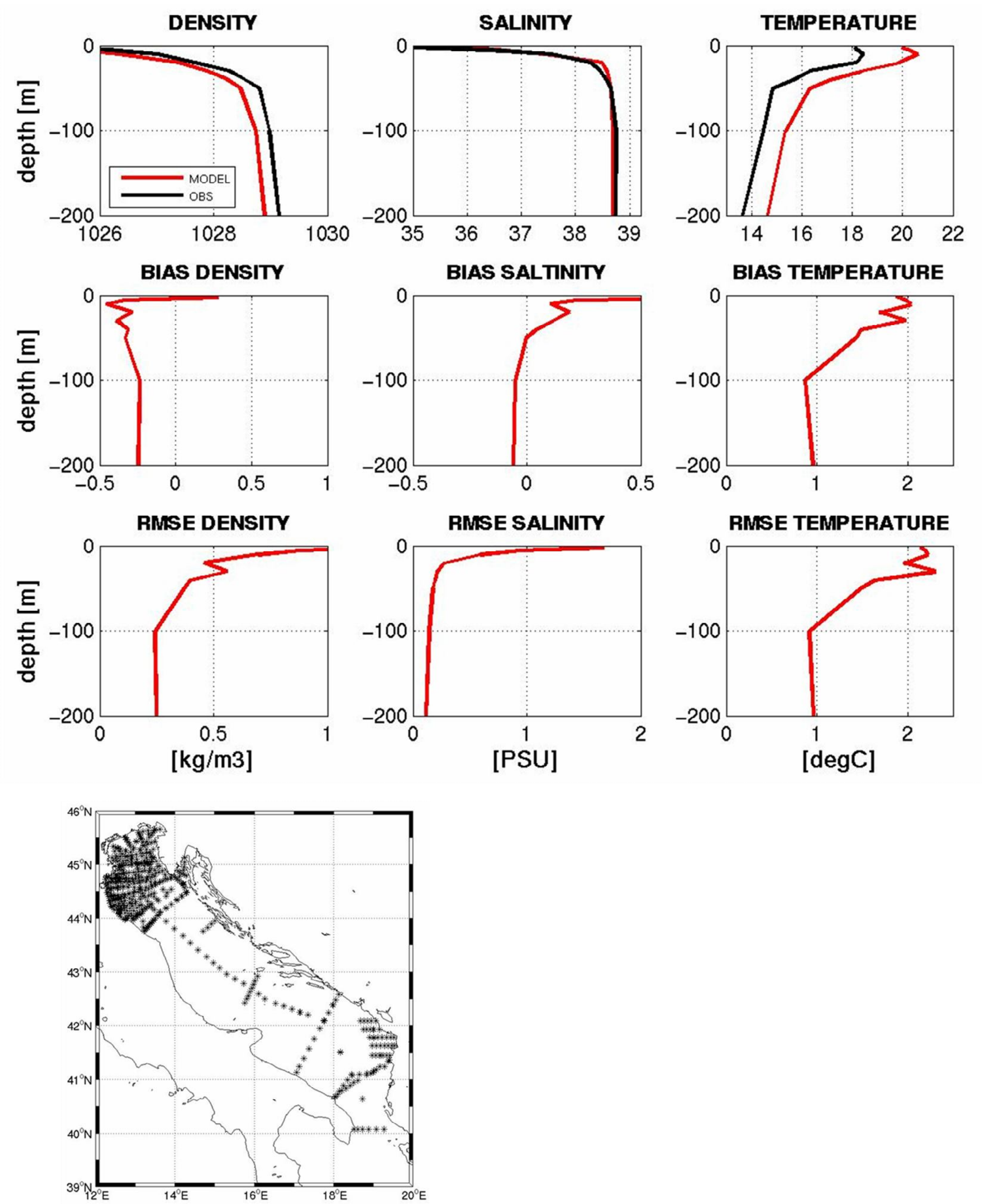

Figure 4.7: Validation of the climatic ocean model. The map in the bottom shows the locations where the data were collected (2002-2008). In the upper panels the mean profiles of density, salinity and temperature are plotted (the red is the scenario model, black is the observations), in the second and third rows the bias and rmse of the same variables are presented.

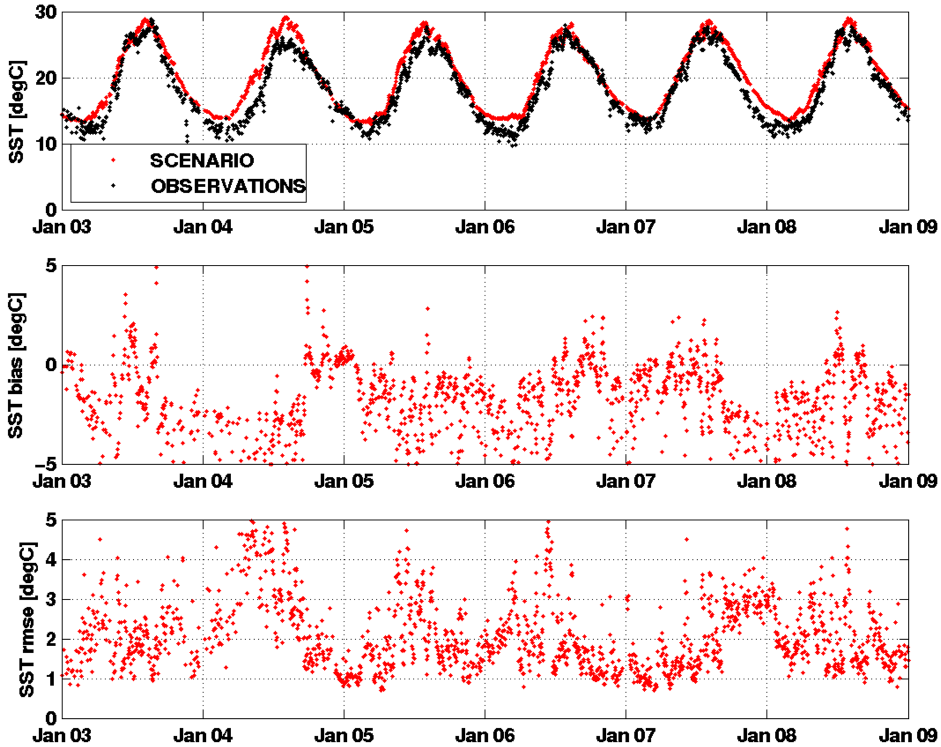

Figure 4.8: Analysis of SST (°C) in the period 2003-2008. The first panel shows the time-series of daily SST as a mean value over the entire domain. The red dots represent the simulated scenario, and the black ones the observations. In the second and third panel the bias and root mean square error are presented.

In fact the rmse is approximately 2 °C for all the years between 2003 and 2009, except for the year 2004, which presents an anomalous rmse, of approximately 2.8°C.

It is important to underline how this approach of validation of the climatic model based on day-to-day comparisons between the model and the data is different from the usual approaches of validation of atmospheric climate models, which are based on the comparison of average values of the variables over much, much longer periods, of the order of years. We believe this is a rather pioneering approach to this issue, very important from the perspective of the regionalization of the climate models.

4.5 Circulation, temperature and salinity changes in the next decades

In this section of the thesis the evaluation of temperature, salinity and circulation between the present and the future scenarios are analyzed. To carry out the analysis all the variables have been time averaged over windows of the same length: what we call "present" refers to the mean values of the variables for the period 2003-2008, while with the term "future" we refer to the mean values of the variables in the period 2025-2030. The analysis refers to the results from the ocean circulation regional model forced under the A1B IPCC scenario, as described in Chapter 4.2.

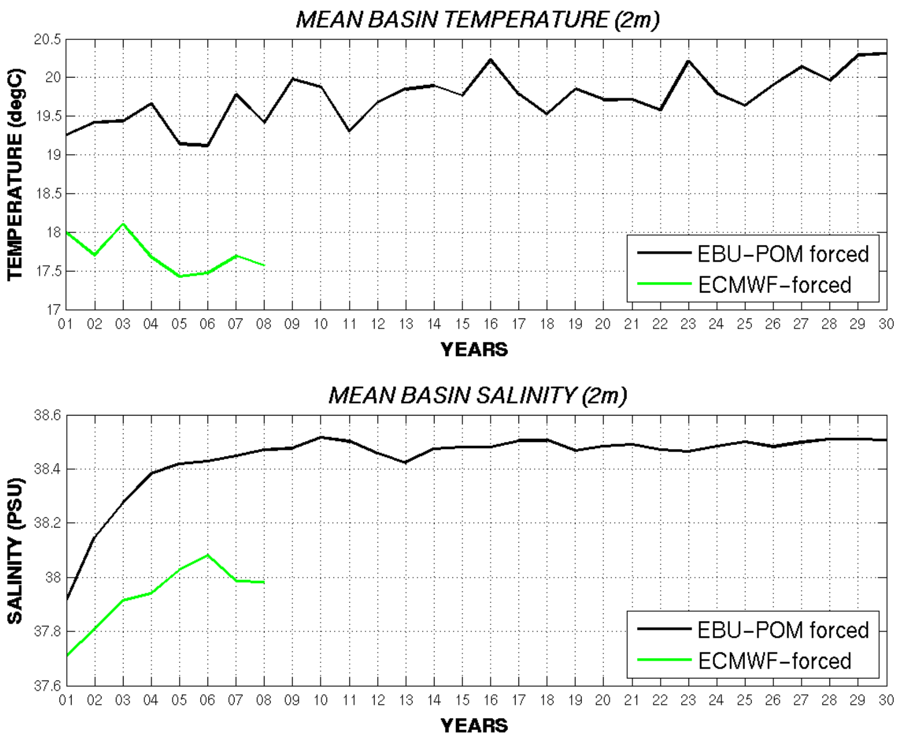

Figure 4.9: Time series of surface temperature (top panel) and salinity (bottom panel). The data are yearly averaged over the whole basin. The black lines refer to the climatic model, forced with the EBU-POM atmospheric forcings, while the green ones refer to the data of the most realistic model forced with ECMWF forcings.

Figure 4.9 shows surface temperature (top panel) and salinity (bottom panel) averaged yearly in time and over the whole basin in space from the beginning to the end of the integration. The green lines refer to the results of the ocean model forced with the most realistic atmospheric forcings of ECMWF, while the black line refers to the climatic ocean model, forced with the EBU-POM atmospheric forcings. It is very important to see how both the models have a similar behaviour in the overlapping time. This can be considered as a sort of additional validation, and again seems to hint how, beside biases, the climatic model seems to be able to capture the general dynamics and trends of the system. If we consider the first two years as spin-up time, especially for salinity, we can conclude that at a regional scale the surface mean temperature of the basin seems to have a visible trend of increase, still keeping its interannual variability. For what concerns salinity, things seem to be similar, but at a much lower trend.

Figures from 4.10 to 4.13 show the differences between the future and the present time surface fields of (from top to bottom respectively) temperature (°C), salinity (PSU), and current intensity (m/s), for the seasons of winter (Jan, Feb, Mar, Apr), spring (May, Jun), summer (Jul, Aug, Sep, Oct) and fall (Nov, Dec) respectively. The left panels show the entire domain of the Adriatic Sea, the right ones show a zoom on the coastal zone of interest for the integration of the different models. For each variable its mean value in the corresponding domain is shown (bottom left for the left panels and top right for the right panels).

As we can see from the images of temperature and salinity the boundary conditions have a very strong influence on the fields' variation, since the imposition at the open boundary consists of a daily climatology calculated in the period 1998-2008, thus is not linked anyhow to dynamics of climate change in the analyzed period. This is why the differences between the future and the present periods are always close to zero in the vicinity of the open boundary. In the calculation of the mean values of temperature, salinity and currents shown in the figures the part of the domain from 39°N to 40°N of latitude has not been considered.

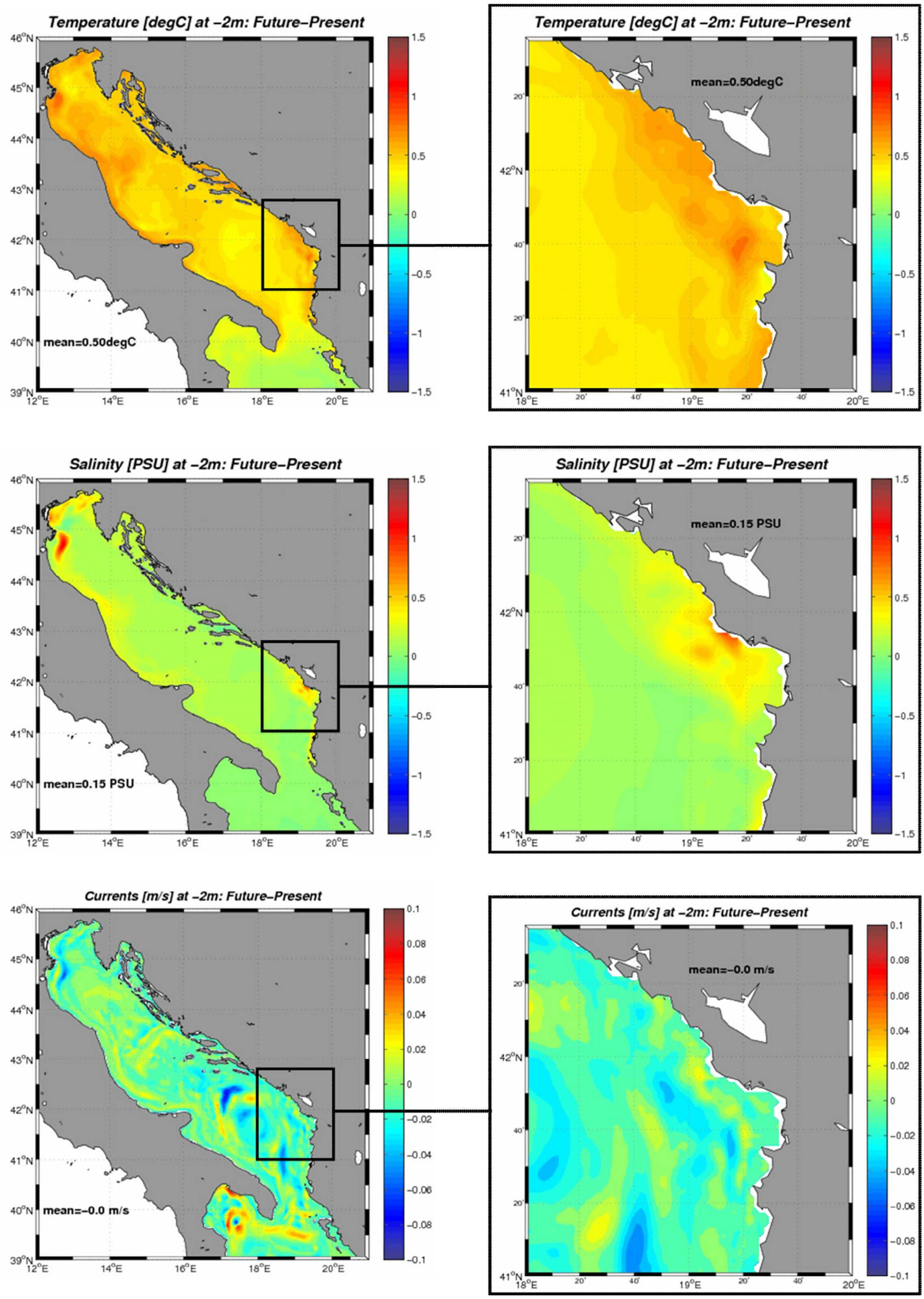

Figure 4.10; From top to bottom: maps of difference between temperature, salinity and current intensity at 2 meters for the mean winter seasons of the periods 2025-2030 (future) and 2003-2008 (present). The left panels show the results on the whole model domain while the right panels focus on the coastal areas of Montenegro and Albania.

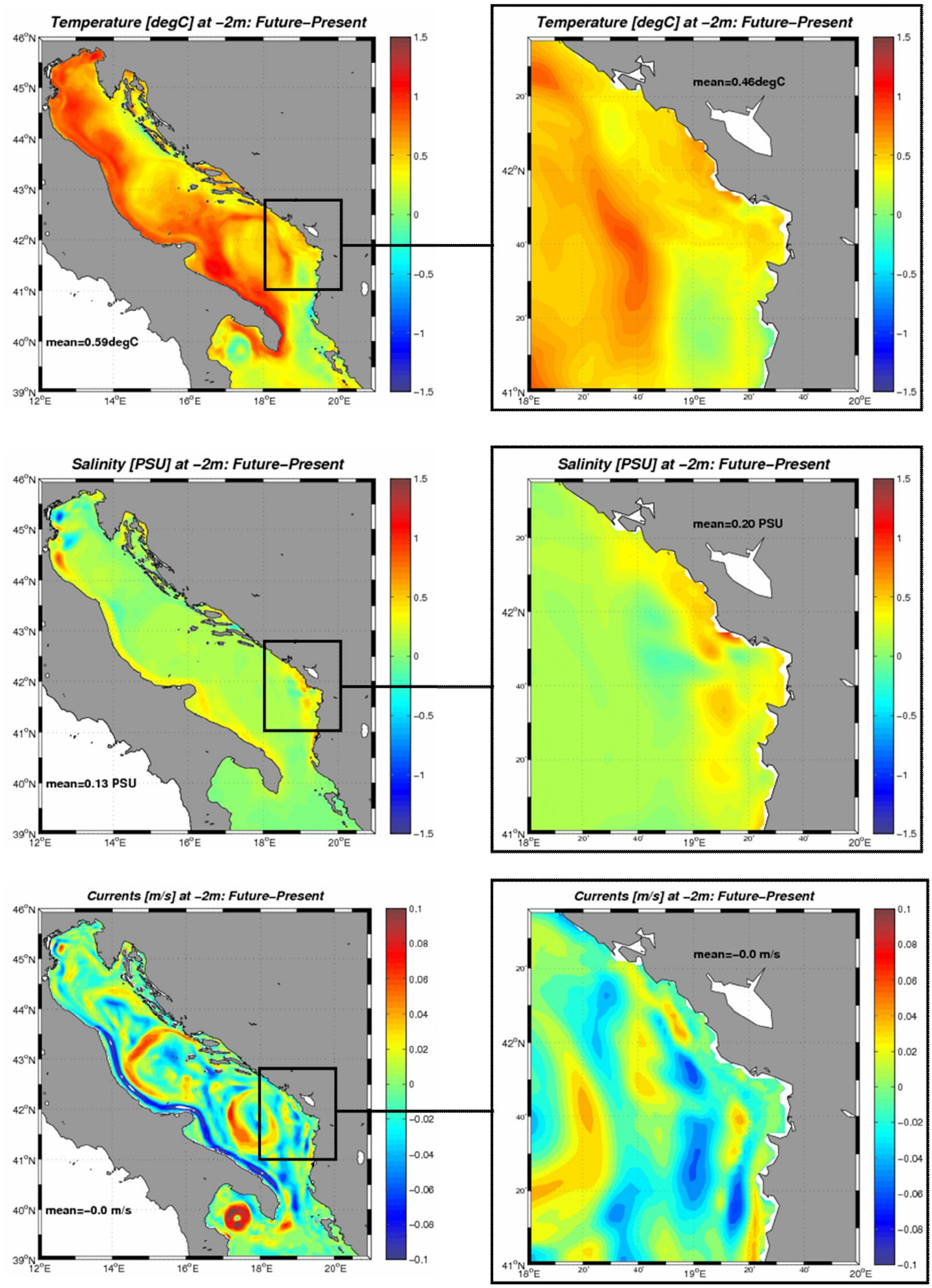

Figure 4.11: same as fiugre 4.10 but for Spring

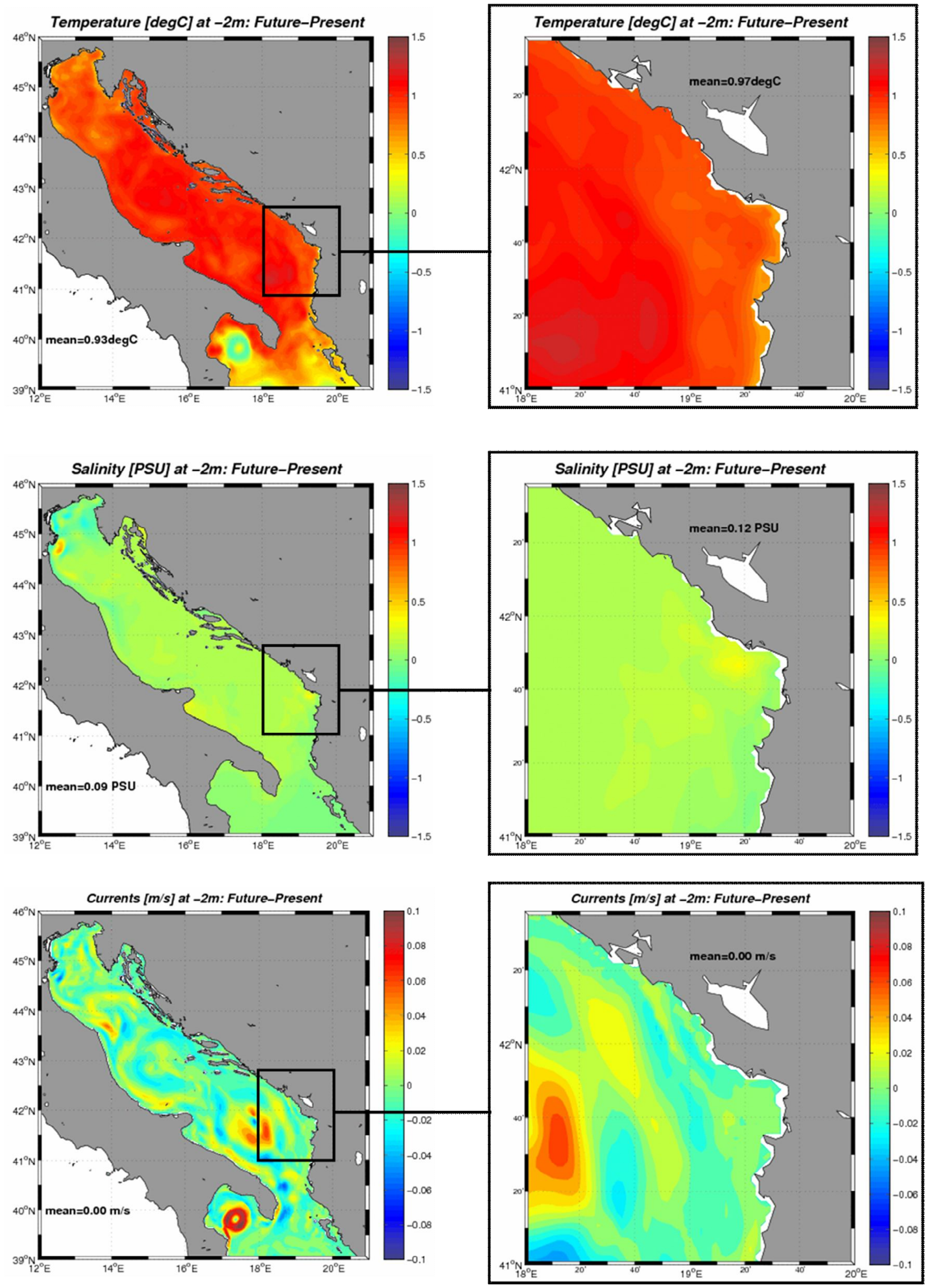

Figure 4.12: Same as figure 4.10 but for Summer

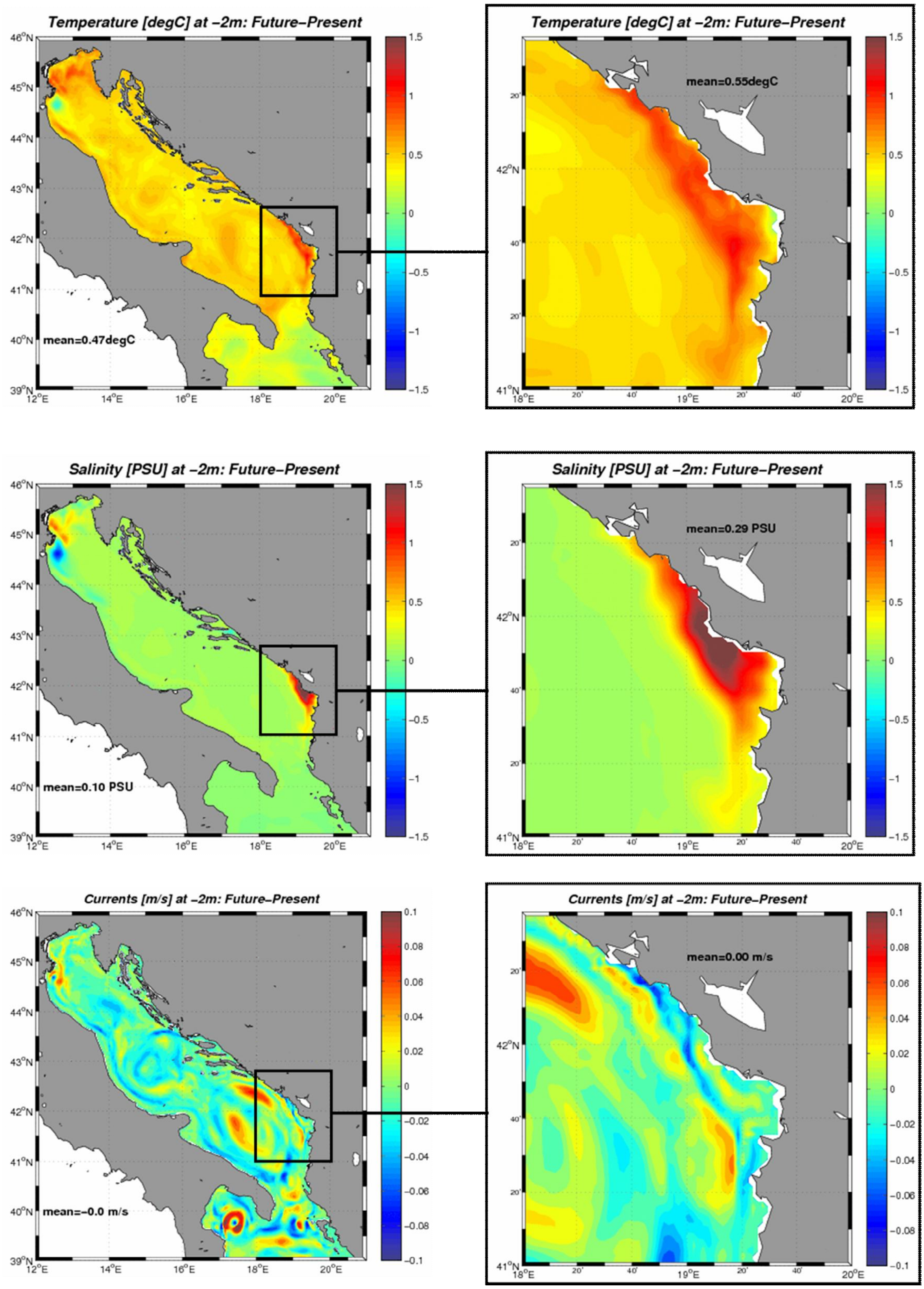

Figure 4.13: Same as figure 4.10 but for Autumn.

The clearest signal evidenced in the difference maps of figures 4.10 to 4.13 is a generalized increase in temperature all around the basin and during all the seasons of the year. As it happens in the atmospheric forcings the strongest increase in temperature is detected in summer (fig. 4.12), with a generalized increase of approximately 1 °C all around the basin. Contrarily to what happens for the atmospheric forcings the increase in temperature detected in spring is higher than the one detected in winter, and the main increases happen in the western region of the basin. The lowest warming happens in autumn, with a regional averaged value of approximately 0.5°C. An exception is the coastal zone of Montenegro and Albania for this season, where the increase in temperature reaches values close to 1°C (similarly to what happens in summer), probably due to an effect of compensation between salinity and temperature (see central right panle of fig. 4.13). For what concerns the other seasons this area behaves similarly to the rest of the basin, except for spring, where the influence of the boundary conditions intrudes this domain, reaching the latitude 42.60°N.

For what concerns salinity a generalized increase in the whole domain is detected as well in the future (2025-2030), even if the intensity of the increase is much lower than that detected for temperature. The highest variations in salinity are localized in the areas of influence of the two main rivers, Po and Buna/Bojana, and particularly high in the autumn season is the increase in the area of influence of this latter river, where salinity increases in the future scenario by up to 1.5 PSU. This very strong signal is due to the future strong decrease in the Buna/Bojana river discharge in this season compared to the climatology used for the “present” period. This might also explain the very strong increase in temperature in autumn which could be due to an effect of compensation (as anticipated ubove). It is interesting to notice a clear signal of increase in salinity along the WACC in spring, partly visible also in winter in the same area. In the portion of the basin further away from the Po river, the Buna/Bojana river and the western Adriatic coast the future scenario doesn’t present substantial differences in surface salinity compared to the present period.

Contrarily to the evolution of temperature and salinity, whose generalized surface increase in the basin is quite evident in the future scenario, currents do not present an evolution so well marked and clear. The field of difference between current intensity in the periods 2025-2030 and 2003-2008 averaged over the whole basin is approximately zero for every season of the year, both in the full domain of the a Adriatic Sea and in the restricted domain of the study case area of the costal strip of Albania and Montenegro. The clearest signal evidenced (fig. 4.11) is a strong decrease in the intensity of the WACC, of up to 10 cm/s, and a quite important intensification of the cyclonic gyres of the South and Mid Adriatic, of up to 6 cm/s in spring. A similar behavior (except for the Mid Adriatic cyclone) happens in autumn (fig. 4.13), even if the variations of the intensity of the currents are much lower than in spring: approximately 3 cm/s the decrease in the WACC intensity and approximately 4 cm/s the increase in the southern Adriatic cyclone, which is also much larger in this season than in spring.

In winter and in summer an intensification of the WACC is detected in the future period, of a couple of cm/s, while a more evident intensification of the Southern cyclone is appreciable in summer, of up to 6 cm/s.

In the coastal area of the study case region of Montenegro and Albania an interesting alternation of decrease and increase in the coastal currents is visible, especially in autumn (fig. 4.13), but also in summer (fig. 4.12), and spring (fig. 4.11).

A comparison of the patterns of the circulation (not shown here), shows that the differences in the direction of the surface flow are not very strong in the whole basin. In the Montenegrin coastal strip we can generally always detect the South Eastern Shelf coastal Current (SESC - Marini et al. 2010), which detaches a few tens of kilometers from the coast, and an eddy-like recirculation between the coast and the SESC current itself, which helps the rivers plumes expand towards offshore, both in present time and in future time.

One last comment needs to be spent on the heat flux budget (W/m^2) for the integrated period, shown in figure 4.14, as daily means over the entire basin. The variability of heat fluxes is very high from periods of maximum gains to periods of maximum loss of heat, and the amplitude of the oscillation is driven by very low episodic heat losses, more than by very high heat gains. A comparison of this result with the most accepted and consolidated heat budgets for the Adriatic (Artegiani et al. Part I, 1997, for example) evidences how the negative peaks of heat fluxes are much stronger in the present climatic integration than in the calculations estimated from datasets of the end of the 20th century. This may be a proxy of the intensification of strong winter storms, as often projected by climate change models.

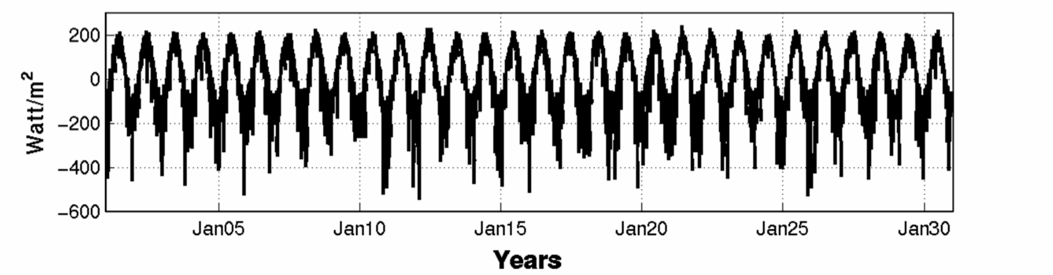

Figure 4.14: Net basin averaged heat fluxes for the period 2001-2030 under the climate change scenario A1B.

What is very important to underline is that the average budget of heat fluxes for the entire period 2001-2030 (which was calculated north of the Otranto Strait) is positive: approximately 6 W/m^2, ranging from -5 W/m^2 to 15 W/m^2 over the 30 years of integration. The climatological heat budget of the Adriatic Sea basin, on the contrary, is negative, and it would be very difficult to imagine an Adriatic Sea basin gaining heat from the atmosphere, but unfortunately it is very difficult to validate this scenario, due to lack of observational fields in this sense.

If this budget would be true, though, it could have a very strong impact on the convective mixing, changing its dynamics and its cycles.

4.6 Summary and conclusions

In this chapter we analyzed the impact that climate changes will have in the Adriatic main physical ocean parameters in the period 2001-2030 by means of numerical simulations. By adopting a strategy of integration of different numerical models in the fields of atmosphere, hydrology, river hydraulics and oceanography, a methodology of regionalization for the study of climate changes in the ocean was delineated, at regional and local scale.

The Adriatic REGional model was coupled with climatic models of atmosphere, hydrometeorology and river, integrated under the IPCC A1B scenario in the period 2001-2030, and validated in an unusual way for climatic models: following a day-by-day comparison of the model results with observed data, instead of comparing long period means of model simulations with long period means of data. This allowed to quantify how reliable a model of climate change can be at a local scale, showing that, in spite of an evident bias in temperature, the dynamics of the ocean climate are represented fairly well by the climatic model.

An analysis of the evolution of the most important physical ocean variables – temperature, salinity and currents – showed the following general results:

- A generalized increase in temperature, of the whole basin, following the increase in the atmospheric forcings, is evidenced in all the seasons between the future (2025-2030) and the present (2003-2008) time. The increase is much more evident in summer, when it reaches values up to 1 °C, than in the rest of the seasons, and considering the whole year it is approximately of 0.8°C.
- Also surface salinity showed an increase in the future period, even if at a much lower extent than surface temperature. The mostly sensitive areas to salinity increase proved to be the coastal zones influenced by the two main rivers of the basin: the Po in the north west and the Buna/Bojana in the south east. In this region in particular, following a decrease in precipitations, and thanks to the realistic hourly coupling of the ocean model with the local hydrology, a much stronger increase in salinity than in the rest of the basin is detected in all the seasons and particularly in autumn, where the local increase is up to 1.5 PSU.
- The influence of climate change on currents appears to be mostly evident along the WACC and in the Southern and Mid Adriatic cyclonic gyres, with different behaviours: the WACC future intensity evidently decreases in transition seasons, and within these, in spring much more than in

autumn, while it moderately increases in summer and in winter. The Southern Adriatic cyclone significantly intensifies in all the seasons but winter, while the Mid Adriatic cyclone intensifies considerably in spring and moderately in summer. According to our results the mostly sensitive season to climate change for what concerns circulation is spring, while the least sensitive is winter.

We believe the ocean climate change integrations carried out and just described and analyzed are pioneering in the field of climate change study, and beside the importance of the results just described strictly related to climate change projections, we believe the present work is very important because the numerical modelling platform that was built in its framework can be considered as a prototype for the local studies of climate change in general, following the twofold approach of numerical integration of models, and of regionalization of climate impacts, and it can be used as a Decision Support System for climate change issues.

Chapter 5

5. *CLIMATE IMPACTS ON SEDIMENT TRANSPORT FOR THE PERIOD 2020-2030*

5.1 **Introduction**

The main interest of climate change studies has been, until recently, related to the impacts climate change have on the air temperature, on the sea level rise, on the melt down of big glaciers, and on precipitations. Only more recently the attention of climate change is widening its focus on a much bigger variety of side issues, all related to the atmosphere changes, but on different scales, thus involving different fields of science and different applications. One of these, which at our knowledge has still never been investigated, at least in the Adriatic Sea basin, is the impact that climate has on sediment transport at sea. There are many practical interests of this issue, beside the pure scientifical aspect related to the better understanding of climate processes. The knowledge on the evolution of sediment transport in the future scenarios can help us understand the future preferential tracks of river pollutants, since sediment is one of the major vehicle of pollution into the sea. Its different future mean concentration along the water column will affect the light penetration into the water and most likely have an impact on subsurface growth of phytoplankton. Under a more engineering oriented point of view major interest is focused on transport of sediment related to coastal protection and to sea mining. In areas of vivid tourism activities and of strong impact of sediment transport linked to river input in the sea, such as the case of the Buna/Bojana coastal area (see fig. 4.1), deep interest in the future evolution of sediment plumes is drawn for tourism purposes.

Climate change may affect sediment transport from two different points of view.

Firstly, the hydrological cycle is very sensitive to atmospheric changing, especially to precipitations. This may have a relevant impact on sediment eroded from rivers and all around the hydrological river catchments, altering the supply of solid matter to those coastal areas where a dynamical equilibrium is guaranteed by the twofold action of coastal erosion by the sea and supply of solid matter by the river system.

Secondly, the change in wind intensity and distribution can severely affect the wave climate, altering sediment concentrations, distributions and transports also from the bottom boundary of the sea. Recent results of the project Adricosm-Star (http://gnoo.bo.ingv.it/adricosm-star/), as a matter of fact, evidenced how the the average number of sea storms during the year time will progressively decrease, and on the contrary the mean duration of the storm events will progressively increase. Moreover, the direction of the peak of the storms and the mean direction of the waves during the storm will undergo non significant changes, while the mean height of the sea storm's peak will increase of about 10% in the next decade (2020-2030).

In the present chapter of the thesis the first results on sediment transport in the Adriatic Sea will be shown, in particular in the coastal area of the Buna/Bojana river, for the period 2020-2030. The system used to carry out this investigation consists of the integration of the coupled wave-current-sediment model presented in chapter 3 under the conditions of the A1B scenario of IPCC. The configuration of the circulation model is the one described in chapter 4, with the only difference of the bottom boundary coupling with the wave model SWAN, which reflects also in a different distribution of the velocity profile, from bottom to surface.

In chapter 5.2 we describe the model configuration and general conditions for the sediment transport integration in the A1B scenario of climate change, and the calibration carried out on the wave bottom orbital velocity. In chapter 5.3 we present the results of the scenario coupled integrations and do some analysis of the results, while in chapter 5.4 we summarize the work done and the main conclusions drawn on sediment transport climate changes in the study case area of the Montenegrin-Albanian coastal strip.

5.2 Sediment transport integration in the time window 2020-2030 under the A1B IPCC scenario

Similarly to what was done for the impact on the circulation due to climate change, and described in chapter 4, to investigate the changes in sediment transport in the future scenario A1B of IPCC, the Adriatic REGional model described in chapter 3 (i.e. general circulation model coupled with tides and sediment transport) has been integrated for 11 years, in the time window 2020-2030. This climatic integration is the result of a chain of numerical model couplings, schematized in figure 5.1.

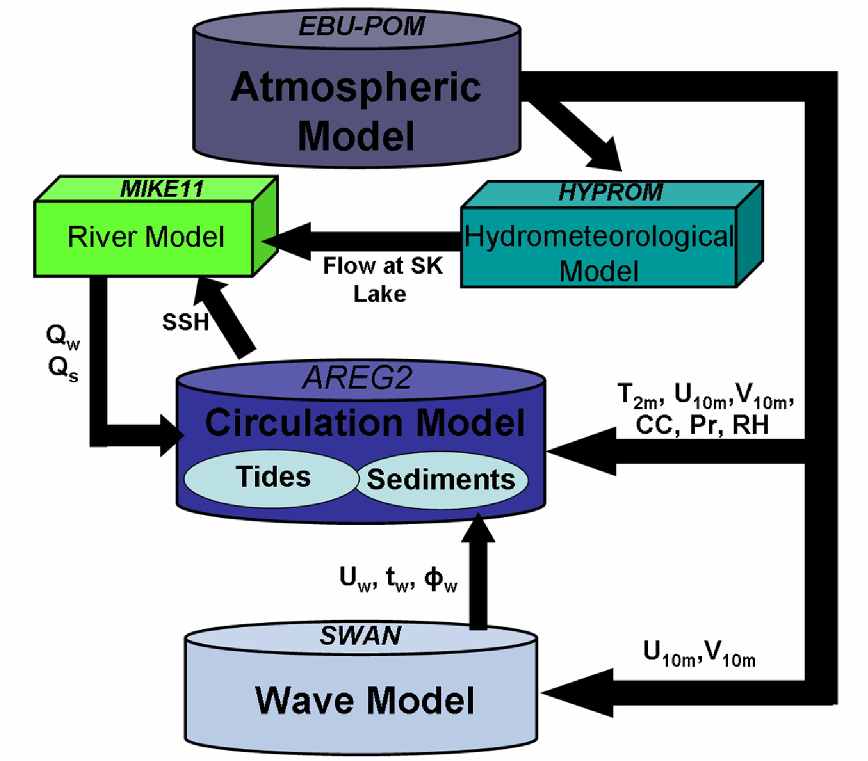

Figure 5.1: Scheme of coupling of numerical models used in the sediment transport scenario simulation. CC, Pr and RH stand respectively for cloud cover, precipitation, and relative humidity, SK stands for Skadar, SSH stands for sea surface height, Q_w and Q_s respectively stand for water and solid flow, U_w, t_w, ϕ_w respectively stand for wave bottom orbital velocity, period and direction. U_{10m} and V_{10m} are the wind zonal and meridional components at 10 meters.

The majority of the components of the integration scheme of figure 5.1 has already been discussed in chapter 4, and in the present sediment transport integration there are no changes in the atmospheric and hydrological forcings compared to the one presented in chapters 4.3.1 and 4.3.2. Compared to the scheme of figure 4.2 the one of figure 5.1 presents the only difference in the introduction of the wave and sediment models that are now part of the integrated platform. The wave model takes in input the wind field from the EBU-POM atmospheric climate model and gives as output the wave bottom orbital velocity (m/s), the wave period (s) and direction (degrees), needed by the sediment transport model, to which they are an input. Last, beside the water flow (m^3/s) the river model provides the solid flow (m^3/s) at the two branches of the Buna/Bojana river.

Table 5.1 summarizes the general conditions and configuration of the integrated model during the 11 year integration undertaken, in the time window 2020-2030.

Sediment transport A1B scenario configuration

Time Frame	Jan 2020- Dec 2030
Model	coupled Wave-CUrrent-Sediment (based on AREG2)
OGCM Initial Condition	AREG2 climate change
Sediment Initial Condition	- 1 kg/m^2 constant on the sea bottom - 0.002 kg/m^3 along the water column
Bojana River Solid and Water Flow	A1B Scenario Hourly Modelled data (2020-2030)
Other Rivers' Solid and Water Flow	Climatology
Atmospheric Forcings	EBU-POM Model (0.25°, 6 hr)
Wave Forcings	SWAN model forced by EBU-POM (A1B scenario)
L.O.B.C	MFS Daily Climatology (1998-2008)
Output Frequency	Daily (Daily Means)

Table 5.1: Configuration and general conditions of the climate change scenario integrated simulation for the analysis of climate impact on sediment transport.

The circulation model used is the one described in chapter 3. The model has been initialized in January 2020 from instantaneous conditions of the climate model discussed in chapter 4. The river flows used are the same used for the integration described in chapter 4 in the period 2020-2030. The lateral input of sediment transport is climatological for all the rivers except for the Buna/Bojana river, where the hourly modelled data under the A1B scenario were used. The initial conditions for sediment in the water were constant all around the basin domain, equal to 1 kg/m^2 of solid matter deposited on the bottom, and 0.002 kg/m^3 of concentration suspended along the water column. Again the classes of sediment considered were two (as described in chapter 3), equally divided on the sea bottom at the beginning of the integration, and equally supplied by the rivers. The wave forcings were the 6-hourly output of the wave model SWAN simulated under the A1B IPCC scenario wind conditions in the period 2020-2030. The lateral open boundary conditions were again those used for the integration of chapter 4: a daily climatology of the fields of the Mediterranean Forecasting System.

5.2.1 Calibration of the orbital velocity under the scenario simulation

The factor mainly responsible for resuspension in the sea water is the orbital bottom velocity due to wave activity, and its interaction with the water bottom currents, as introduced in chapter 3.

As one of the results of the project Adricosm-Star, the fields of velocity of the wind at 10 metres resulting from the climate model EBU-POM present some major differences compared to the more realistic fields provided by the European Center for Medium-Range Weather Forecast, such as, for example, a generalized lower intensity of the climatic simulated winds compared to observed ones or to those simulated with more realistic models (i.e. ECMWF).

To take these differences into account, some calibration was carried out to find a correction coefficient in order to have a better fit of the bottom wave orbital velocities resulting from the wave model forced with climate change forcings on the ones resulting from the model forced with realistic forcings.

Figure 5.3 shows the distribution of the bottom orbital velocities into bins of 5 cm/s, for the two different datasets of results of the wave model: one forced with ECMWF atmospheric forcings (blue bars, left panel), and one forced with EBU-POM climate atmospheric forcings (red bars, right panel). The analysis has been conducted where the realistic model had been validated, i.e. in the WHOI tripod location (see chapter 3), in front of the Po river delta (fig 3.2). As we can see the distributions are similar, even if the population of the first bin is higher for the EBU-POM forced model by approximately 10%, on the contrary, all the populations relative to the other bins are higher in the ECMWF forced model. This reflects the fact that EBU-POM winds are generally weaker than those of ECMWF.

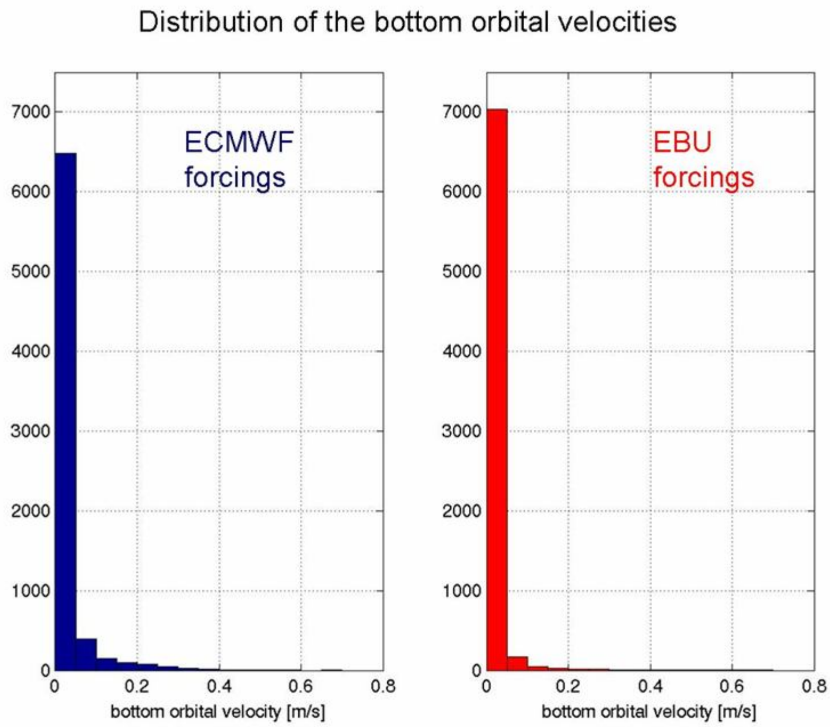

Figure 5.2: Distribution of the bottom orbital velocities for the period 2004-2008 in front of the Po river delta simulated with SWAN forced with ECMWF (left) and EBU-POM (right)

The correction factor applied to the bottom orbital velocity of the EBU-POM forced SWAN model has been calculated as follows:

$$Fac = \frac{\overline{U}_{ECMWF}}{\overline{U}_{EBU}}$$

Where *Fac* is the correction factor, $\overline{U}_{ECMWF}$ is the mean bottom orbital velocity calculated on the period 2004-2008 with the wave model forced by the ECMWF atmospheric forcings, $\overline{U}_{EBU}$ is the mean bottom orbital velocity calculated on the same period with the wave model forced by the EBU-POM atmospheric forcings.

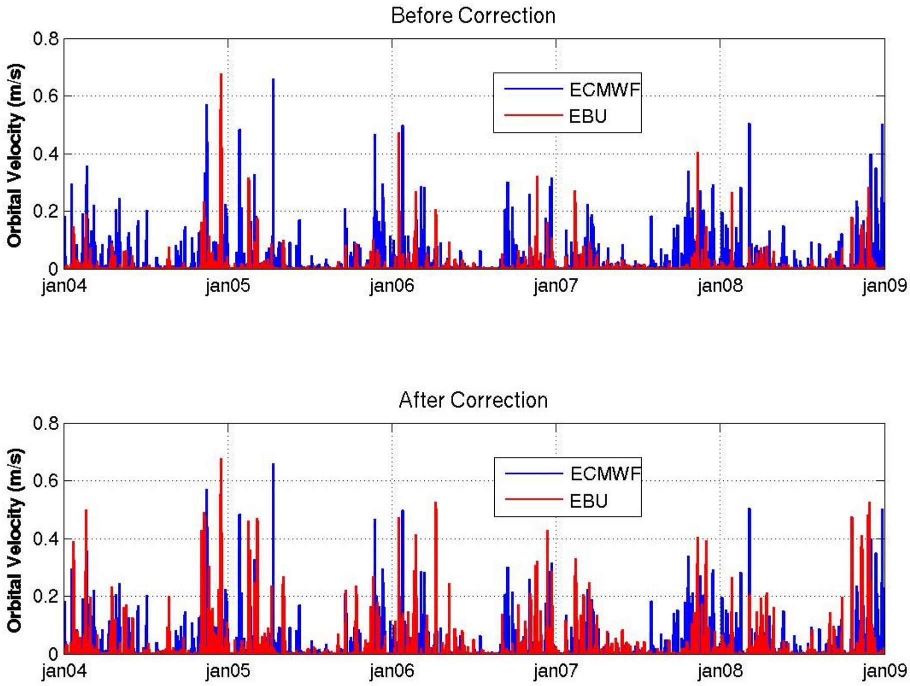

Figure 5.3: Bottom orbital velocities before (upper panel) and after (lower panel) the application of the correction factor. Blue line: SWAN model forced with ECMWF; red line: SWAN model forced with EBU-POM

Figure 5.3 shows the comparison between the bottom orbital velocities resulting from the realistic model (blue curve) and the climate model (red curve) for the period 2004-2008 before (upper panel) and after (lower panel) the correction. The correction factor found on the velocities was 2.6. Since the 98% of the entire population covered the first four bins (velocities up to 20 cm/s), and since the SWAN model forced with EBU forcings seems to be able to reproduce several peaks of bottom orbital velocities, to avoid overestimated non-realistic high values of velocity the correction factor has only been applied to velocities lower than 20 cm/s.

5.2.2 Buna/Bojana river sediment input

As introduced in chapter 3 the wave-current-sediment model has been coupled with the Buna/Bojana river model at the time frequency of 1 hour in terms of water discharge (m^3/s) and of sediment flux inflowing to the Adriatic Sea through the final cross sections of the river. Figure 5.4 shows the input of sediment in the sea in terms of solid flow (m^3 of solid suspended matter per second). By multiplying the solid flow by the density of the porous material (approximately 1700 kg/m^3) we obtained the sediment flux input (kg/s), needed as surface boundary condition by the sediment transport submodel.

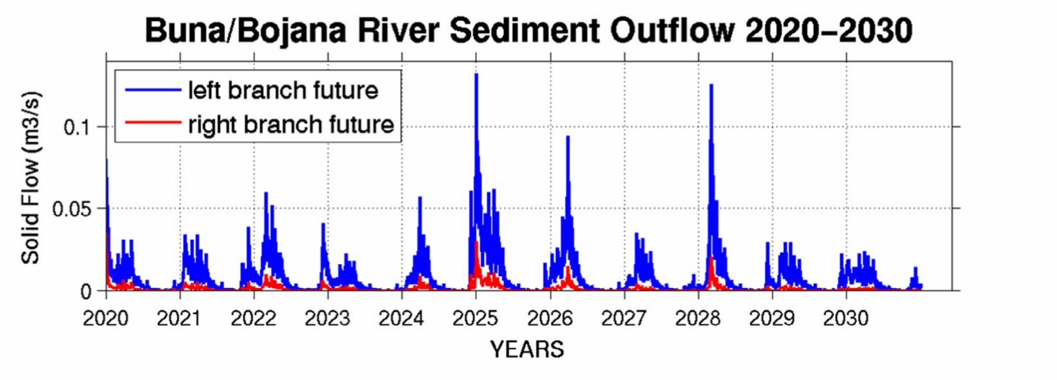

Figure 5.4: Buna/Bojana river sediment outflow time series from January 2020 to December 2030. The flow of the left branch of the river delta is represented with the blue curve, while the flow of the right branch is represented with the red curve.

As clearly visible from the time-series of figure 5.4 the left branch of the river delta is dominating in terms of sediment discharge into the sea. The right branch transport is decreasing, and it is almost nil in the projections at 2030, hinting a depositional trend.

The model and data concerning the Buna/Bojana river climate simulations used for the present work have been implemented and produced by the private company S.G.I. SPA (Studio Galli Ingegneria, Padova, Italy)

5.3 Coastal sediment changes in the next decades

After the calibration on the waves' orbital velocity the wave-current-sediment integrated model, coupled with the river model, has been integrated from January 2020 to December 2030 in the framework of the climate change A1B scenario. As anticipated in chapter 5.2 the solid matter in the sediment transport submodel has been treated, for simplicity, as two non cohesive classes of sediment, respectively fine (diameter of 17 μm) and coarse (diameter of 55 μm), as described also in chapter 3.

Figure 5.5 shows the difference in terms of erosion and deposition in the coastal area of Albania and Montenegro between the first (2020-2024) and last (2026-2030) five years of the coupled scenario integration. This gives a hint of the future trend of erosion/deposition in that area. As it is appreciable from the figure the area of the Drinn bay tends to be an area of sedimentation all along the coast line. In particular, by looking at the very coastal zone in the surroundings of the Buna-Bojana river delta we can see that in spite of the much lower input of sediments from the right branch of the river, the sediment tends to deposit within the first kilometres from the right branch, consistently with the hints of low sediment transport activity for this branch of the river's delta suggested by the river model. A different situation is the one that characterizes the left branch of the river. In fact the grid points immediately surrounding the left mouth are in equilibrium, in terms of sediment evolution, slightly going towards erosion, and the great amount of solid matter out-flowing this branch of the river is mainly advected eastwards, tending to deposit along the coast line immediately south-south/east of the river. The tendency of this part of the Albanian-Montenegrin coastline to be subjected to strong deposition of solid matter from the river was also detected in the past. In fact figure 5.6, provided by sources of the former *Serbian Hydrographic Insitute* in the framework of the project Adricosm-Star, shows the present-time coast-line

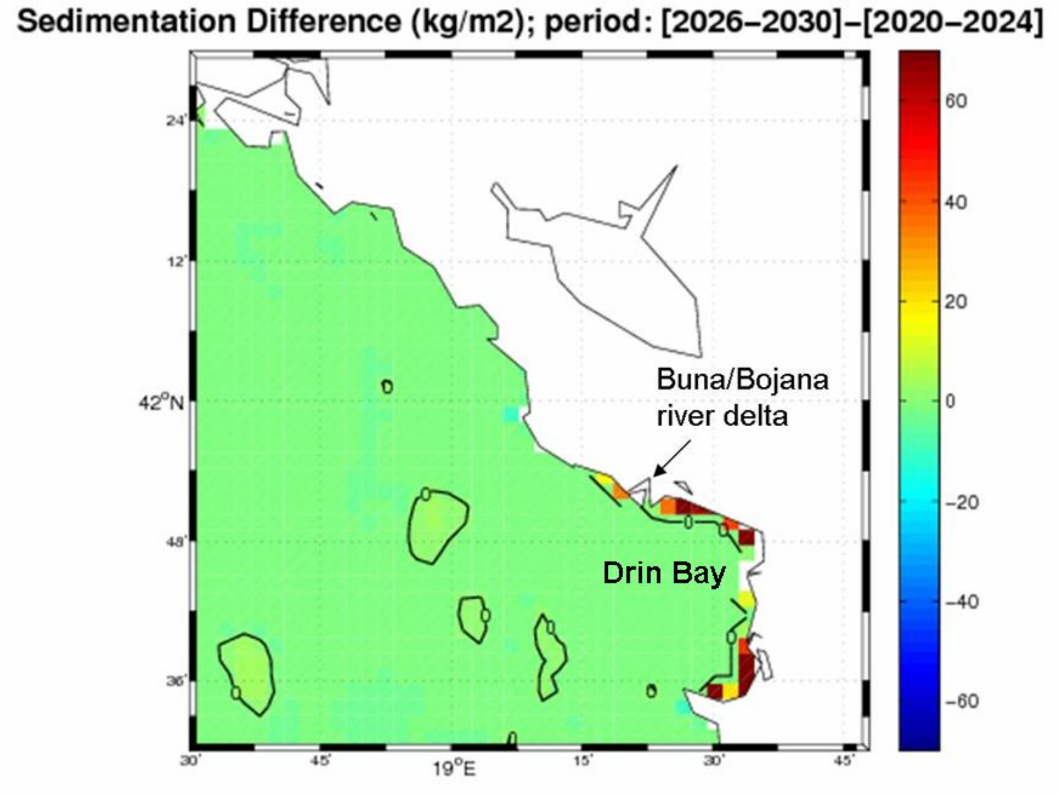

Figure 5.5: Difference patterns of erosion/deposition. To plot the image the deposition in terms of kg/m^2 has been averaged over the two 5-year periods 2020-2024 and 2026-2030, then the mean fields have been subtracted to each others.

(from Google Earth) in the immediate vicinity of the Buna/Bojana river delta, and the old coastline of the 60s, superimposed to it, represented with a red line. It is evident how the left branch of the river used to form a more complex deltaic area, which has eventually been eroded, and how the area immediately south/south east of this river branch is a depositional area. According to the model results in the period 2020-2030 this deltaic evolution will continue with similar dynamics.

Figure 5.6: Old morphology of the coastline in the surroundings of the Buna/Bojana delta. The coastline of the 60s (red line) is superimposed to the present-time Google Earth image of the Buna/Bojana delta and coast line. Image provided by sources of the former Serbian Hydrographic Insitute

Figures 5.7 and 5.8 show an analysis of the evolution of different physical and sediment transport parameters respectively in front of the left and right branch of the Buna/Bojana river. In panels *a, b* and *c* the wind stress (Pa), bottom currents (m/s) and bottom maximum shear stress (Pa) averaged over the four dots of panel *g* are presented, while in panels *d, e* and *f* respectively the sea bottom evolution (kg/m^2) for fine (red curve) and coarse (blue curve), the concentration of fine and coarse sediment at the surface (blue curve) and at the bottom (red curve) are shown, again averaged over the four dots of panel *g*. The data are plotted as daily means for the entire period of the scenario integration.

The dynamics of sedimentation in front of the right branch and of erosion in front of the left branch of the river is also visible through panels *d* of the two figures:

the evolution of the zone immediately in front of the left branch is basically in equilibrium in time, and it tends to follow a sort of seasonality: the high sediment

inputs from the river in the winter periods are followed or happen together with favourable resuspension and erosion conditions (sea storms, see panel *a* and *c*), but usually the sediment input is dominant with respect to erosion in the winter time, so we have deposition until the end of the summer, and then in the autumn season, the sediment input from the river is almost absent, while the bottom stress (panel *c*) is usually strong enough, due to wind conditions (panel *a*), to keep alive the process of resuspension/erosion. The eroded material is then advected elsewhere. Particularly interesting is the example of the period from the end of December 2024 to the end of December 2025. In the beginning of this period we have a river input of sediment from the left branch of up to 200 kg/s (approximately 0.12 m^3/s of solid flow, see figure 5.4). This strong input, evident in panel *d* of figure 5.7, is only partially equilibrated by the erosion due to resuspension induced by bottom stress which is also strong (figure 5.7, panel *c*), as also reflected from the bottom concentration of sediment (fig. 5.7, panel *f*) which occasionally reaches extremely high values of up to 0.5 g/l, witnessing the availability of material for erosion and the intense wind and wave action. In autumn then the sediment river input is practically absent, while the bottom stress is strong again, inducing the erosion of all the material that had deposited during the previous part of the year.

A very different situation is that one concerning the right branch of the Buna/Bojana river and its coastal surroundings (figure 5.8). Panel *d* clearly indicates the that the evolution of the sea bottom, in spite of a much lower input of sediment from the right branch of the river (fig. 5.4), is subjected to a depositional regime. The events of erosion, mainly in autumn and in the beginning of winter characterize the waters with occasional very high concentration of sediment (panels *e* and *f*), even if lower and less frequent than those experienced in front of the left branch of the river.

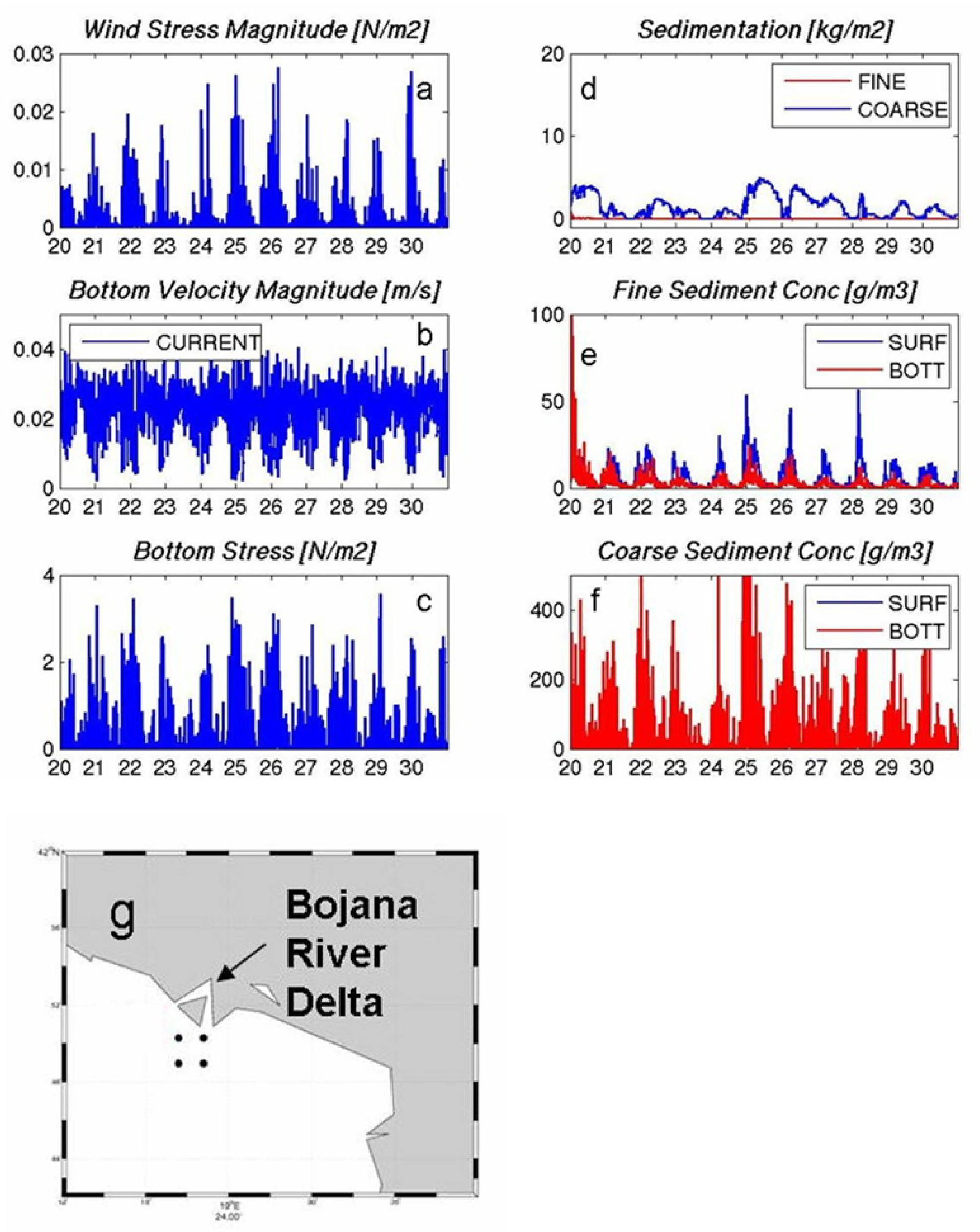

Figure 5.7*: Analysis of the coastal surroundings of the left branch of the Bojana River under the IPCC climate change conditions for the period 2020-2030. The analysis has been done considering the spatial average of the variables' values in the locations represented by the black dots of the map (g). The analyzed fields are: wind stress amplitude (a), bottom current intensity (from the circulation model, without considering the orbital velocity) (b), maximum wave-current combined bottom shear stress (c), bed evolution (d), concentration of fine sediment: red line at the bottom, blue line at the surface (e), concentration of coarse sediment: red line at the bottom, blue line at the surface (f)*

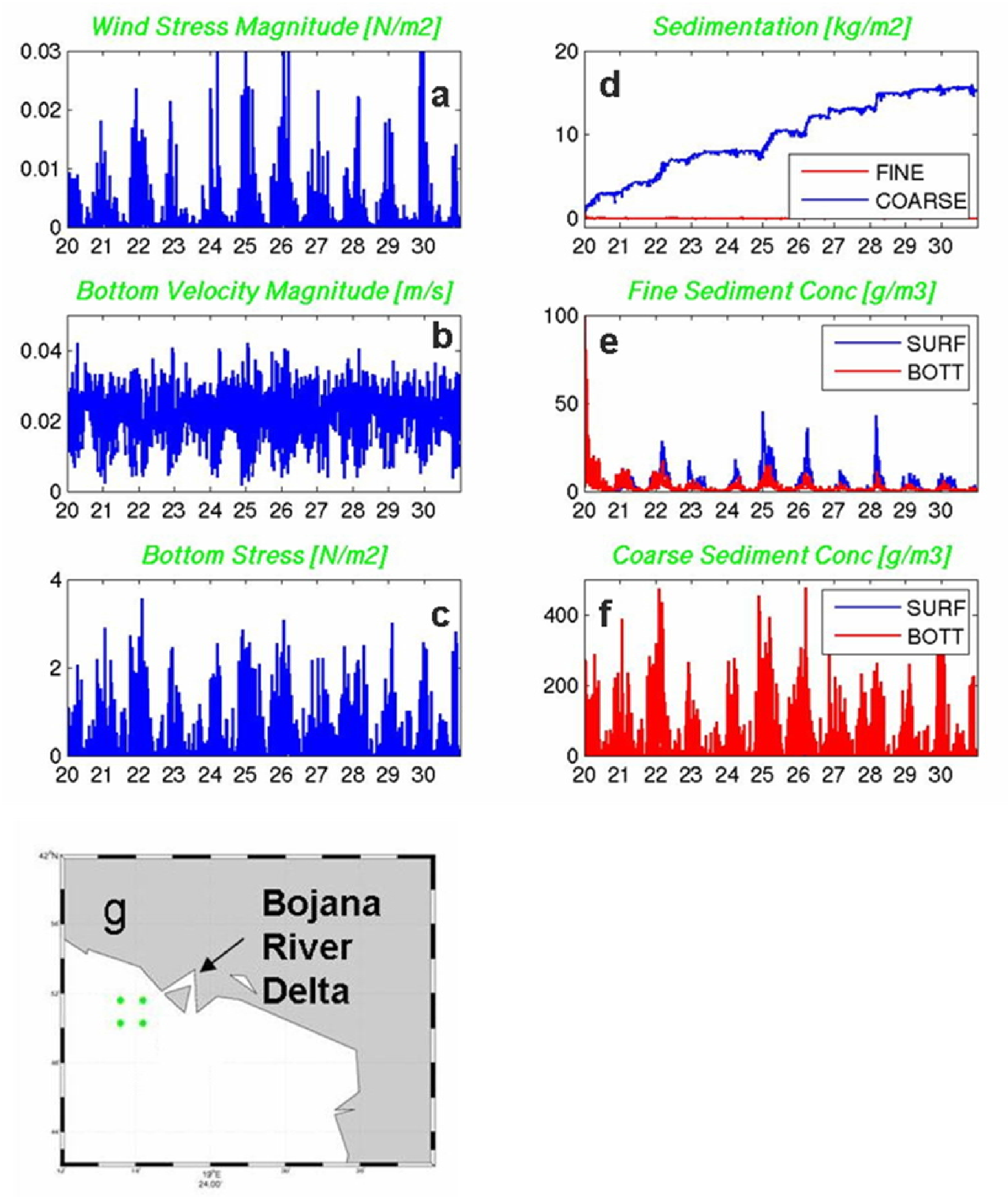

Figure 5.8: *Analysis of the coastal surroundings of the right branch of the Bojana River under the IPCC climate change conditions for the period 2020-2030. The analysis has been done considering the spatial average of the variables' values in the locations represented by the green dots of the map (g). The analyzed fields are: wind stress amplitude (a), bottom current intensity (from the circulation model, without considering the orbital velocity) (b), maximum wave-current combined bottom shear stress (c), bed evolution (d), concentration of fine sediment: red line at the bottom, blue line at the surface (e),), concentration of coarse sediment: red line at the bottom, blue line at the surface (f)*

5.4 Summary and conclusions

The impact brought by climate change to the transport of sediment at sea, in particular in the coastal area of the Buna/Bojana river, in the south east of the Adriatic Sea basin, was presented and discussed in the present chapter. This area is very sensitive to sediment transport, mainly for the presence of the Buna/Bojana river, which is the second largest supplier of sediment in the whole Adriatic Sea basin after the Po river. The simulation was carried out for the period 2020-2030, through a series of coupling of numerical models, all forced under the climate atmospheric conditions of the A1B scenario of the IPCC, in order to make it as realistic as possible, even if still in the framework of climate simulations.

The results of the integration showed some major results:

- The coastal area surrounding the Buna/Bojana river is very active in terms of sediment transport, both for the presence of high concentrations of sediment coming from the river, and from a strong process of resuspension. Typical values of sediment concentration during intensive activity exceed 0.5 g/l in the vicinity of the river delta. The central part of the decade 2020-2030 seems to be the most extreme in terms of erosion/deposition and sediment concentration along the water column, and the last part of the decade seems to be more erosive than the first part of it, at least in the shelf area.
- The observed tendency of erosion of the past 50/60 years in the area immediately offshore of the left branch of the Buna/Bojana river and of deposition of the area immediately south/south-east of it seems to be maintained also in the future decades. The whole coastal area of the Drinn Bay (fig. 5.5) is subjected to deposition of sediment.
- A moderate depocenter is evidenced approximately 50 km west of the coast of the Drinn Bay.

CHAPTER 6

6. OVERALL SUMMARY AND CONCLUSIONS

This study describes the effects of high frequency processes on the Adriatic Sea dynamics and on the sediment transport, and introduces a methodology of integration and regionalization of numerical models in the framework of climate change, in order to analyze its impact on the circulation of the Adriatic Sea basin, and, for the very first time, on the patterns of sediment transport in the coastal area of the basin.

In order to improve the modelling of the Adriatic Sea and to have more realistic simulations, especially for what concerns the higher frequency processes, a baroclinic ocean general circulation model was successfully coupled with a tidal model through a particular nesting condition at the lateral open boundary. The resulting sea surface elevation fits well the observed data all around the basin, and the accuracy in tidal prediction is comparable to that of barotropic tidal models.

The baroclinicity of the model allowed to analyze for the first time the impact of tides on the dynamics and state variables of the system, and on the mixing of the water column in different seasons. It was shown that tides produce a stronger impact in the along shore rather than in the cross shore near bottom transport of heat and salt in the Po river ROFI. In the along shore direction the tidal transport was shown to be almost completely associated to semidiurnal frequencies, while in the cross shore direction the transport related to diurnal frequencies becomes quite important too. Tide induced mixing was found in the Northern Adriatic, even if it was not powerful enough to induce a complete mixing of the water column. Nevertheless, a clear oscillation of salinity and density, following the current shear stresses was found both in winter and summer, and it appeared to be even more evident and enhanced in winter season, and after episodes of strong wind. In general tides showed to induce a higher stratification along the water column.

The comparison between the models with and without tides allowed also to highlight the two different temporal scales characterized by the effects of tides on the circulation: the fact that important differences in the distribution of mean temperatures and salinities between the model with tides and the model without tides is often observed, even in absence of big differences in vertical mixings, suggests that on long time scales tides have a stronger impact on advection rather than on diffusion.

The tidal coupled model was further integrated with a wave and a sediment transport model, in order to include more processes and to simulate the particular dynamics of the coastal sediment transport. The implementation of the integrated models was successful and the results of modelled sediment concentration along the water column, of sediment transport at sea and of bottom maximum stress were in good agreement with observations. Some deficiencies of the sediment model were also evidenced, such as its excessive erosive component and the fact that it is not well balanced between the different classes of sediments. Moreover a very simplified representation of the sea bottom such as the one presented, combined with the several assumptions adopted (constant critical shear stress for erosion in time and space, and equal in magnitude for all the classes of sediment considered) proved not to allow to reproduce correctly enough the long timescales of sediment transport, such as maps of erosion/deposition patterns, at least far away from important sources of sediment. The model was used for the first time to analyze the patterns of sedimentation and erosion along the Montenegrin coastal zone, where the Buna/Bojana river supplies for high amount of sediments. The coupling of the wave-current-sediment model with a river model for the Buna/Bojana increased considerably the reliability of the investigation, even if, unfortunately, observed sedimentological data to support our conclusions are still not available.

Finally, by adopting a strategy of integration of different numerical models in the fields of atmosphere, hydrology, river hydraulics and oceanography, a methodology of regionalization for the study of climate changes in the ocean was delineated, at regional and local scale. All these models were coupled together and integrated in the period 2001-2030 under the atmospheric conditions of the A1B scenario of climate change of the IPCC, to investigate in a realistic way and on a local spatial scale the climate impact on coastal circulation and on sediment transport. The results of the integrations showed a generalized increase in temperature and salinity of the Adriatic Sea basin, and some important changes in the circulation, such as the future weakening of the intensity of the Western Adriatic Coastal Current in transition seasons, and within these, in spring much more than in autumn, and a moderate intensity increase in summer and in winter. The Southern Adriatic cyclone significantly intensifies in all the seasons but winter, while the Mid Adriatic cyclone intensifies considerably in spring and moderately in summer. According to the scenario results for what concerns circulation, the season mostly sensitive to climate change is spring, while the least sensitive is winter.

The study of sediment transport in the future scenarios is something very new, but still very preliminar. However, the analysis of the results showed a moderate depocenter, approximately 50 km west of the Montenegrin and Albanian coast, and the tendency of (i) erosion, in the area immediately offshore the left branch of the Buna/Bojana river (South-East of the basin) and (ii) of deposition, in the area immediately to its South/South-East. This tendency had already been observed in the past 50/60 years in the same areas.

Further development in the modelling of the presented integrated platform is however required, particularly in the sediment transport component, mainly to overcome the problems of excessive erosion in the basin, especially in its deepest parts. More work is also needed in the scenario integrations through a more exhaustive analysis of the results, and forcing the described ocean coupled model with different atmospheric climate models in order to assess the different responses of the model to different climate forcings and to analyze the similarities and the discrepancies in the results.

In spite of all the uncertainties related to climate change studies, we believe that the present work was very important because it contributed in building a numerical modelling platform that can be considered as a prototype for the local studies of climate change in general, following the twofold approach of numerical integration of models, and of regionalization of climate impacts.

7. *APPENDIX A: ITERATIVE PROCEDURE TO CALCULATE THE WAVE CURRENT FRICTION FACTOR*

To estimate the friction factor f_{cw} between wave and current it is firstly necessary to determine the oscillatory component of the stress, i.e. that component related only to the wave activity, defined as:

$$\tau_w = \rho u_{*w}^2 = \frac{1}{2}\rho f_w u_w^2 \tag{7.1}$$

Where f_w is the friction factor only due to waves motion, u_w is the magnitude of the representative bottom orbital velocity, and u_{w*} is the bottom shear velocity due to waves. τ_w can be estimated through the relation proposed by Jonsson (1966):

$$f_w = \exp\left(-6 + 5.2\left(A_\delta k_b\right)^{-0.19}\right) \tag{7.2}$$

where z_0, again, is the scale of the bottom roughness ($z_0=0.001\ m$), k_b is the characteristic dimension of the physical bottom roughness and A_δ is the amplitude of the wave velocity near the bottom, and is determined by:

$$A_\delta = \frac{2T_w \cdot u_w}{\pi} \tag{7.3}$$

being T_w the wave period, with the limit that $f_{wmax}=0.3$ for $A_\delta / k_b \le 1.57$. According to the experimental results of Schilchting (1968) it can be assumed that

$$k_b = 30 z_0 \tag{7.4}$$

Once u_{*w} has been estimated through (7.1) and (7.2), f_{cw} can be determined through an iterative procedure as it follows:

A first tentative value for f_{cw} is assumed (in this work we assumed 0.01, as often used in literature). The steady shear component of the flow (i.e. the one related to the mean flow) can be calculated as

$$u_{*c} = \sqrt{f_{cw}} u_c \tag{7.5}$$

And the combined wave-current shear velocity is determined as

$$u_{*cw} = \sqrt{\frac{\tau_b}{\rho}} \tag{7.6}$$

(where τ_b is the bottom maximum wave-current shear stress as introduced in equation (3.12)) and can be calculated through the shear velocities related to the oscillatory component of the stress alone (wave) and to the steady component of the stress alone (current) as it follows:

$$u_{*cw} = \sqrt{(u_{*c}^2 + u_{*w}^2 + 2u_{*c}u_{*w}\cos\theta} \tag{7.7}$$

where θ is the angle between wave and current direction. Now the effective (or apparent) bottom roughness (Grant and Madsen 1979) can be estimated as:

$$k_{bc} = k_b\left(24\frac{u_{*cw}}{u_w}\frac{A_\delta}{k_b}\right)^{[1-(u_{*c}/u_{*cw})]} \tag{7.8}$$

Now the apparent roughness is used to calculate the velocity in the bottom boundary layer:

$$u_c = \frac{u_{*c}}{\kappa}\ln\left(\frac{\delta_b}{k_{bc}/30}\right) \tag{7.9}$$

which will update equation (7.5) in the next iteration of the procedure.

By combining equation (7.9) with equation (7.5) the current related shear stresses cancel out and we obtain the new estimate of f_{cw}:

$$f_{cw} = \left(\frac{\kappa}{\ln\left(\frac{30\delta_b}{k_{bc}}\right)}\right)^2 \tag{7.10}$$

The procedure is now reiterated until the difference δ_{fcw} between two successive estimates of f_{cw} is smaller than δ'_{fcw} - a small value decided a priori. In the present work we used $\delta'_{fcw} = 10^{-5}$.

REFERENCES

- Ariathurai, R., and R. B. Krone, Mathematical modelling of sediment transport in estuaries, in Estuarine Processes, vol. II, edited by M. Wiley, pp.98– 106, Academic, San Diego, Calif., 1976.
- Artegiani, A., Bregant, D., Paschini, E., Pinardi, N., Raicich, F., Russo, A.: The Adriatic Sea general circulation. part I: Air-sea interactions and water mass structure, J. Phys. Oceanogr., 27, 1492–1514. 1997a.
- Artegiani, A., Bregant, D., Paschini, E., Pinardi, N., Raicich, F., Russo, A.: The Adriatic Sea general circulation. part II: Baroclinic circulation structure, J. Phys. Oceanogr., 27, 1515–1532. 1997b.
- Beniston, M., D.B. Stephenson, O.B. Christensen, C.A.T. Ferro, C. Frei, S. Goyette, K. Halsnaes, T. Holt, K. Jylhä, B. Koffi, J. Palutikof, R. Schöll, T. Semmler and K. Woth, 2007: Future extreme events in European climate: an exploration of regional climate model projections. Climatic Change, 81, S71-S95.
- Bever et al., 2009, Deposition and flux of sediment from the Po River, Italy: an idealized and wintertime numerical modeling study, Marine Geology, 260, 69–80
- Blumberg, A.F.,Mellor G.L.1987. A description of a three-dimensional coastal ocean circulation model. In: Heaps NS, editor. Three-dimensional coastal ocean models. Washington, DC7 American Geophysical Union; 208 pp.
- Booij, N., R.C. Ris and L.H. Holthuijsen, 1999, A third-generation wave model for coastal regions, Part I, Model description and validation, J.Geoph.Research, 104, C4, 7649-7666.
- Book J., Perkings H., Wimbush M.2009. North Adriatic tides: observations, variational data assimilation modeling, and linear tide

dynamics, Geofizika, 26, pp 115-143.

- Bortoluzzi G., Frascari F., Giordano P., Ravaioli M., Stanghellini G., Coluccelli A., Biasini G. and Giordano A. 2006. The S1 Buoy station, PoRiver Delta: data handling and presentation. Acta Adriatica, 47(Suppl):113-131.
- Cacchione, D.A., Drake, D.E., Kayen, R.W., Sternberg, R.W., Kineke, G.C., Tate, G.B., 1995. Measurements in the bottom boundary layer on the Amazon subaqueous delta. Mar. Geol. 125, 235–257.
- Cardin, V., M. Gacic, . 2003. Long term heat flux variability and winter convection in the Adriatic Sea. J Geophys Res;108(C9): n. 8103.
- Cavaleri, L, Malanotte-Rizzoli, P., 1981. Wind wave prediction in shallow water: theory and applications.Journal of Geophisical Reaserch, VOL. 86, No. Cll, Pages 10,961-10,973, November 20, 1981.
- Chen, F., K. Mitchell, J. Schaake, Y. Xue, H. Pan, V. Koren, Y. Duan, M. Ek, and A. Betts. 1996. Modeling of land-surface evaporation by four schemes and comparison with FIFE observations. J. Geophys. Res., 101, 7251-7268.
- Chiggiato, J., M. Zavatarelli, S., Castellari, M. Deserti, 2005. Interannual variability of surface heat fluxes in the Adriatic Sea in the period 1998–2001 and comparison with observations. Science of the Total Environment 353, 89–102.
- Cushman-Roisin, B., Naimie, C. E., 2002. A 3-D finite element model of the Adriatic tides. Journal of Marine Systems 37, 279– 297.
- Djurdjevic, V., and Rajkovic B. 2010. Development of the EBU-POM coupled regional climate model and results from climate change experiments, in Advances in Environmental Modeling and Measurements, Editors: T. D. Mihajlovic and Lalic B, Nova Publishers.

- Estubier A., and Lévy M. Quel schéma numérique pour le transport d'organismes biologiques par la circulation océanique. Note Techniquesdu Pôle de modélisation, Institut Pierre-Simon Laplace ;2000 : 81pp.
- Fain A.M.V, Ogston A.S, Sternberg R.W. 2007.Sediment transport event analysis on the western Adriatic continental shelf, Continental Shelf Research 27, 431–451
- Flather, R.A., 1976. A tidal model of the northwest European continental shelf. Memoires de la Societe Royale des Sciences de Liege 6 (10), 141–164.
- Frascari F., Frignani M., Guerzoni S., Ravaioli M. 1988. Sediments and Pollution in the Northern Adriatic Sea. Reprented from Living in a Chemical World, Volume 534.
- Frignani M., Langone L.,Ravaioli M., Sorgente D.,Alvisi F., Albertazzi S. 2005. Fine-sediment mass balance in the western Adriatic continental shelf over a century time scale. Marine Geology 222–223 (2005) 113– 133.
- Grant W. D., Madsen O. C.. 1986. The Continental shelf bottom boundary layer. Ann. Rev. Fluid Mech. 1986. 18 : 265
- Grant, W. D., Williams, A. J. 3rd, Glenn, S. M. 1984. Bottom stress estimates and their prediction on the northern California continental shelf during CODE-l: The importance of wave-current interaction. J.Phys. Oceanogr. 14(3): 506-27
- Grant, W.D., Madsen, O.S., 1979. Combined wave and current interaction with a rough bottom. Journal of Geophysical Research 84, 1797–1808.
- Gualdi, S., E. Guilyardi, A. Navarra, S. Masina, and P. Delecluse, 2003b: The interannual variability in the tropical Indian Ocean as

simulated by a CGCM. Clim. Dyn., 20, pp567-582.

- Gualdi, S., E. Scoccimarro, and A. Navarra, 2008: Changes in tropical cyclone activity due to global warming: Results from a high-resolution coupled general circulation model. Results from a high-resolution coupled general circulation model. J. Climate, 21, 5204–522
- Guarnieri, A., Oddo, P., Pastore, M., Pinardi, N. 2010. The adriatic basin forecasting system new model and system development. In: Coastal to global operational oceanography: achievements and challenges. Dahlin, H., Fleming, N.C., Petersson, S.E. (Eds.), Proceeding of 5th EuroGOOS Conference, Exeter.
- Hellerman S, Rosenstein M. 1983. Normal monthly wind stress over the world ocean with error estimates. J Phys Oceanogr;13: 1093–104.
- Holthuijsen, L.H., Booij, N. and T.H.C. Herbers, 1989: A prediction model for stationary, short-crested waves in shallow water with ambient currents, Coastal Engineering, 13, 23-54.
- Janjić, Z. 1984. Non-linear advection schemes and energy cascade on semistaggered grids, Mon. Wea. Rev., 112, 1234–1245.
- Janjić, Z. I. 1977. Pressure gradient force and advection scheme used for forecasting with steep and small scale topography., Contrib. Atmos. Phys.,, 50, 186–199.
- Janjić, Z. I. 1979. Forward-backward scheme modified to prevent two-grid-interval noise and its application in sigma coordinate models., Contrib. Atmos. Phys., 52, 69–84.
- Janjić, Z. I. 1990. Physical package for step-mountain, eta coordinate model., Mon. 272 Wea. Rev., 118, 1429–1443.
- Janjic, Z. I. 1996. The surface layer parameterization in NCEP Eta model, pp. 4.16–4.17, WMO, Geneva, CAS/C WGNE, 4.16-4.17.

- Janjic, Z., and Black T. 2003. Response to the ‘White Paper’ by Skamarock And Baldwin. Available at http://www.mmm.ucar.edu/individual/skamarock/spectra discussion.html
- Janjić, Z.I.,1994. The step-mountain eta coordinate model: Further developments of the convection, viscous sub-layer, and turbulence closure schemes. Mon. Wea. Rev., 122, 927-945
- Janssen P. 1991.Quasi-linear theory of wind wave generation applied to wave forecasting. Journal of Physical Oceanography, Vol 21. pp. 1631-1642
- Jerlov NG.1976. Marine optics. Elsevier, Amsterdam
- Jones, P.D. and A. Moberg. 2003: Hemispheric and large scale surface air temperature variations: an extensive revision and an update to 2001. J. Clim., 16, 206- 223.
- Kjellström, E., L. Bärring, D. Jacob, R. Jones and G. Lenderink. 2007: Modelling daily temperature extremes: recent climate and future changes over Europe. Climatic Change, 81, S249-S265.
- Klein Tank, A.M.G. and Können. 2003. Trends in indices of daily temperature and precipitation extremes in Europe. J. Clim., 16, 3665-3680.
- Legates DR, Wilmott CJ. 1990. Mean seasonal and spatial variability in a gauge corrected global precipitation. Int J Climatol;10: 121–7.
- Lou, J., D. J. Schwab, D. Belesky, and N. Hawley, A model of sediment resuspension and transport dynamics in southern Lake Michigan, J. Geophys. Res., 105, 6591–6610, 2000.
- M., Grilli, F., Guarnieri, A., Jones, B., Kljaji´c, Z., Pinardi, N., Sanxhaku, M., 2010. Is the Southern Adriatic coastal strip an eutrophic area? Estuarine, Coastal and Shelf Science 88 (3), 395–406.

- Madec, G., P. Delecluse, M. Imbard, and C. Levy.1999. OPA 8.1 Ocean General Circulation Model reference manual, Internal Rep. 11, Inst. Pierre--Simon Laplace, Paris, France.
- Madsen, O.S., Poon, Y.-K., Graber, H.C., 1988. Spectral wave attenuation by bottom friction: theory. In: Proceedings of the 21th International onference on Coastal Engineering, ASCE, New York, pp. 492-504.
- Malacic, V., Viezzoli, D., Cushman-Roisin, B., 2000. Tidal dynamics in the northern Adriatic Sea. J. Geophysical. Research. 105, 26265–26280.
- May PW. 1986. A brief explanation of Mediterranean heat and momentum flux calculations NORDA Code 322. Stennis Space Center, Miss.7 Nav Oceanogr Atmos Res Lab; 5 pp.
- Mellor, G. L. & T. Yamada. 1982. Development of a turbulence closure submodel for geophysical fluid problems. Rev. Geophys. Space Phys., 20: 851-875.
- Mesinger, F., Z. Janjić, S. Nicković, D. Gavrilov, and D. Daven. 1988. The step mountain coordinate: model description and performance for cases of alpine lee cyclogenesis and for a case of an Appalachian redevelopment, Mon. Wea. Rev., 116, 1493–1518.
- Mihanovic, H., Orlic, M., Pasaric, Z., 2009. Diurnal thermocline oscillations driven by tidal flow around an island in the Middle Adriatic. Journal of Marine Systems 78 (2009) S157–S168.
- Mllor, G. L., Yamada, T. 1982. Development of a turbulence closure submodel for geophysical fluid problems. Rev. Geophys. Space Phys., 20: 851-875.
- Mosetti, R.. 1986. Determination of the current structure of the M2 tidal component in the northern Adriatic by applying the rotary analysis to

the Taylor problem, Boll. Oceanol. Teor. Appl., IV, 165–172.

- Nickovic S., Pejanovic G., Djurdjevic V., Roskar J., Vujadinovic M. 2010. HYPROM hydrology surface-runoff prognostic model, Water Resources Reaserch, VOL. 46, W11506, 18 PP.
- Norrant, C. and Douguédroit A. 2006: Monthly and daily precipitation trends in the Mediterranean. Theor. Appl. Climatol., 83, 89-106.
- Oddo P, Pinardi N, Zavatarelli M, Colucelli A. 2006. The Adriatic Basin Forecasting System. Acta Adriatica, 47 (suppl). 169-184.
- Oddo P., Pinardi N.,. 2008 . Lateral Open Boundary Conditions for Nested Limited Area Models: Process selective approach. Ocean Modeling. Vol.20, 2, pag 134-156.
- Oddo, P., Pinardi, N., Zavatarelli, M. 2005. A numerical study of the interannual variability of the Adriatic Sea (1999–2002). Science of the Total Environment 353, 39–56.
- Oddo.P and Guarnieri A.2011. A Study of the Hydrographic Conditions in the Adriatic Sea from Numerical Modelling and Direct Observations (2000-2008). Ocean Science, submitted.
- Palinkas, C.M., Nittrouer, C.A., Wheatcroft, R.A., Langone, L., 2005. The use of 7Be to identify event and seasonal sedimentation near the Po River delta, Adriatic Sea. Marine Geology 222–223, 95–112.
- Pawlowicz, R., B. Beardsley, and S. Lentz, "Classical Tidal armonic Analysis Including Error Estimates in MATLAB using T_TIDE", Computers and Geosciences, 28, 929
- Pinardi, N., Arneri, E., Crise, A., Ravaioli, M., Zavatarelli, M., 2006. In: Robinson, A.R., Brink, K. (Eds.), The Physical, Sedimentary and Ecological Structure and Variability of Shelf Areas in the Mediterranean Sea, the Sea, vol. 14. Harvard University Press,

Cambridge, USA, pp. 1243e1330.

- Pinardi, N., I. Allen, E. Demirov, P. De Mey, G. Korres, A. Lascaratos, P.Y. Traon, C. Maillard, G. Manzella & C. Tziavos. 2003. The Mediterranean ocean forecasting system: first phase of implementation (1998-2001). Ann. Geophys., 21: 3-20.
- Polli, S., 1960. La Propagazione delle Maree nell'Adriatico: Atti del Convegno dell' Associazione Geofisica Italiana, Roma, 1959. 11 pp.
- Raicich F., 1994. Note on flow rates of the Adriatic rivers. Istituto Talassografico Sperimentale Trieste. Technical Report;RF02:94, 8.
- Raicich, F,1996. On the fresh water balance of the Adriatic Sea. Journal of Marine Systems 9, 305-319.
- Räisänen, J., U. Hansson, A. Ullerstig, R. Döscher, L.P. Graham, C. Jones, M. Meier, P. Samuelsson and U. Willén. 2004: European climate in the late 21st century: regional simulations with two driving global models and two forcing scenarios. Climate Dynamics., 22, 13-31.
- Ravaioli, M., Albertazzi S., Mercuriali C., Marozzi G., Bioturbazione e veloctà di sedimentazione, scientific report within the framework of the Project PRISMA 1
- Reed RK. 1977. On estimating insolation over the ocean. J Phys Oceanogr;1:854 – 71.
- Reed RK.1975. An evaluation of formulas for estimating clear sky insulation over the ocean. NOAA-ERL 352-PMEL Technical Report 1975 ;26:25.
- Ris, R.C., N. Booij and L.H. Holthuijsen, 1999: A third-generation wave model for coastal regions, Part II: Verification, J. Geophys. Res., 104, C4, 7667-7681.

- Roeckner E, and Coauthors. 1996. The atmospheric general circulation model Echam-4: model description and simulation of present-day climate. Max-Planck-Institut fur Meteorologie, Rep. No 218, Hamburg, Germany, 90 pp.
- Russo, A., A. Coluccelli, I. Iermano, F. Falcieri, M. Ravaioli, G. Bortoluzzi, P. Focaccia, G. Stanghellini, C.R. Ferrari, J. Chiggiato e M. Deserti 2009. An operational system for forecasting hypoxic events in the northern Adriatic Sea. Geofizika, 26(2), 191–213.
- Sanchez-Arcilla, A. and Simpson, J.H. 2002. The narrow shelf concept: couplings and fluxes.Continental Shelf Research 22 (2002) 153–172
- Smagorinsky, J. 1993. Some historical remarks on the use of nonlinear viscosities. In: Galperin, B. & S.A. Orszag (Editors). Large eddy simulations of complex engineering and geophysical flows. Cambridge Univ. Press, New York, pp. 3-36.
- Smith, J.D., 1977. Modeling of sediment transport on continental shelves, The Sea. Wiley-Interscience, New York.
- Souza A.J., Holt J. T., Proctor R.2007. Modelling SPM on the NW European shelf seas.
- Souza A.J.,Neil R. Fisher, John H. Simpson, and M. John Howarth. 2008. Effects of tidal straining on the semidiurnal cycle of dissipation in the
  Rhine region of freshwater influence: Comparison of model and measurements. JOURNAL OF GEOPHYSICAL RESEARCH, VOL. 113, C01011, doi:10.1029/2006JC004002, 2008
- Tonani M., N.Pinardi, S. Dobricic, I. Pujol and C. Fratianni, (2008). A High Resolution Free Surface Model on the Mediterranean Sea. Ocean Science, 4, 1-14.
- Traykovski et al. 2007, Observations and modeling of wave-supported

sediment gravity flows on the Po prodelta and comparison to prior observations from the Eel shelf, Continental Shelf Research 27, 375-399.

- Tsimplis, M.N., Proctor, R., Flather, R.A., 1995. A two-dimensional tidal model for the Mediterranean Sea. J. Geophys. Res. 100, 16223–16239.
- UNEP, 1996. Mediterranean Action Plan (MAP), Implications of Climate Change for the Albanian Coast, Technical Reports Series No. 98.
- Vichi, M., N. Pinardi, M. Zavatarelli, G. Matteucci, M. Marcaccio, M. C. Bergamini, and F. Frascari, One-dimensional ecosystem model tests in the Po Prodelta area (Northern Adriatic Sea), Environ. Model. Software, 13, 471– 481, 1998.
- Wang, X.H., Pinardi, N., 2002. Modeling the dynamics of sediment transport and resuspension in the northern Adriatic Sea. J. Geophys. Res. 107 (C12), 18–1–18-23.
- Wang, X.H., Pinardi, N., Malacic, V., 2007. Sediment transport and resuspension due to combined motion of wave and current in the northern Adriatic Sea during a Bora event in January 2001: a numerical modeling study. Cont. Shelf Res. 27, 613–633.
- Warren, R., and J. Johnsen, Cohesive sediment modelling for coastal lagoons, paper presented at International Colloquium and Exposition on Computer Applications in Coastal and Offshore Engineering (ICE-CA COE’93), Kuala Lumper, Malaysia, June 14– 16, 1993.
- Zavatarelli M, Pinardi N, Kourafalou VH, Maggiore A. 2002. Diagnostic and prognostic model studies of the Adriatic Sea circulation Seasonal variability. J Geophys Res;107(C1).
- Zavatarelli M, Pinardi N. 2003. The Adriatic Sea modelling system: a

nested approach. Ann Geophys;21:345–64.

- Zore-Armanda, M., 1979: Physical characteristics of the sea-water in the region of the Island of Hvar. Acta Biol. 8, 65– 78.